NASA TECHNICAL NOTE

NASA TN D-2247

C. 1

NASA TN D-2247

WIND TUNNEL INVESTIGATION OF TURBULENT BOUNDARY LAYER NOISE AS RELATED TO DESIGN CRITERIA FOR HIGH PERFORMANCE VEHICLES

by J. S. Murphy, D. A. Bies, W. W. Speaker, and P. A. Franken

Prepared under Contract No. NASr-110 *by*
DOUGLAS AIRCRAFT COMPANY, INC.
Long Beach, California
for

NATIONAL AERONAUTICS AND SPACE ADMINISTRATION • WASHINGTON, D. C. • APRIL 1964

WIND TUNNEL INVESTIGATION OF TURBULENT BOUNDARY LAYER NOISE AS RELATED TO DESIGN CRITERIA FOR HIGH PERFORMANCE VEHICLES

By J. S. Murphy, D. A. Bies, W. V. Speaker, and P. A. Franken

Prepared under Contract No. NASr-110 by
DOUGLAS AIRCRAFT COMPANY, INC.
Long Beach, California

NATIONAL AERONAUTICS AND SPACE ADMINISTRATION
For sale by the Office of Technical Services, Department of Commerce, Washington, D. C. 20230 -- Price $2.25

ACKNOWLEDGEMENT

The authors acknowledge the advice and support of Prof. Anatol Roshko, California Institute of Technology and Consultant, Douglas Aircraft Company; Dr. William J. Galloway, Bolt Beranek and Newman Inc.; and Drs. H. H. Hubbard and I. E. Garrick, Langley Research Center, NASA, during the course of the investigation. The investigation was supported by the National Aeronautics and Space Administration under Contract NASr 110.

NATIONAL AERONAUTICS AND SPACE ADMINISTRATION

WIND TUNNEL INVESTIGATION OF TURBULENT BOUNDARY LAYER NOISE AS RELATED TO DESIGN CRITERIA FOR HIGH PERFORMANCE VEHICLES

By

J. S. Murphy*
D. A. Bies△
W. V. Speaker*
P. A. Franken△

SUMMARY

Experimentally determined data on the magnitude of wall pressure fluctuation levels for turbulent boundary layers are presented in this report. The measurements were made on the sidewall of the Trisonic One-Foot Tunnel of the Douglas Aerophysics Laboratory which was modified to eliminate background noise in the test stream normally associated with choked flow over the pressure control valve. A small condenser microphone was used which limited measurements to frequencies below 88,000 cps, a range to which practical vehicle structure can respond. Results are presented for the zero pressure gradient or flat plate boundary layer on an insulated surface for free stream Mach numbers of .43, .59, .86, 1.41, 1.80, 2.52, and 3.46 and Reynolds number based on momentum thickness in the range $14 \times 10^3 < R_\theta < 50 \times 10^3$. These results are in agreement with other measurements at subsonic speeds and indicate a spectral distribution which is flat to values of non-dimensional frequency $f\delta^*/u_\infty = 0.45$ and a truncated fluctuation level of $\sqrt{\overline{\Delta p_T^2}}/\tau_o \simeq 2.8$. At supersonic speeds, the spectra also are flat to values of $f\theta/u_\infty \simeq 0.15$ with truncated overall levels of $\sqrt{\overline{\Delta p_T^2}}/\tau_o \simeq 1.2$ to 1.7. At Mach 3.46, the effects of various strength shock waves impinging on the boundary layer, surface roughnesses and surface pressure gradients on the magnitude of wall pressure fluctuation are shown to increase the truncated levels by factors of 5 to 20 times the level in the undisturbed boundary layer.

* Douglas Aircraft Company, Inc.
△ Bolt Beranek and Newman Inc.

INTRODUCTION

The high speed motion of a vehicle through a gas is resisted by the action of viscosity. This resistance is generated in a thin region near the surface of the vehicle, the boundary layer, in which large mean velocity gradients normal to the surface exist. Under conditions of major interest, the Reynolds number is large enough so that the motion within the boundary layer is turbulent; i.e., unsteady or fluctuating velocities of a random nature are superimposed on the mean motion. These fluctuating velocities produce pressure fluctuations which are evident as sound associated with the turbulence and as a fluctuating force acting on the vehicle surface. The vehicle designer is greatly interested in the magnitude of this fluctuating force since it can cause vibration of the structure which can contribute to fatigue failure and generate sound within the vehicle (ref. 1). Hence the designer must provide proper treatment for protection of passengers and equipment. The problem is particularly important for designers of advanced vehicles such as supersonic transport aircraft (ref. 2) and manned spacecraft.

The mechanism of noise generation for turbulent flows over rigid surfaces has been studied theoretically by Curle (ref. 3) and Phillips (refs. 4 and 5) while theories on noise radiated by flexible flat plates excited by turbulent boundary layers have been presented by Corcos and Liepmann (ref. 1), Ribner (ref. 6) and Kraichnan (ref. 7). Dyer (ref. 8) and Tack and Lambert (ref. 9) have considered the response of plates and bars subjected to boundary layer pressure fluctuations using the approach suggested by Lyon (ref. 10).

All of these theoretical treatments require empirical information on the characteristics of the pressure fluctuation field. Most laboratory measurements of wall pressure fluctuation characteristics have been made on smooth, rigid surfaces. The measurements of Willmarth (ref. 11) and Harrison (ref. 12) were made at subsonic speeds for the case of zero pressure gradient flow (flat plate) on a smooth surface. Skudrzyk and Haddle (ref. 13) made measurements at subsonic speeds on the wall of a water tunnel and on a rotating cylinder with both a smooth and rough surface (sandpaper type roughness). Kistler and Chen (ref. 14) and Williams (ref. 15) measured the fluctuating pressure field on smooth surfaces with zero pressure gradient flow at supersonic speeds. Unfortunately for the vehicle designer, the results show a rather wide variation - particularly between the subsonic and supersonic measurements. To further complicate the designer's dilemma, measurements made in flight by Von Gierke (ref. 16), Mull and Algranti (ref. 17, 18), McLeod and Jordon (ref. 19) Hilton et.al. (ref. 20), Shattuck (ref. 21) and McLeod (ref. 22) indicate that it is not possible generally to relate the laboratory results directly to flight

measurements. Thus the present experimental program of wind tunnel measurements was initiated in order to: (1) examine the Mach number effect on wall pressure fluctuations for zero pressure gradient flows at both subsonic and supersonic speeds in a single experimental set-up; and (2) introduce into the laboratory experiments some of the elements of non-uniform flow such as surface roughness, pressure gradient and shock wave impingement which exist for practical vehicle configurations on which flight measurements were made.

The need for improved information on boundary layer pressure fluctuations increases in urgency with the advent of supersonic transport vehicles since the dynamic pressure corresponding to cruise (at 60,000 - 70,000 feet altitude) is greater by a factor of two to three than existing subsonic transports (at 30,000 feet altitude). The location of critical regions of high fluctuation levels may require special treatment for protection of vehicle structure, equipment and passengers. With these applications in mind, the emphasis was placed on obtaining measurements in the frequency range to which a structure can respond.

A small condenser microphone was used as the pressure transducer, thereby eliminating the problems of vibration sensitivity that are encountered with piezoelectric transducers. Although the use of such a transducer (effective surface diameter of approximately 0.13 inch) meant that the investigation was restricted to the relatively lower frequency range, and that no direct measure of overall pressure fluctuation level could be obtained, it was believed that the results would be useful in the frequency range of primary interest in practical vehicle design problems.

SYMBOLS

A area of microphone diaphragm, in^2

a speed of sound, ft/sec

b constant in eq. C2, dimensionless

c_f skin friction coefficient = τ_o/q, dimensionless

da element of area, in^2

D diameter of microphone diaphragm, inches

D_e effective diameter of microphone diaphragm, inches

f frequency of pressure fluctuations, cps

$F(f)$ pressure spectral density

H form parameter = δ^*/θ, dimensionless

J_n Bessel function of the nth order, dimensionless

M Mach number = u/a, dimensionless

P steady pressure, lb/in^2

P_o pressure amplitude of a plane progressive wave, lb/in^2

$\tilde{p}$ fluctuating pressure, lb/in^2 or db re 2.9×10^{-9} lb/in^2(.0002 microbar)

$\Delta\tilde{p}_T$ increment of overall pressure fluctuation level for limited frequency range

Pr Prandtl number, dimensionless

q dynamic pressure, lb/in^2

r temperature recovery factor = $\frac{T_w - T_e}{T_{t_e} - T_e}$, dimensionless

R radius in polar coordinates, inches

R_θ Reynolds number based on momentum thickness, dimensionless

t height of roughness element, inches, or time, seconds

T temperature, deg. Rankine

u velocity of fluid, ft/sec

V output of microphone, volts

x longitudinal distance, parallel to tunnel centerline, with x = 0 at center of sidewall insert, inches

X_P longitudinal distance along centerline of pressure gradient generator, inches

y transverse distance, normal to sidewall, with y = 0 at the wall, inches

Y_P distance from centerline to contour of pressure gradient generator, inches

β angle between tunnel centerline and shock generator surface, degrees

γ ratio of specific heats, dimensionless, ($\gamma = 1.4$)

δ	boundary layer thickness, defined as y at $u/u_e = 0.99$, inches
δ^*	boundary layer displacement thickness, inches
θ	boundary layer momentum thickness, inches
λ	wave length, inches
μ	absolute viscosity, lb-sec/ft^2
ν	angle between tunnel centerline and expansion generator surface, degrees
ρ	density, lb-sec^2/ft^4
$\sigma(r)$	sensitivity function, volts/in^2 - lb/in^2
σ_o	sensitivity constant, volts/in^2 - lb/in^2
τ_o	wall shearing stress, lb/in^2
ω	angular frequency, rad/sec
ψ	angle in polar coordinates, degrees

SUBSCRIPTS

e	condition at edge of boundary layer
i	incompressible conditions
n	condition at microphone; i.e., n = 1, 3, 4, 5, 7, 8, 11
t	stagnation condition
w	condition at wall
y	condition at y inches from wall
∞	freestream condition

SUPERSCRIPT

'	reference condition

APPARATUS AND TEST PROCEDURE

Wind Tunnel

The measurements were made on the sidewall of the Trisonic One-Foot Tunnel of the Douglas Aerophysics Laboratory. The tunnel is a blowdown-to-atmosphere facility operating over the Mach number range 0.2 to 3.5. Mach number in the tunnel is generated by fixed nozzle blocks at supersonic speeds. Speeds in the subsonic and transonic range are controlled by changing the area of a second throat downstream of the test section. Design features of the tunnel are shown in Figure 1. The tunnel is particularly suitable for research in boundary layer pressure fluctuations because it was designed with an acoustic muffler in the stilling chamber (ref. 23) which reduces background noise and because the choked second throat prevents sound propagation upstream from the diffuser even at subsonic speed in the test section. Thus, it provides the inherent advantages of high test stream dynamic pressure with low background noise. The facility was specifically modified for this study to eliminate background noise normally associated with choked flow over the control valve. By connecting the 8,000 ft^3 reservoir of the tunnel with an adjacent 26,000 ft^3 reservoir, it is possible to operate with stagnation pressure equal to reservoir pressure thereby completely eliminating choked valve noise. The piping modification required to accomplish this is shown in Figures 2 to 4. A hydraulically operated butterfly valve was installed in the 18-inch line connecting the two reservoirs. Both this 18-inch valve and the 12-inch control valve were operated simultaneously as on-off valves for the boundary layer pressure fluctuation tests. Corrections for the slight decay in stagnation pressure resulting from the above mode of operation were made during data reduction. Further details concerning the wind tunnel may be found in ref. 35.

Boundary Layer and Static Pressure Measurements

The measurements were made on a 14.5-inch circular insert in the side wall of the test section. The turbulent boundary layer developed naturally for approximately eight feet upstream of the measuring station. Pressure distributions along the sidewall were measured with Statham 5-psid differential transducers (using a vacuum reference). Boundary layer total pressures were measured using a 3-tube rake (Figure 5). Pressures were sensed by Statham 15-psid differential transducers. The position of the rake was varied by means of a traverse gear driven by a 28-volt Globe dc motor and was measured by a shaft position encoder with a resolution of 36,000 counts per inch of rake travel.

Static and total pressure data were reduced to absolute pressures on an IBM 1620 computer using appropriate transducer calibration factors

and ambient pressures. The static pressure data was also reduced to Mach number by means of the isentropic relationship between static and stagnation pressure. The boundary layer total pressures were reduced to local Mach numbers and velocities by the isentropic static-to-stagnation pressure ratio at subsonic speeds and by the Rayleigh pitot formula at supersonic speeds. In both cases, the local Mach number was calculated using the static pressure taken from the wall pressure orifice nearest to the boundary layer rake which was unaffected by the presence of the rake. To calculate the velocity, constant total temperature across the boundary layer was assumed.

The local-to-freestream velocity ratio within the boundary layer was plotted as a function of distance from the wall on a Benson-Lehner Electroplotter, and values of δ were determined by setting $y = \delta$ at $u/u_e = .99$. Typical boundary layer velocity profiles are shown in Figure 6. Values of other boundary layer parameters were determined as shown in Appendix A.

Fluctuating Pressure Measurements

Boundary layer pressure fluctuations were measured by a series of flush-mounted Bruel and Kjaer Model 4136 condenser microphones installed in a second insert in the sidewall of the wind tunnel. Figure 7 shows the locations of the microphones and an accelerometer on the test plate. Figure 8 is a block diagram of the acoustic data acquisition system. During the first series of acoustic tests, the microphone signals were recorded in the FM mode to provide data over the frequency range from 0.01 to 10 kcps. During the final series of tests, the microphone signals were recorded in the direct record mode to provide data over the frequency range from 0.1 to 100 kcps. Most of the acoustic data presented in this report were obtained during the final series of tests. Further information concerning the acoustic data acquisition instrumentation and procedures, including discussions of calibration procedures and microphone vibration sensitivity, is given in Appendix B.

A typical wind tunnel run lasted for approximately 15 seconds, including tunnel starting and shut-down time. The frequency analyses of the acoustic data were accomplished by re-recording the data on a multichannel continuous loop of approximately 10 seconds duration. The data on a loop thus represented that portion of the wind tunnel run during which essentially steady-state conditions prevailed.

In Figure 9 are block diagrams of the acoustic data processing systems that were used for the direct and FM recorded data. The FM data from the first series of acoustic tests were reduced in one-third octave bands of frequency. The direct record data from the final acoustic tests were reduced in octave bands of frequency. For convenience of

comparison, the one-third octave band levels have been converted to octave band levels, and all the acoustic data in this report are presented as octave band levels.

Corrections were applied to the raw data to account for record and playback characteristics of the acquisition and analysis system, for the resonance of the condenser microphone at reduced ambient pressures, and for the finite size of the microphone diaphragm. Further information concerning the derivation and form of these corrections is given in Appendices B and C.

Model Description

In addition to the two sidewall inserts used for static and fluctuating pressure measurements, other items of hardware are noteworthy. Two-dimensional shock wave and pressure gradient generators were provided as shown in Figure 10. The shock generator spanned the height of the tunnel and was simply rotated about one of two pivot points to change the shock angle between 0° and 10°. It was possible to obtain expansion angles from 0° to 5° also with the same arrangement using the forward pivot point. The adverse pressure gradient generator was originally designed by the method of characteristics to provide a change in Mach number of about -1.0 in eight inches along the sidewall using the contour $Y_p = 0.00551\ X_p^2$ located three inches from the wall. To eliminate choking in the channel between the contour and the wall, the generator was moved farther from the wall and the resulting change in Mach number was then equal to -0.8 in four inches. (See the section entitled "Measurements" for other ramifications of this problem.)

A number of roughness elements were fabricated for investigation of the effects of local perturbations on tunnel sidewall boundary layer pressure fluctuation levels. These are shown in Figure 11. Four thicknesses of two-dimensional roughness between 0.012 and 0.125 inch were provided and a second 0.125-inch strip was rounded on the leading edge for comparison with the square leading edge. All were one inch in width. A simulated half-scale window (Figure 11) with a thickness of 0.050 inch was also provided.

Test Procedure

The supersonic test section was used for both subsonic and supersonic investigations. Clear tunnel measurements of turbulent sidewall boundary layer pressure fluctuation levels, static pressure distributions, and boundary layer velocity profiles were conducted at subsonic Mach numbers of 0.43, 0.59, 0.77, and 0.86 and at supersonic Mach numbers of 1.41, 1.80, 2.52, and 3.46. Effects of shock wave boundary

layer interaction, surface roughness elements, and favorable and adverse pressure gradients on pressure fluctuation level were measured at Mach 3.46.

All pressure fluctuation measurements were made with tunnel stagnation pressure equal to reservoir pressure. Stagnation pressure was maintained nearly constant by using a 34,000 ft^3 reservoir connected to the stilling chamber by two hydraulically operated butterfly valves - a 12-inch diameter valve normally associated with the tunnel and an 18-inch diameter valve. These valves were used as on-off valves for the pressure fluctuation tests. The resulting variation in stagnation pressure during these tests varied from $\pm$ 6% at Mach number 0.30 to $\pm$ 12% at Mach 0.86 and $\pm$ 1.5% at Mach 3.56. Tunnel Mach number was maintained constant during all runs, which normally lasted for 15 seconds. The deviation in sound pressure level as a result of the stagnation pressure change was not readily discernible. Thus, the pressure fluctuation level is referred to average dynamic pressure during a run. Static pressure distributions and boundary layer velocity profiles were measured using normal tunnel operation at constant stagnation pressure. For these runs, Reynolds number was maintained nearly constant at a value equal to the average value occurring in the acoustic tests. Deviations in data introduced by the slight Reynolds number variation of the acoustic tests are considered to be of second order.

MEASUREMENTS

The primary data obtained in this experimental investigation is the magnitude of wall pressure fluctuations as a function of frequency for various types of turbulent boundary layers. Measurements were limited to the frequency range $32 \leq f \leq 88{,}000$ cps. Results are presented and discussed for the zero pressure gradient or flat plate turbulent boundary layer on an insulated wall in the range of free stream Mach numbers $0.43 \leq M \leq 3.46$ and Reynolds numbers based on momentum thickness and free stream conditions in the range $14 \times 10^3 \leq R_\theta \leq 50 \times 10^3$. At one representative supersonic Mach number, Mach 3.46, the effects of various strengths of shock and expansion waves impinging on the boundary layer, surface roughness and favorable and adverse pressure gradients on the magnitude of wall pressure fluctuation are presented.

Boundary Layer Characteristics

To be useful for design purposes, wall pressure fluctuations ideally should be related to suitable characteristics of the turbulent boundary layer which can be calculated or estimated by conventional

boundary layer theory. In the present experiments, the boundary layer velocity profile was measured at a single station on the sidewall at all test Mach numbers. This station was located four (4) inches ahead of the centerline of the instrumented sidewall insert and corresponded to microphone position #4. (See Figure 7).

Non-dimensional velocity profiles are shown in Figure 12. Using the data reduction procedure presented in Appendix A, boundary layer total thickness, displacement thickness, momentum thickness, and skin friction coefficient have been calculated from the measured velocity profile. These boundary layer characteristics are presented in Figure 13 as a function of free stream Mach number and are tabulated in Table 1.

For the zero pressure gradient cases, estimates of boundary layer characteristics at stations upstream or downstream of the measurement station may be made using the assumption that the velocity profile shape parameter, H, remains constant and determining the change in momentum thickness from the momentum integral equation (ref. 24).

$$\frac{d\theta}{dx} = c_{f/2} \qquad (1)$$

Estimated boundary layer characteristics at microphone position #1 (station +6.625) using this procedure are tabulated in Table 2.

No attempts were made in the present study to measure detailed boundary layer velocity profiles for cases where the base or clear tunnel boundary layer was disturbed by shock impingement, favorable or adverse pressure gradients, and surface roughness. Instead, the pressure fluctuation measurements for these cases have been referred to the boundary layer characteristics in the undisturbed flow ahead of the shock or roughness element.

Mach Number Effect

Mach number and static pressure distributions along the instrumented sidewall insert are presented in Figure 14 (A-H) while wall pressure fluctuation levels as a function of frequency are presented in Figures 15 to 21 inclusive. The study of these data indicates three separate phenomena. At each Mach number there are a group of data points which define a straight line with a rise of three decibels (3db) per octave, indicating a constant spectrum above a certain frequency, up to the highest measured (88kcps). At Mach numbers M = 0.43, 2.52, and 3.46, all microphones indicate this constant spectrum characteristic irrespective of microphone position along the plate.

The flat spectrum holds for all frequency bands measured except for those below 1000 cps at Mach 0.43, where a relative maximum is evident at about the 100 cps band. This same relative maximum appears at Mach numbers M = 0.59, 0.86, 1.41, and 1.80. Also at Mach numbers M = 0.59, 0.86, and 1.41, and 1.80, a second group of data points indicate a pressure fluctuation level well above that corresponding to a flat spectrum for frequencies between the 250-cps octave band and the 8000-cps band. These points are most prominent at Mach 1.41. However, at these Mach numbers, the spectrum is again flat at frequencies above 10 k cps.

For later convenience, these observed phenomena are summarized as follows:

Phenomenon	"a"	- linear slope with 3 db rise per octave
Phenomenon	"b"	- elevated fluctuation levels between .25 and 8.0 kcps
Phenomenon	"c"	- relative maximum below 0.25 kcps

The data presented in Figures 15 through 21 were obtained during three separate series of tests in November, 1962 and January and March, 1963. In each test series, measurements were made at all Mach numbers noted above. In each series, at Mach numbers between 0.59 and 1.80, all three phenomena were measured whereas at other Mach numbers phenomenon "a" predominated. Thus at Mach 1.41 for tests conducted in November, microphone position #1 showed phenomenon "a" and microphone position #5 showed phenomenon "b". In the March tests at Mach 1.41, microphone position #1 showed phenomenon "b" and microphone position #5 showed phenomenon "a". The above measurements were repeated in each test series with results found to be repeatable within $\pm$ 1 db as shown in Figure 18. Thus, no interchange of phenomena "a" and "b" at any given microphone location during a single series of runs was ever observed. No explanation for phenomena "b" and "c" may be offered at this time. It should be pointed out that they are not in conflict with the work of other investigators, however, since they occur in a frequency range below that generally investigated and where available data has been considered uncertain. Some speculations regarding their origin are presented in "Discussion".

At Mach 3.46, the data of Figure 21 clearly indicate a flat spectrum over the entire frequency range for which measurements were made. The scatter in pressure fluctuation level as measured at six different microphone positions (including #11 which is located 4 inches below the sidewall centerline) and several repeat runs is on the order of $\pm$ 3 db at any given frequency. Some of this scatter may be associated with the change in boundary layer characteristics resulting from the

change in Reynolds number corresponding to the various microphone locations.

Effects of Shock Wave Impingement

Based on the work of Ribner (ref. 27) it is expected that impingement of a shock wave on the turbulent boundary layer should bring about a marked increase in the surface pressure fluctuation level which is due to the interaction of vorticity and entropy spottiness with the shock wave. In order to determine whether such increases do occur, several shock waves with flow deflection angles, β, between 0° and 10° were impinged on the sidewall boundary layer at M = 3.46. Detailed pressure distributions in the region of shock boundary layer interaction exhibit the well known (refs. 28 and 29) steep, unbroken wall pressure gradient over a distance of 2δ for weak shock angles ($\beta \leq 2.5^\circ$); and the occurrence of a pressure "plateau" for $\beta = 5^\circ$ which increases in extent for $\beta = 7.5^\circ$ to indicate incipient separation. At $\beta = 10^\circ$, the shock strength was so large that the channel between the generator and the sidewall was probably choked as the result of the strong shock and the reduced area ratio between the base of the generator and its leading edge. Qualitative wall static pressure distributions for various shock angles are presented in Figure 22. The data for $\beta = 0^\circ$ indicate that in this configuration there was actually a weak shock of $1/2^\circ$ deflection angle impinging on the sidewall boundary layer.

The effects of shock angle on the fluctuating pressure level spectra at several microphone locations are shown in Figures 23 through 25. The shock generator reference angle β was set at 0°, 5.0°, and 7.5°. For convenience the theoretical point of impingement of the shock and the region of expansion is given schematically in the upper left-hand corner along with the microphone locations. In all three cases the spectrum measured at microphone position #1 is the same as for a clear tunnel. However, the data indicate that the effect downstream of the shock is quite pronounced.

Figure 23 presents the acoustic data for a shock generator angle of 0°. The presence of phenomenon "b" in addition to phenomenon "a" is indicated by the spread of the data points at frequencies below 10 kcps. Presumably this is due to the presence of the weak shock wave, (approximately 0.5°).

In Figure 24 are shown the results of runs conducted in January and in March for a shock generator angle of 5.0°. In both cases the pressure fluctuation levels are greatly increased downstream of the point of shock impingement, but the data are not as repeatable as might be desired. This result may be due to a slight variation in the shock generator angle in the two runs. In one test the levels in

the area of microphone position #3, #4, and #5 were raised above the clear tunnel levels by 15 db, while in the other test the levels in this region were raised 10 db. In both cases the levels at microphone position #8 were lower than those at positions #3, #4, and #5 but higher than those at microphone position #1 which gives clear tunnel levels.

In Figure 25 are shown the results of runs conducted in January and in March for a shock angle of 7.5°. The results are much the same as for the 5° shock angle case except that the levels in the vicinity of microphone positions #3, #4, and #5 were raised about 24 db above clear-tunnel levels.

The microphone at position #4 was always downstream of the shock wave and as shown above, the levels measured there were similar to the levels measured at microphone positions #3 and #5. We may infer from this that the pressure fluctuation levels downstream of the shock are not strongly dependent upon distance from the shock in the region of the steep pressure rise, but are strongly dependent upon the shock strength as shown in Figure 26 where the pressure fluctuation levels measured at microphone position #4 have been plotted for several angles β of the shock generator. Clear-tunnel measurements have also been included for comparison. The data for $\beta = 10°$ are shown (although the tunnel was probably choked, as noted above) to allow comparison of levels in both separated and unseparated flows.

Effect of Pressure Gradients

The effects of pressure gradient on wall pressure fluctuation were studied briefly at Mach 3.46. Favorable pressure gradients were obtained by simply rotating the shock generator until an expansion took place. The static pressure and Mach number distributions are shown in Figure 27. The adverse gradient was obtained by designing a curved surface in an attempt to obtain a constant gradient at the wall. As shown in Figure 28, the gradient was much steeper and was located further downstream than desired.

The acoustic spectra for the favorable gradients are shown in Figure 29 and 30 while Figure 31 is a favorable gradient summary at microphone position #4. The data in Figure 31 for $\nu = 0$ are identical with the data in Figure 23 for $\beta = 0$ and differ from the clear tunnel data at the same microphone positions because of the presence of a mild shock for $\beta = \nu = 0$. Figure 30 for $\nu = 5°$ reveals a curious correspondence when compared with Figure 24, the spectra for $\beta = 5°$. Although microphone #1 (Figure 30) is located at the beginning of the influence region of the expansion, its data are almost identical to the data for $\beta = 5°$, which in turn reflect the clear-tunnel levels shown in Figure 21. Data from microphones #3, #4, and #5 are nearly

the same for both $\nu = 5^\circ$ and $\beta = 5^\circ$, particularly at the higher frequencies. In the frequency range 0.125-4.0 kcps there are some deviations, although these do not generally exceed 3.5 - 4.0 db. Data at microphone #8 are the only ones to indicate a difference. For the case of $\beta = 5^\circ$ microphone #8 is at the beginning of the expansion region from the end of the wedge (Figure 22) and the acoustic levels are some 4-5 db lower than the average for microphones #3, #4, and #5 but are still much higher than for clear-tunnel. For the expansion case, $\nu = 5^\circ$, the data show lower than clear-tunnel levels, the only condition in the entire investigation that has produced values below the basic clear-tunnel levels.

The acoustic spectra for the adverse pressure gradient are shown in Figure 32. As can be seen from Figure 28, microphones #1, #3, #4, and #5 were essentially at clear-tunnel conditions and only microphone #8 was in a disturbed region. Strangely, the pressure fluctuations at microphone #8 (Figure 32) differ very little from clear-tunnel levels despite the fact that the microphone is located at the very peak pressure. This result may be due to the fact that precisely at that location the adverse gradient meets a favorable gradient resulting from the expansion at the base of the generator. Clearly, additional investigating of the effects of adverse pressure gradients is required.

Effects of Surface Roughness

In describing the aerodynamic effects which are due to the two-dimensional roughness elements tested in this investigation, it can be stated that conditions upstream are analagous to those with a forward-facing step. Conversely, conditions downstream are those for a rearward-facing step. Considerable background material exists concerning the fluid mechanic effects of steps (refs. 30-34) although most investigators have reported on flows over steps that are large compared to the boundary layer thickness. In the case described herein, the steps range in height from 0.017δ to 0.17δ at M = 3.46 (nominal). Figure 33 (a) presents the pressure and Mach number distributions for the four roughness thicknesses investigated and Figure 33 (b) compares the distributions for a 0.125-inch strip with blunt or rounded leading edges. While the pressure orifices were not sufficiently dense to describe the flow in detail, the measurements show the approximate pressure levels and gradients at the various microphone locations. It can be seen that there is little difference between the upstream effects for the two smallest strips but in the region immediately downstream the differences for all four strips are distinguishable.

Although the static pressures at microphone positions #1 and #3 show an effect of roughness for all thicknesses, no appreciable effect on local pressure fluctuations was observed (Figure 34) up to t = 0.025".

A large effect was noted for the 0.050-inch roughness as is shown in Figure 35. The downstream levels are all raised roughly 6 db above clear-tunnel levels and the upstream levels (at microphone #1) are increased up to 20 db below the 16 kcps octave band. In addition, the upstream levels exhibit the behavior of clear-tunnel phenomenon "b".

The levels were increased still further with a 0.125-inch roughness, Figure 36. The pressure fluctuation levels at microphone positions #4 and #8 are up 10 db above clear-tunnel levels. The levels at microphones #1 and #5 are similar to each other and show the phenomenon "b" behavior, indicating as much as 20 db above clear-tunnel levels in the lower frequency range.

Figures 37 and 38 summarize the effects just upstream (microphone #1) and downstream (microphone #3) of the roughness and compare them to the clear-tunnel levels. For microphone #3, clear-tunnel levels have been estimated from the data of microphone #1.

The effect of rounding the leading edge of the 0.125-inch strip was not conclusive (Figures 37 and 38), although the levels upstream appear to be slightly lower than for the blunt strip.

Figures 39 and 40 present static pressure and fluctuating pressure data, respectively, for a simulated half-scale window at M 3.46. The spacing of pressure orifices is limited but microphones #1, #7, and #8 are seen to be in relatively undisturbed regions. Microphone #11 (not shown), might be considered to be influenced by the simulated window, being about 1-1/2 inches below it and nearly 2 inches behind the leading edge. The fluctuating pressures (Figure 40) at microphone #1 are indeed unaffected but microphones #7 and #8 give levels 5-6 db above clear-tunnel levels. Microphone #11 once again exhibits the phenomenon "b" effects at frequencies of 2 kcps and lower.

DISCUSSION

It is of interest to compare the present results with previous measurements of wall pressure fluctuations. Perhaps the most complete measurements are those of Willmarth (ref. 38) at subsonic speeds. His results at speeds of 206 ft/sec show a spectrum which is almost flat to $f\delta^*/u_\infty = 0.5$ and a measured overall fluctuation level of $\sqrt{\widetilde{p^2}}/\tau_o = 2.2$ compared to his previous measurements of $\sqrt{\widetilde{p^2}}/\tau_o = 2.3$ to 2.5 (ref. 11). When corrections to Willmarth's measurements are made for transducer size in accordance with Corcos' technique (ref. 25), the resulting overall values are $\sqrt{\widetilde{p^2}}/\tau_o = 3.5$. In order to compare these results with our measurements, it is necessary to determine the contribution to the overall level of fluctuations contained in the frequency range

up to $f\delta^*/u_\infty = 0.45$, the range of frequency covered by our measurements at M = 0.43. If this contribution is defined as a truncated mean square pressure, $\sqrt{\widetilde{\Delta p_T^2}}$, the resulting valve from ref. 38 is $\sqrt{\widetilde{\Delta p_T^2}}/\tau_o = 1.9$, when transducer size corrections are included. Our measured spectrum at M = .43, shown in Figure 15, has been integrated over the frequency range $0 \leq f \leq 44$ kcps, yielding $\sqrt{\widetilde{\Delta p_T^2}}/\tau_o = 2.8$ and $\sqrt{\widetilde{\Delta p_T^2}}/q = 7.5 \times 10^{-3}$. Thus reasonable agreement with Willmarth's subsonic measurement is exhibited.

At supersonic speeds, the only detailed measurements of spectra which have been reported to date are those of Kistler and Chen (ref. 14). They showed that their spectra could be brought into coincidence, independent of Mach number in the range between M = 1.33 and M = 5, by use of frequency in the non-dimensional form, $f\theta/u_\infty$. Likewise they showed that their measured values of overall fluctuation level were almost independent of Mach number above M = 2 . Thus according to their measurements, they found

$$\widetilde{p^2} = \int_o^\infty F(f)df = \frac{\tau_o^2\theta}{u_\infty} \quad \frac{u_\infty}{\theta} \int_o^\infty \frac{Fu_\infty}{\tau_o^2\theta} \quad d\left(\frac{f\theta}{u_\infty}\right) \tag{2}$$

where the value of the integral is approximately 25. Hence,

$$\frac{\sqrt{\widetilde{p^2}}}{\tau_o} = 5 \tag{3}$$

or

$$\sqrt{\widetilde{p^2}} = 5 \quad \frac{\gamma P_\infty}{2} \quad M_\infty^2 \, c_f \tag{4}$$

Equation (4) exhibits the dependence of the root-mean-square pressure fluctuation on skin friction coefficient, static pressure and Mach number, when contributions from all portions of the spectrum are present. Thus, the measurements of Kistler and Chen indicate that the quantity $\sqrt{\widetilde{p^2}}/\tau_o$ increases from about 3 at subsonic speeds to about 5 at supersonic speeds.

A direct comparison of the present data with the measurements of Willmarth and Kistler and Chen is shown in Figure 44. Reasonable agreement is exhibited at subsonic speeds. The transducer size correction contained in our data accounts for the deviation from Willmarth's curve at the higher frequencies since this correction is not included in his data. Our data falls below the previous supersonic measurements.

However, the numerous transducers and test series represented by the current measurements and the knowledge that they are free from vibration effects lends credence to the present results.

For some applications the contributions to $\sqrt{\widetilde{p^2}}$ from limited frequency intervals of the spectrum may be of interest e.g. in a measurement in which there is a frequency cut-off, f_c, imposed by instrumentation limitations. Similarly, the response of a structure may be negligible beyond some cut-off frequency, fc. In such cases, we define a truncated mean square pressure,

$$\widetilde{\Delta p_T^2} = \int_0^{f_c} F(f)df \tag{5}$$

For measurements, fc is chosen so that the portion of the spectrum from 0 to f_c is practically flat, as indicated by the spectra shown in Figures 15 to 21. Then,

$$\widetilde{\Delta p_T^2} = F_o f_c = \frac{\tau_o^2 \theta}{u_\infty} \frac{F_o u_\infty}{\tau_o^2 \theta} f_c = \text{const} \frac{\tau_o^2 \theta}{u_\infty} f_c \tag{6}$$

where F_o is the value of the spectral function in the flat portion. Since

$$u_\infty = a_\infty M_\infty \tag{7}$$

Equation (6) yields

$$\sqrt{\widetilde{\Delta p_T^2}} = K \frac{\gamma P_\infty}{2} M_\infty^{3/2} c_f \sqrt{\frac{f_c \theta}{a_\infty}} \tag{8}$$

Based on the present measurements, the value of the constant K has been determined to be approximately

$$K = 3.6 \tag{9}$$

as shown in Figure 43. The data points shown in Figure 43 were obtained by integrating the spectra of Figures 15-21. In performing this integration, phenomena "b" and "c" have been neglected since phenomena "a" predominates in all cases at frequencies above 10 kcps. Since both the subsonic and supersonic data of the present study can be correlated with a single value of K, our results tend to indicate a relationship between wall pressure fluctuation level and skin friction which is independent of Mach number. Of course, our measurements are limited to f - 88 kcps so that significant contributions to overall fluctuation level may exist at higher frequencies which could alter this conclusion.

At Mach 3.46, the influence of various types of disturbances to the boundary layer on the magnitude of wall pressure fluctuation level are summarized in Table 3. As indicated therein, shock waves impinging on the boundary layer produce increases in pressure fluctuation levels as great as twenty (20) times the undisturbed case. Within the limited frequency range of the measurements, the spectra again are flat, as shown in Figure 26. The values of $\sqrt{\overline{\Delta p_T^2}}$ shown in Table 3 for shock impingement were obtained by the integration of these spectra.

Favorable gradients were generated by a Prandtl-Meyer expansion of $\nu = 2.5^\circ$ and $\nu = 5^\circ$. In one case ($\nu = 2.5^\circ$), this favorable gradient had little influence on magnitude of wall pressure fluctuation level, whereas, in the other case ($\nu = 5^\circ$) it increased the level by a factor of five above the undisturbed case. The increase in local skin friction accompanying the favorable pressure gradient was not determined.

The adverse gradient of .96 psi/in produced no measurable change in the magnitude of wall pressure fluctuation level. In these tests, however, the microphone locations with respect to the pressure distributions were not optimal. Hence, the effects of favorable and adverse pressure gradient at Mach 3.46 from the present study must be considered inconclusive.

The influence of two-dimensional, square-edge, roughness elements on wall pressure fluctuations are found to be appreciable as shown in Table 3. These elements increase the level of pressure fluctuations at a location ahead of the elements (element downstream) by a factor of six compared with the undisturbed case. This is shown by the measurements presented in Figure 37 for cases where the element is large enough in height to ensure that the normal shock ahead of the element is upstream of the fixed microphone position #1 ($t \geq 0.05"$). Likewise, the level downstream of the element is increased by as much as a factor of five above clear-tunnel values.

In addition to the change in fluctuation level, the roughness elements modify the spectrum of the pressure so as to increase the fluctuation level at intermediate frequencies. Thus it may be speculated that the appearance of increased levels in the middle frequency range for the undisturbed boundary layer, as shown in Figure 18 for Mach 1.41, may be the manifestation of a relatively small local flow disturbance arising from some change in tunnel configuration between the three test series. The increase in levels over the entire frequency range measured, shown in Figures 24 and 25 for shock angles $\beta = 5^\circ$ and 7.5°

and in Figure 30 for $\nu = 5^{\circ}$, may be the manifestation of a relatively larger flow disturbance. In these latter cases, the larger flow disturbance may give rise to level increases over a broader frequency range, and these appear as uniform level increases in the present measurements.

In terms of conditions which may be encountered in flight at Mach 3.5 at 60,000 ft. altitude, the results of this study indicate that thin turbulent boundary layers on insulated surfaces (R_θ = 50,000, c_f = 0.0011) will generate pressure fluctuation levels of magnitude $\sqrt{\widetilde{\Delta p_T^2}} \simeq$ .015 lbs/in^2 in the frequency range $f \leq 88$ kcps. However, in the neighborhood of surface roughness elements or impinging shock waves, the pressure fluctuation levels increase to $\sqrt{\widetilde{\Delta p_T^2}} \simeq 0.10$ and $\sqrt{\widetilde{\Delta p_T^2}} \simeq 0.20$ lbs/in^2 respectively.

CONCLUDING REMARKS

Results of the present experimental investigation of turbulent boundary layer wall pressure fluctuations lead to the following conclusions:

1. The modification of the blowdown wind tunnel, enabling operation with stagnation pressure equal to reservoir pressure, produced a facility which has satisfactory characteristics (low background noise level) to enable boundary layer noise to be measured over the Mach range $0.4 \leq M \leq 3.5$ in a single experimental arrangement.

2. Measurements under the zero-pressure gradient boundary layer are in agreement with other results at subsonic speeds and indicate a pressure spectrum which is flat to values of non-dimensional frequency $f\delta^*/u_\infty = 0.45$ and a truncated fluctuation level of $\sqrt{\widetilde{\Delta p_T^2}} / \tau_o \simeq 2.8$ for $f \leq 44$ kcps.

3. Zero-pressure gradient results at supersonic speeds show pressure spectra which are flat to $f0/u_\infty \simeq .15$ and truncated fluctuation levels of $\sqrt{\widetilde{\Delta p_T^2}}/\tau_o = 1.2$ to 1.7 for $f \leq 88$ kcps, a frequency range to which practical vehicle structure can respond.

4. Measurements of the influence of favorable and adverse pressure gradients on wall pressure fluctuation levels at Mach 3.46 are inclusive.

5. At Mach 3.46, impingement of shock waves on the turbulent boundary layer can increase the pressure fluctuation level by a factor of twenty (20) above the undisturbed case.

6. At Mach 3.46, two-dimensional, square-edge roughness elements increase pressure fluctuation levels by a factor of five or six above the undisturbed boundary layer levels.

APPENDIX A - BOUNDARY LAYER DATA REDUCTION PROCEDURES

The characteristics of the turbulent boundary layer on the sidewall were determined by measurement of the total pressure profile and the local wall static pressure. Velocity ratio, u/u_e, was calculated from these measurements using the Rayleigh pitot formula. The Crocco relationship between velocity and temperature was used to define a mean temperature profile. Since measurements of wall temperature showed that the mean wall temperature during a 10-15 second run was equal to stagnation temperature, this relationship is simplified to:

$$T = T_{t_e} - (T_{t_e} - T_e)\left(\frac{u}{u_e}\right)^2 \tag{A1}$$

Using the normal boundary layer assumptions $p = p(x)$ and the perfect gas equation of state, the following expression for density profile is obtained:

$$\frac{\rho}{\rho_e} = \frac{T_e}{T_{t_e} - (T_{t_e} - T_e)\left(\frac{u}{u_e}\right)^2} \tag{A2}$$

From the velocity and density profiles, the turbulent boundary layer thickness, displacement thickness, and momentum thickness were evaluated by use of the following equations:

$$y = \delta \text{ when } u/u_e = .99 \tag{A3}$$

$$\delta^* = \int_o^\infty (1 - \rho u/\rho_e u_e)\, dy \tag{A4}$$

$$\theta = \int_o^\infty \frac{\rho u}{\rho_e u_e}\left(1 - \frac{u}{u_e}\right) dy \tag{A5}$$

$$H = \delta^*/\theta \tag{A6}$$

Values of skin friction coefficient were determined by use of Eckert's reference enthalpy method (ref. 36) which relates the compressible flow skin friction coefficient to the incompressible coefficient by the equation

$$\frac{c_f}{c_{f_i}} = \left(\frac{\rho'}{\rho_\infty}\right)^{5/6} \left(\frac{\mu'}{\mu_\infty}\right)^{1/6} \tag{A7}$$

where the incompressible coefficient is given by Falkner (ref. 37)

$$\frac{c_{f_i}}{2} = \frac{0.006534}{R_\theta^{1/6}} \tag{A8}$$

In the above,

$$\frac{\rho'}{\rho_\infty} = \frac{T_\infty}{T'} = \frac{T_\infty}{\frac{T_w + T_\infty}{2} + .22\, r\, \frac{\gamma-1}{2} M_\infty^2 T_\infty} \tag{A9}$$

and

$$\frac{\mu'}{\mu_\infty} = \left(\frac{T'}{T_\infty}\right)^{3/2} \frac{T_\infty + 200}{T' + 200} \tag{A10}$$

The turbulent recovery factor is

$$r = (Pr')^{1/3} \tag{A11}$$

Values of δ, δ^*, θ, c_f, c_{fi} and τ_o based on the above relations are tabulated in Table 1 for each Mach number. All measurements of velocity profiles were limited to clear-tunnel configurations at a station 4 inches upstream of the sidewall center line, i.e., no measurements were attempted downstream of roughness elements or shock boundary interaction regions.

APPENDIX B

INFORMATION ON ACOUSTIC INSTRUMENTATION AND PROCEDURES

The acoustic transducer used to measure boundary layer pressure fluctuations was the Bruel and Kjaer Model 4136 condenser microphone. With the protective grid removed, the microphone can be mounted in a flat plate with the outer surface of the diaphragm flush with the plate surface.

The microphones were installed utilizing compressed O-rings to hold them in place and also to provide an adequate seal. Using an opaque thin straight edge in conjunction with a concentrated light source, it was possible to align the surface of the diaphragm with the surface of the plate to within $\pm$ 0.0005 inch.

A small annular gap existed between the edge of the diaphragm and the plate. In the earlier wind tunnel runs, lacquer was used as a filler to provide a completely smooth surface from the edge of the plate mounting hole to the diaphragm. Identical wind tunnel runs were made with and without the gap filled with lacquer. Because the noise spectra measured without the lacquer were indistinguishable from those measured with the lacquer, the use of lacquer was discarded in the later wind tunnel runs.

In the microphone installation, provision was made for static pressure equalization between the front and the back of the microphone diaphragm by means of a small air passage. In order that equilibrium be maintained across the diaphragm, it was necessary to seal carefully all possible leaks to the outside of the wind tunnel. After some of the earlier wind tunnel runs, it was discovered that some of these seals may not have been airtight, thereby leading to a static pressure differential across the diaphragm and a consequent reduction in microphone sensitivity. Data affected by the apparent lack of pressure equalization are considered suspect and are not presented in this report.

A special low-noise cable adapter developed by Bolt Beranek and Newman, Inc. was used to connect the microphone output to the input of a suitable cathode follower. The cable adapter serves as a mechanical isolator between the microphone and the cathode follower. When the microphone is subjected to 1 g rms, the equivalent sound pressure level at the cathode follower output is 85 db re 0.0002 microbar. By comparison, the use of a standard rigid adapter can exhibit an equivalent sound pressure level as high as 145 db under similar conditions. The special adapter introduces an overall loss in sensitivity which is 3 db

greater than the standard rigid adapter. The microphone sensitivity with the special adapter is -83 db re 1 volt/microbar measured at the cathode follower output.

During several of the tests, the signal from a calibrated accelerometer fastened directly to the test plate (see figure 7) was recorded, to permit calculation of the vibration-induced signal of the acoustic transducer. Acceleration measurements at a Mach number of 0.86 indicated that the equivalent sound pressure level resulting from microphone vibration sensitivity was a maximum of 65 db, in the octave band centered at 500 cps. A review of the acoustic and vibration data indicated a minimal signal-to-noise ratio of 45 db was due to vibration sensitivity. Thus there was no need for vibration isolation of the instrumented insert from the remainder of the tunnel.

For linear reproduction of signal voltages in the desired amplitude and frequency range, the total load impedance seen by the cathode follower output must be greater than 5×10^4 ohms. For this reason, cables utilized in this part of the system were kept under a maximum length of 10 feet.

The microphones were acoustically calibrated by means of a Bruel and Kjaer Model 4220 pistonphone used in conjunction with a BBN acoustic coupler. This combination provided a reference sound pressure level of 128 db, accurate to $\pm$ 0.2 db, at 250 cps. Calibration levels were noted and recorded on tape at periodic intervals throughout the series of noise measurements.

As mentioned in the body of this report, during the first series of tests the data signals were recorded in the wide band FM mode of a Precision Instruments tape recorder using a 54 kcps carrier frequency, $\pm$ 40% record bandedge, and 60 in/sec tape speed. During the final series of tests, the signals were direct recorded on a Mincom tape recorder at 60 in/sec tape speed.

System record and playback corrections were determined by recording sinusoidal signals on the data channels and playing these signals back through the data processing system. This process was of particular importance in the reduction of the direct record data since in this case the tape recorder playback amplifier with its playback head compensating network was circumvented to reduce electrical noise. Also, the graphic level recorder, used as a read-out device for the first series of data, does not give a true rms output for a random noise input. The level recorder was suitably calibrated to generate an appropriate correction to adjust the readings to true rms values. Typical values of the system corrections are given in Table 4.

A sample of the system noise floor was also recorded, analyzed, and compared with the data. No data that are limited by the system noise floor have been presented in this report. At reduced ambient pressures, the Bruel and Kjaer Model 4136 condenser microphone exhibits a resonance around 48 kcps. During the wind tunnel tests the microphones were exposed to static pressures over the range of 0.5 to 18 lbs/in^2 absolute. It was necessary, therefore, to calibrate the microphone over this range of pressures, and apply a correction for the changes in microphone sensitivity. The pressure sensitivity of the condenser microphones was obtained by the use of a Bruel and Kjar Model 4142 electrostatic driver. The microphone and driver were placed in a sealed chamber, and the microphone was calibrated over a range of static pressure from 0.1 psia to 20 psia. A sinusoidal signal was used to obtain the frequency response from 0.1 kcps to 100 kcps, and a constant-spectrum-level random noise signal was used to obtain the frequency response in the three octave bands centered at 16, 31.5, and 63 kcps. A typical set of response curves generated with the sinusoidal excitation is given in Figure 41, and a typical set of corrections for one microphone is given in Table 4.

The acoustic data were also corrected for the finite size of the microphone diaphragm. Like the pressure sensitivity correction mentioned above, the finite size correction was of importance only in the octave bands above 8 kcps. A set of the finite size corrections for a particular Mach number is also given in Table 4.

The finite size correction is based on the work of Corcos (ref. 25). He has calculated the reduction in pressure fluctuation spectrum that is due to the finite dimension of the measuring transducer. The correction is expressible in terms of the dimensionless quantity of fL/u_c, where f is frequency, L is a characteristic dimension of a uniformly sensitive transducer, and u_c is the turbulence convection speed. For convenience we have replotted Corcos' results for a round transducer in Figure 42, where it has been assumed that the convection velocity, u_c, is 0.8 of the free stream velocity, u_∞. This result is approximately valid through the entire frequency range of concern in the present investigation. Corrections based on Figure 42 have been applied to all of the data in the present test. An effective transducer diameter of 0.13 inch has been used to generate these corrections. The justification for this choice of diameter is given in Appendix C.

The Corcos length correction utilizes measured values of the one-dimensional longitudinal and lateral cross-spectral densities. In order to determine whether the Corcos correction, which is based on subsonic data, is valid for supersonic data also, it is of interest to inquire whether the eddy size at supersonic Mach numbers is the same (on a non-dimensional basis) as the eddy size at subsonic Mach numbers.

Comparison of Figure 14b of Kisler and Chen (ref. 14) with Figure 11 of Willmarth (1962) (ref. 38) indicates that the eddy size in supersonic flow is considerably larger than in subsonic flow. In this case the Corcos correction would be too large for supersonic flow because less cancellation would occur when a larger eddy passes over the transducer face than when a smaller one passes. A quantitative evaluation of this reduction requires the measurement of cross-spectral densities in supersonic flow.

The overall uncertainty of the measurements is $\pm$ 1 db at center-band frequencies of 16 kcps and below and $\pm$ 3 db in the 31.5 kcps band. The data in the 63 kcps band is questionable and its accuracy is not easily determinable.

APPENDIX C

ESTIMATE OF THE EFFECTIVE DIAMETER OF THE CONDENSER MICROPHONE

The Bruel and Kjaer Model 4136 condenser microphone used to measure the boundary layer pressure fluctuations has an overall nominal diameter of 0.250 inch. The diaphragm of this microphone is essentially a stretched and clamped membrane with a geometric diameter of 0.170 inch. As would be expected with a clamped membrane, the microphone diaphragm is more sensitive at its center than at its edges. The finite size correction (see Appendix B) assumes that the microphone diaphragm has uniform sensitivity. Since our microphone does not have uniform sensitivity, it is necessary to determine the diameter of an equivalent microphone in order to apply the finite size correction. It is thus necessary for us to formulate a definition of equivalence and then to calculate the diameter of an equivalent uniformly sensitive microphone.

The problem of the microphone diameter becomes of importance only when the wave length of the sound measured becomes comparable to the microphone diameter. For a grazing incidence plane progressive sound field, a wavelength will exist for which the surface integral of pressure times diaphragm sensitivity will be zero; that is, the microphone output signal will be zero as the wave propagates by the diaphragm. It is proposed that the diameters of two transducers be defined as equivalent when at the same frequency they both give zero output signal for a plane progressive sound wave of grazing incidence.

We shall assume that the diaphragm of our microphone has a circular boundary of diameter D with its center at the origin of a cartesian reference frame. We shall suppose that we have a plane progressive wave of wavelength λ traveling at grazing incidence across the diaphragm in the direction of the ordinate and that the sensitivity of the diaphragm is solely a function of the distance from its center. Our job then is to evaluate the following integral:

$$V = \int_A P_o \cos\left[\left(\omega t - \frac{2\pi y}{\lambda}\right) \sigma(R)\right] da$$

$$V = \int_A P_o \, \sigma(R) \left[\cos \omega t \cos \frac{2\pi y}{\lambda} + \sin \omega t \sin \frac{2\pi y}{\lambda}\right] da$$

The second term is an odd function and thus clearly the integral is zero.

$$V = \int_A P_o \, \sigma(R) \cos \omega t \cos \frac{2\pi y}{\lambda} \, da$$

Thus we need determine D so that

$$0 = \int_A \sigma(R) \cos \frac{2\pi y}{\lambda} \, da$$

We introduce polar coordinates, R and ψ ,

$$0 = \int_0^{D/2} \int_0^{2\pi} \sigma(R) \cos \left(\frac{2\pi R}{\lambda} \sin \psi\right) R \, dR \, d\psi$$

$$0 = \int_0^{D/2} \int_0^{2\pi} \sigma(R) \left[J_0 \left(\frac{2\pi R}{\lambda} + 2J_2 \left(\frac{2\pi R}{\lambda}\right) \cos 2\psi + \ldots \right] R \, dR \, d\psi \right.$$

The integrals with respect to ψ of all of the terms except the first are zero. Thus the above becomes

$$0 = \int_0^{D/2} \sigma(R) \; J_0 \left(\frac{2\pi R}{\lambda}\right) \; R \, dR \qquad (C1)$$

In order to evaluate the sensitivity function σ (R) for the Bruel and Kjaer microphone type 4136, we make use of measurements made of this quantity on a model of a large Bruel and Kjaer microphone type 4131. Bruel and Kjaer show that just below the resonant frequency of the microphone the sensitivity near the edge of the diaphragm is down 20 decibels below the sensitivity at the center (ref. 39) Using this information we propose the following empirical formula for $\sigma(R)$.

$$\sigma(R) = \sigma_0 \left[1 - b \left(\frac{R}{D/2}\right)^2\right], \; b = 0.9 \qquad (C2)$$

If we substitute equation (C2) in equation (C1) and integrate we obtain

$$0 = J_1 \left(\frac{\pi D}{\lambda}\right) \left[(1 - b) \left(\frac{\pi D}{\lambda}\right)^2 + 4b\right] - 2b \left(\frac{\pi D}{\lambda}\right) J_0 \left(\frac{\pi D}{\lambda}\right) \qquad (C3)$$

If we substitute the empirical value for b of 0.9 and solve for the first significant root of equation (C3) we obtain

$$\frac{\pi D}{\lambda} = 4.89 \qquad (C4)$$

In order to determine the diameter of a uniformly sensitive equivalent diaphragm we set b = 0 in equation (C3) and obtain

$$J_1 \left(\frac{\pi D_e}{\lambda}\right) = 0 \qquad (C5)$$

The first significant root of equation (C5) gives

$$\frac{\pi D_e}{\lambda} = 3.83 \qquad (C6)$$

We determine the equivalent diameter from equations (C4) and (C6).

$$D_e = .170 \times \frac{3.83}{4.89} = .133 \text{ inches}$$

REFERENCES

1. Corcos, G. M. and Liepmann, H. W.: On the Contribution of Turbulent Boundary Layers to the Noise Inside a Fuselage, NACA Technical Memorandum 1420, December, 1956.

2. Staff of Langley Research Center: The Supersonic Transport - A Technical Summary, NASA Technical Note D-423, June, 1960.

3. Curle, N.: The Influence of Solid Boundaries Upon Aerodynamic Sound, Proc. Royal Society, Series A, Vol. 231, No. 1187, 1955.

4. Phillips, O. M.: Surface Noise from a Plane Turbulent Boundary Layer, British Aeronautical Research Council 16,963-FM 2099, August, 1954.

5. Phillips, O. M.: On the Aerodynamic Surface Noise from a Plane Turbulent Boundary Layer, Proc. Royal Society, Series A, Vol. 234, No. 1198, Jan., 1956.

6. Ribner, H. S.: Boundary Layer - Induced Noise in the Interior of Aircraft, University of Toronto Institute of Aerophysics, Report No. 37, April, 1959.

7. Kraichnan, R. H.: Noise Transmission from Boundary Layer Pressure Fluctuations, Journal of Acoustical Society of America, Vol. 29, No. 1, January, 1957.

8. Dyer, I.: Response of Plates to a Decaying and Convecting Random Pressure Field, Journal of Acoustical Society of America, Vol. 31, No. 7, July, 1959.

9. Tack, D. H. and Lambert, R. F.: Response of Bars and Plates to Boundary Layer Turbulence, Journal Aerospace Sciences, Vol. 29, No. 3, March, 1962.

10. Lyon, R. H.: Response of Strings to Random Noise Fields, Journal Acoustical Society of America, Vol. 28, No. 3 , 1956.

11. Willmarth, W. W.: Space-Time Correlations and Spectra of Wall Pressure in a Turbulent Boundary Layer, NASA Memorandum 3-17-59W, March, 1959.

12. Harrison, M.: Pressure Fluctuations on the Wall Adjacent to a Turbulent Boundary Layer, David Taylor Model Basin Report 1260, December, 1958.

13. Skudrzyk, E. J. and Haddle, G. P.: Noise Production in a Turbulent Boundary Layer by Smooth and Rough Surfaces, Journal Acoustical Society of America, Vol. 32, No. 1, Jan., 1960.

14. Kistler, A. L. and Chen, W. S.: The Fluctuating Pressure Field in a Supersonic Turbulent Boundary Layer, Jet Propulsion Laboratory Technical Report, No. 32-277, August, 1962.

15. Williams, D. J. M.: Measurements of the Surface Pressure Fluctuations in a Turbulent Boundary Layer in Air at Supersonic Speeds, University of Southampton, AASU Report 162, Dec., 1960.

16. Von Gierke, H. E.: Types of Pressure Fields of Interest in Acoustical Fatigue Problems, WADC - University of Minnesota Conference on Acoustical Fatigue, WADC ASD TR 59-676, March, 1961.

17. Mull, H. R. and Algranti, J. S.: Preliminary Flight Survey of Aerodynamic Noise on an Airplane Wing, NACA RME55K07, March, 1956.

18. Mull, H. R. and Algranti, J. S.: Flight Measurements of Wall Pressure Fluctuations and Boundary Layer Turbulence, NASA TN D-280, Oct., 1960.

19. McLeod, N. J. and Jordon, G. H.: Preliminary Flight Survey of Fuselage and Boundary Layer Sound Pressure Levels, NACA RM #58B11, May, 1958.

20. Hilton, D. A., Mayes, W. H., and Hubbard, H. H.: Noise Considerations for Manned Re-entry Vehicles, NASA TN D-450, Sept., 1960.

21. Shattuck, R. D.: Sound Pressures and Correlations of Noise on the Fuselage of a Jet Aircraft in Flight, NASA TN D-1086, August, 1961.

22. McLeod, N. J.: Flight-Determined Aerodynamic Noise Environment of an Airplane Nose Cone up to a Mach Number of 2, NASA TN D-1160, March, 1962.

23. Murphy, J. S.: Pressure Fluctuations in a Blowdown Wind Tunnel, Journal of Aeronautical Sciences, Vol. 26, No. 1, Jan., 1959.

24. Schlichting, Hermann: Boundary Layer Theory, McGraw-Hill Book Co., Inc., 1955.

25. Corcos, G. M.: Resolution of Pressure in Turbulence, J. Acoust. Soc. Am., Vol. 35, No. 2, pp. 192-199, February, 1963.

26. Bull, M. K. and Willis, J. L.: Some Results of Experimental Investigations of the Surface Pressure Field Due to a Turbulent Boundary Layer, Aeronautical Systems Division TDR-62-425, August, 1962.

27. Ribner, H. S.: Shock-Turbulence Interaction and the Generation of Noise, NACA TN 3255, July, 1954.

28. Liepmann, H. W., Roshko, A., and Dhawan, S.: On Reflection of Shock Waves from Boundary Layers, NACA Rep. 1100, 1952.

29. Vas, I. E. and Bogdonoff, S. M.: Interaction of a Shock Wave with a Turbulent Boundary Layer at M = 3.85. Princeton Univ. Dept. of Aero. Engr. Rep. 294, April 1955.

30. Chapman, D. R.: An Analysis of Base Pressures at Supersonic Velocities and Comparison with Experiment. NACA Report 1051, 1951.

31. Moeckel, W. E.: Flow Separation Ahead of Blunt Bodies at Supersonic Speeds, NACA TN 2418, 1951.

32. Chapman, D. R., Kuehn, D. M., and Larson, H. K.: Investigation of Separated Flows in Supersonic and Subsonic Streams with Emphasis on the Effect of Transition. NACA Report 1356, 1958.

33. Sterrett, J. R., and Emery, J. C.: Extension of Boundary-Layer-Separation Criteria to a Mach Number of 6.5 Utilizing Flat Plates with Foreward-Facing Steps, NASA TN D-618, December 1960.

34. Smith, R. R.: Investigation of Flow Variables Over a Series of Rearward Facing Stepped Flat Plates at a Nominal Mach Number of 4.15, Rep. ASD-TDR-63-131, April 1963.

35. Trisonic One-Foot Wind Tunnel - Description of the Facility and Provisions for Testing, Douglas Aircraft Co., Inc. Report ES 29278, January 1959.

36. Eckert, E. R. G.: Engineering Relations for Friction and Heat Transfer to Surfaces in High Velocity Flow, Jour. Aero. Sci., Vol. 22, No. 8, pp. 585-587, August 1955.

37. Falkner, V. M.: The Resistance of a Smooth Flat Plate with Turbulent Boundary Layer, Aircraft Engineering, Vol. 15, p. 63, 1943.

38. Willmarth, W. W. and Wooldridge, C. E.: Measurements of the Fluctuating Pressure at the Wall Beneath a Thick Turbulent Boundary Layer, University of Michigan Technical Report 02920-1-T, April 1962.

39. Bruel and Kjaer Technical Review, April 1959, p. 6.

TABLE 1

BOUNDARY LAYER PROPERTIES OF THE TRISONIC ONE-FOOT TUNNEL

Mach No.	u_∞ (fps)	q (psi)	δ (in.)	δ^* (in.)	θ (in.)	H	R_θ	C_{f_i}	C_f/C_{f_i}	C_f	τ_o (psi)
0.30	326	1.21	0.580	0.077	0.055	1.40	14,000	0.0028	0.985	0.0027	0.0033
0.43	466	2.28	0.500	0.057	0.041	1.40	13,000	0.0028	0.982	0.0027	0.0062
0.59	631	3.90	0.395	0.048	0.032	1.50	13,300	0.0028	0.967	0.0027	0.0105
0.86	885	6.42	0.350	0.044	0.028	1.57	14,400	0.0026	0.934	0.0026	0.0164
1.41	1320	9.74	0.354	0.068	0.028	2.42	17,400	0.0027	0.840	0.0022	0.0218
1.80	1535	10.47	0.378	0.090	0.031	2.90	21,200	0.0026	0.762	0.0020	0.0204
2.52	1860	11.50	0.492	0.151	0.035	4.31	28,400	0.0024	0.636	0.0016	0.0179
3.46	2120	12.20	0.726	0.306	0.044	6.95	49,000	0.0022	0.500	0.0011	0.0136

TABLE 2

BOUNDARY LAYER PROPERTIES AT MIC. POSITION #1

(CALCULATED FROM DATA AT MIC. POSITION #4)

M	u_∞ (ft/sec)	q (lb/in^2)	δ (in.)	δ^* (in.)	θ (in.)	H	R_θ	C_{f_i}	C_f/C_{f_i}	C_f	τ_o (lb/in^2)
0.30	326	1.21	0.522	0.070	0.050	1.40	12,700	0.0027	0.985	0.0027	0.0032
0.43	466	2.28	0.440	0.050	0.036	1.40	11,300	0.0028	0.982	0.0027	0.0062
0.59	631	3.90	0.333	0.040	0.027	1.50	11,200	0.0028	0.967	0.0027	0.0104
0.86	885	6.42	0.284	0.036	0.023	1.57	11,700	0.0028	0.934	0.0026	0.0165
1.41	1320	9.74	0.301	0.058	0.024	2.42	14,800	0.0026	0.840	0.0022	0.0216
1.80	1535	10.47	0.334	0.080	0.027	2.90	18,750	0.0025	0.762	0.0019	0.0202
2.52	1860	11.50	0.452	0.139	0.032	4.31	26,100	0.0024	0.636	0.0015	0.0176
3.46	2120	12.20	0.692	0.292	0.042	6.95	46,600	0.0022	0.500	0.0011	0.0133

where $\frac{d\theta}{dx} = \left(\frac{C_f}{C_{f_i}}\right)\left(\frac{C_{f_i}}{2}\right) = K_M\, \theta^{-1/6}$

Note: At M = 3.46

Mic. Loc. #4

Measured θ = 0.044

" δ^* = 0.306

" δ = 0.726

Mic Loc. #7

Measured θ = 0.048

" δ^* = 0.335

" δ = 0.794

Calculated θ = 0.046

" δ^* = 0.320

" δ = 0.759

TABLE 3

INFLUENCE OF VARIOUS DISTURBANCES ON

WALL PRESSURE FLUCTUATION LEVEL AT M = 3.46

$R_\theta = 50{,}000$

Type of Disturbance	$\frac{\sqrt{\widetilde{\Delta p}_T^2}}{q} \times 10^3$	$\frac{\sqrt{\widetilde{\Delta p}_T^2}}{\tau_o}$
No disturbance	1.8	1.7
$1/2^\circ$ Deflection Shock	2.7	2.4
2.5° Deflection Shock	4.3	3.9
5° Deflection Shock	9.6	8.7
7.5° Deflection Shock	23.3	21.2
Normal Shock	37.2	33.8
dP/dx = -.19 psi/inch	10.7	9.7
dP/dx = + .96 psi/inch	1.8	1.7
t = .125" Downstream	12.0	10.9
t = .125" Upstream	10.5	9.5

TABLE 4

EXAMPLE OF CORRECTIONS APPLIED TO RAW DATA

Positive numbers represent additions to raw data values.

Octave Band Center Frequency, kcps	Typical direct record corrections*			
	WBFM System Corrections, All Data, db	System Corrections, db	Pressure-dependence Corrections, db	Finite Size Corrections db
0.016	+6		0	0
0.0315	+4		0	0
0.063	+3.5		0	0
0.125	3.5	5.5	0	0
0.250	2.5	0.0	0	0
0.500	2.5	-5.0	0	0
1.00	1.5	-9.5	0	0
2.00	1.0	-14.5	0	0
4.00	0.5	-20.0	0	0
8.00	0.5	-23.0	0	0
16.00		-25.0	1	1
31.5		-22.0	-7	2
63.0		-18.5	-10	4

*microphone serial number 77315, wall static pressure 2.58 psia, data track 2-loop track 1.

FIGURE 3 – DAL TRISONIC ONE-FOOT TUNNEL DESIGN FEATURES

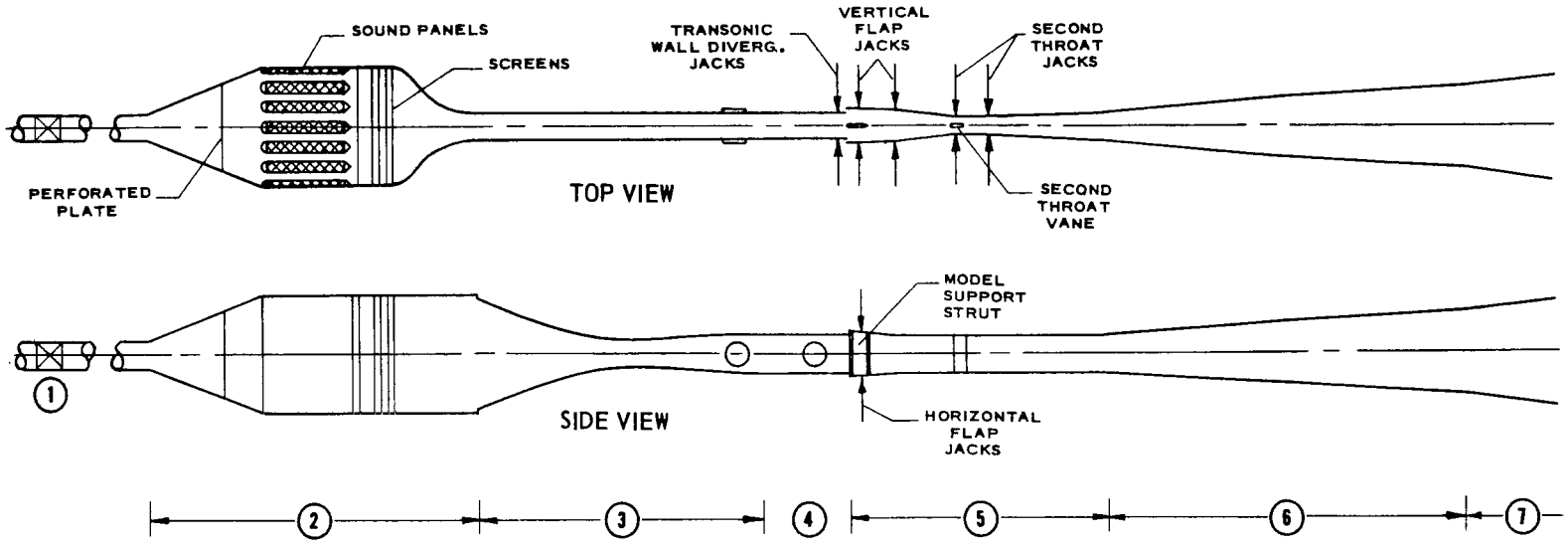

(1) CONTROL VALVE Valve motion controlled during run by pneumatic controller to maintain constant pressure in stilling chamber.

(2) STILLING CHAMBER Perforated plate, 1/4" thick with backup structure, 1/4" holes distributed uniformly. 5 screens consisting of 1-20 mesh, 36% open 4-40 mesh, 51.8% open. 5 internal sound panels reducing maximum pressure fluctuation to ± 0.5% of stilling chamber pressure. Contraction ratio to test section (M_∞ 1.0) is 11.5.

(3) NOZZLE SECTION Removable blocks M_∞ 1.0, 1.4, 1.6, 1.8, 2.5, 3.5, 10" window in supersonic section. Schlieren system.

(4) TRANSONIC 4 walls perforated, 22% open, holes normal to wall. Adjustable divergence on side walls ± 2°. Section removable and downstream circuit moves up. Schlieren system.

(5) MODEL SUPPORT, FLAP & VARIABLE DIFFUSER Variable strut - maximum pitch ± 30°. Horizontal & vertical flaps movable to give variable gap for flow reentry and variable area around strut. Second throat controls M_∞ in range 0-1.2. Variable M_∞ during run possible by rotating throat vane. Variable settings in diffuser improves run time over fixed design.

(6) FIXED DIFFUSER 7° total angle diffuser. Transition from rectangular to circular section.

(7) MUFFLER Sound panels. Flow exhausted to atmosphere.

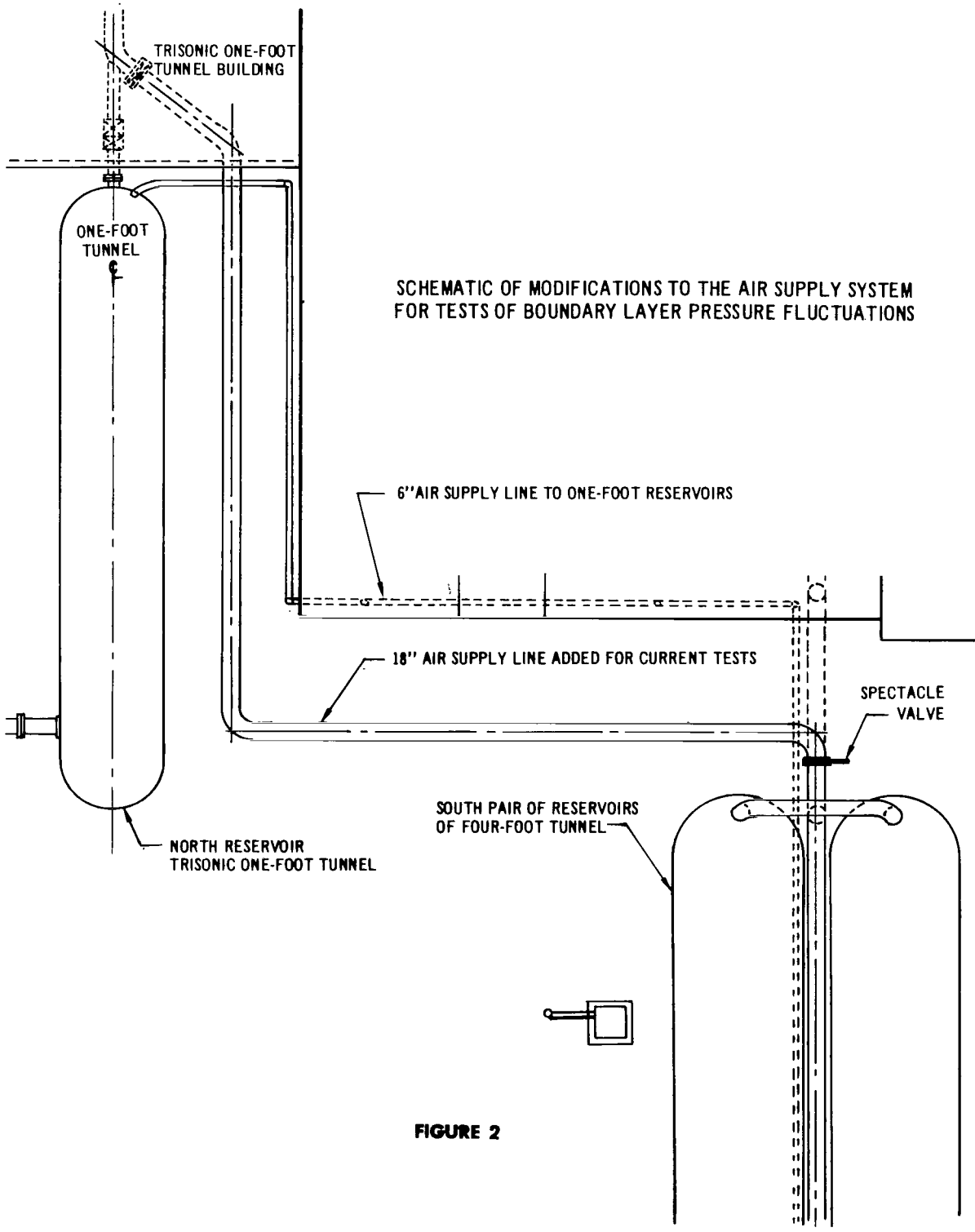
TRISONIC ONE-FOOT
TUNNEL BUILDING
ONE-FOOT
TUNNEL
SCHEMATIC OF MODIFICATIONS TO THE AIR SUPPLY SYSTEM
FOR TESTS OF BOUNDARY LAYER PRESSURE FLUCTUATIONS
6"AIR SUPPLY LINE TO ONE-FOOT RESERVOIRS
18" AIR SUPPLY LINE ADDED FOR CURRENT TESTS
SPECTACLE
VALVE
SOUTH PAIR OF RESERVOIRS
OF FOUR-FOOT TUNNEL
NORTH RESERVOIR
TRISONIC ONE-FOOT TUNNEL

FIGURE 2

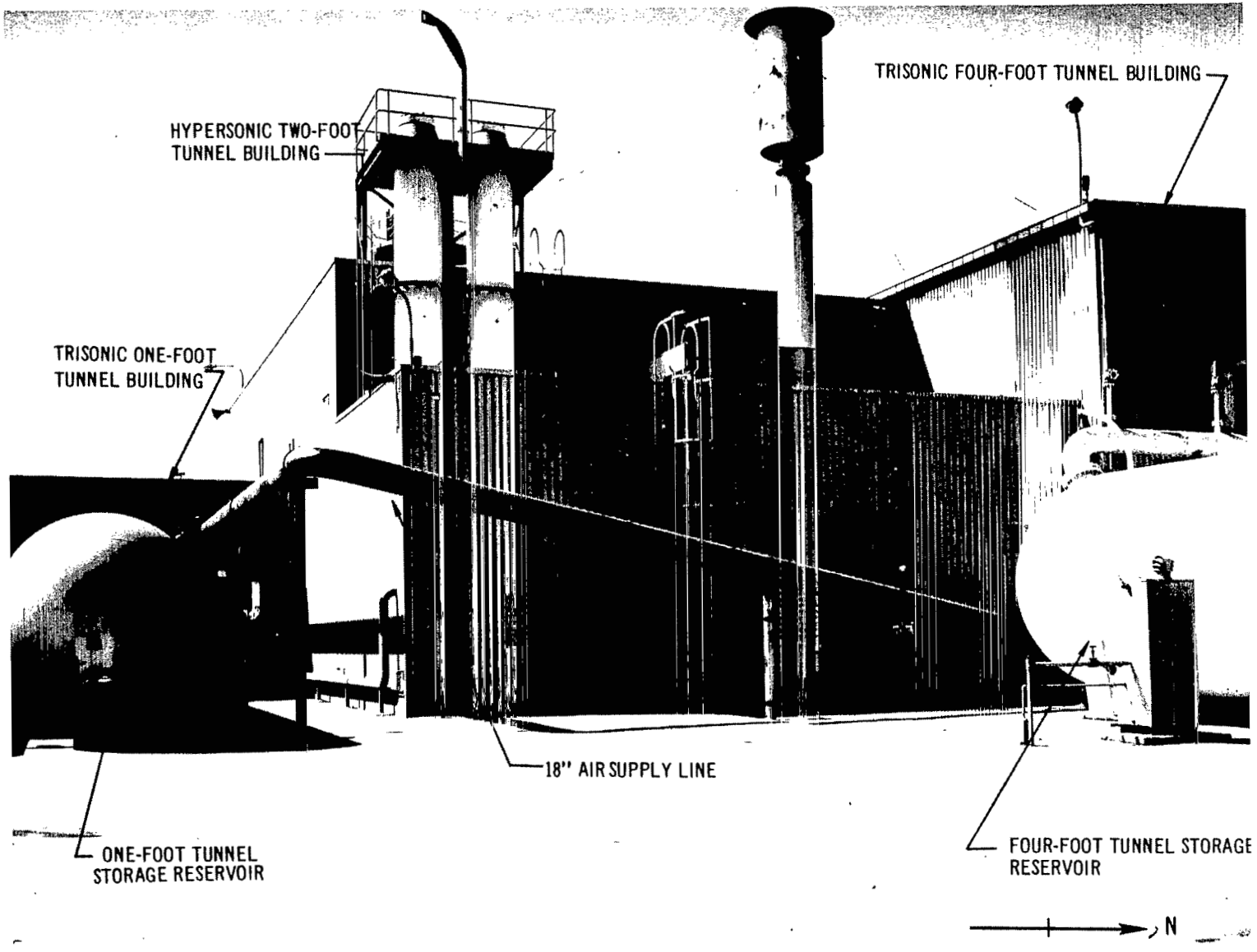

FIGURE 3 PHOTOGRAPH OF MODIFICATIONS TO THE AIR SUPPLY SYSTEM

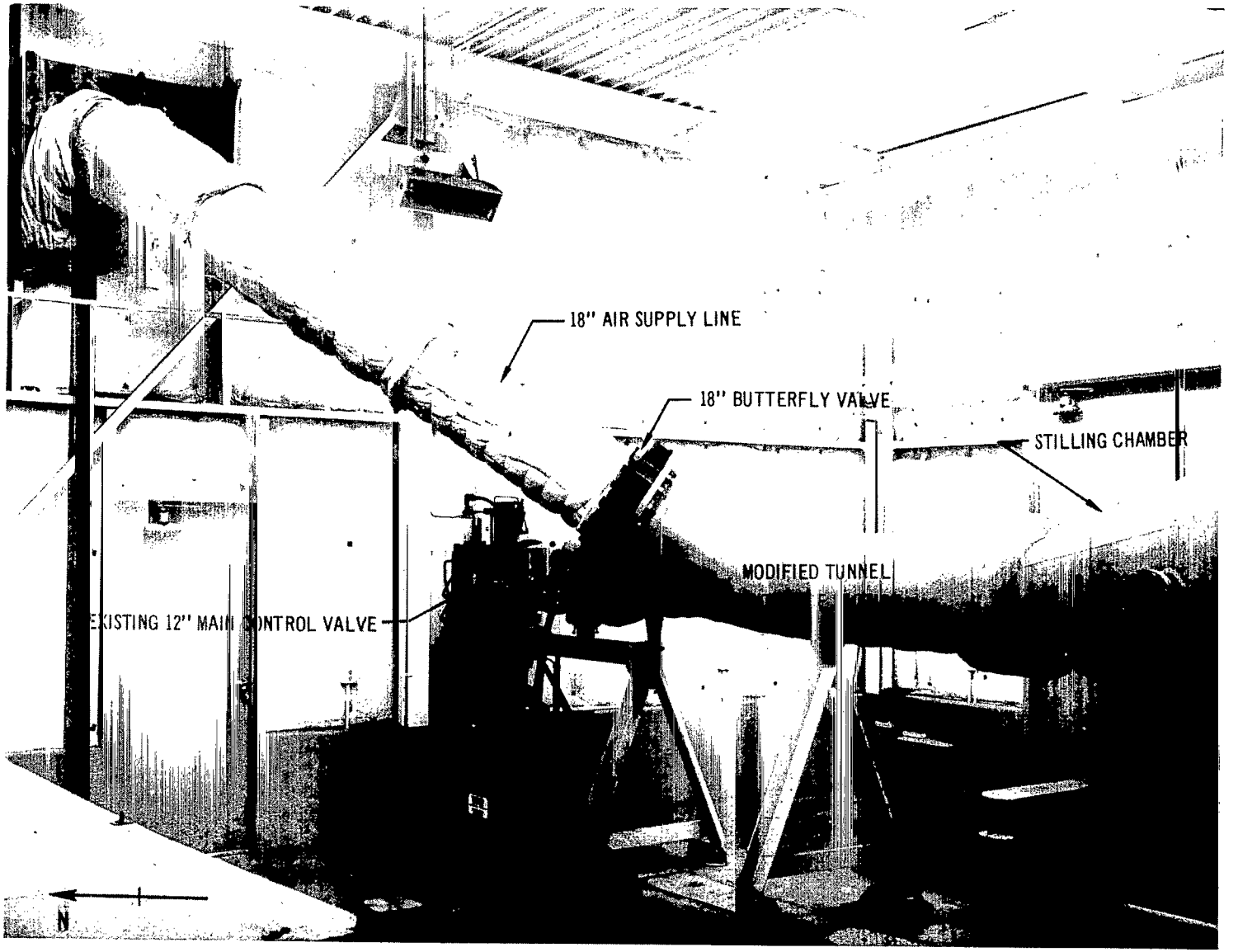

FIGURE 4 PHOTOGRAPH OF MODIFICATIONS TO ONE-FOOT TUNNEL ENTRANCE

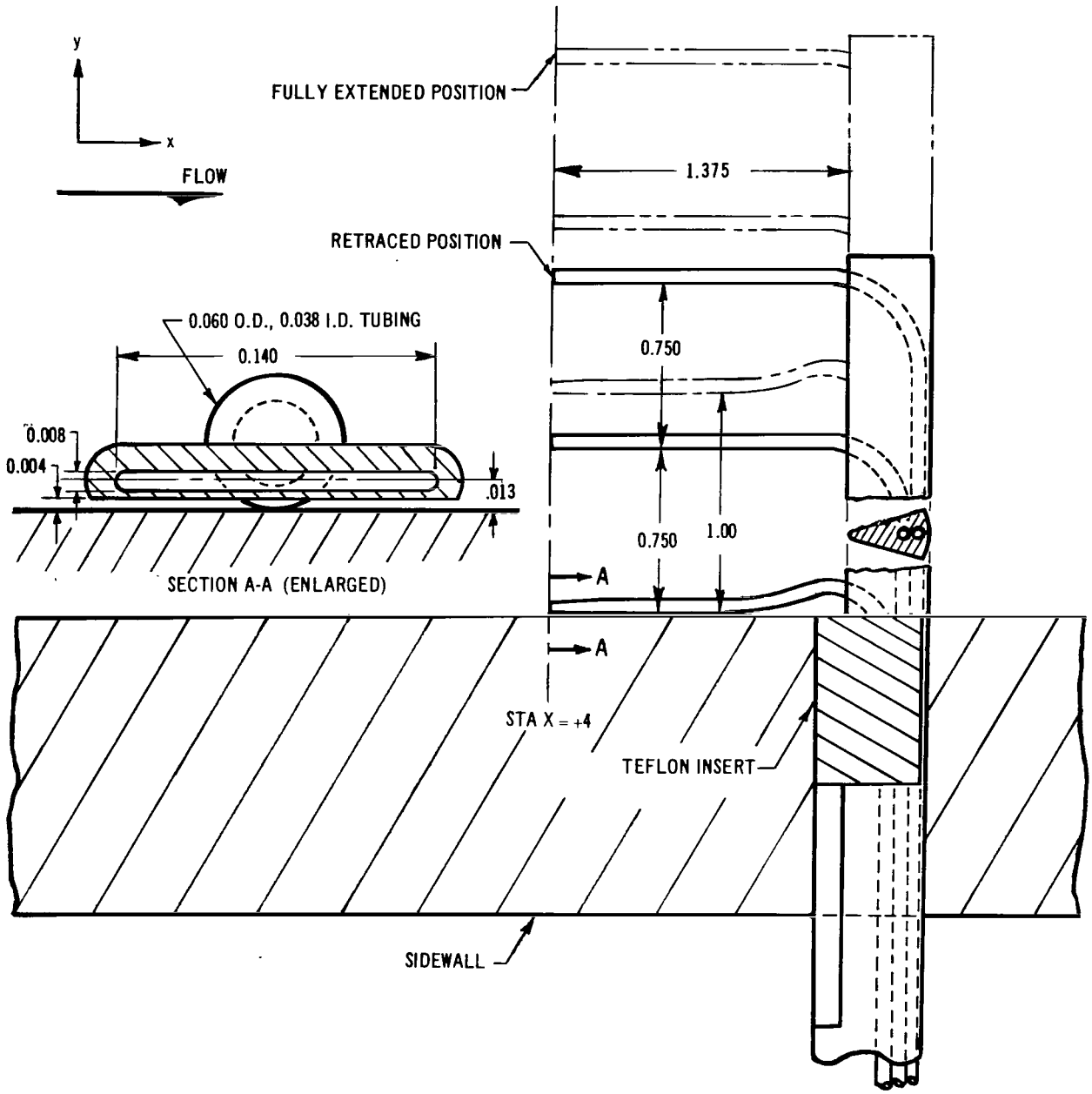

FIGURE 5 SKETCH OF BOUNDARY LAYER TOTAL HEAD PROBE

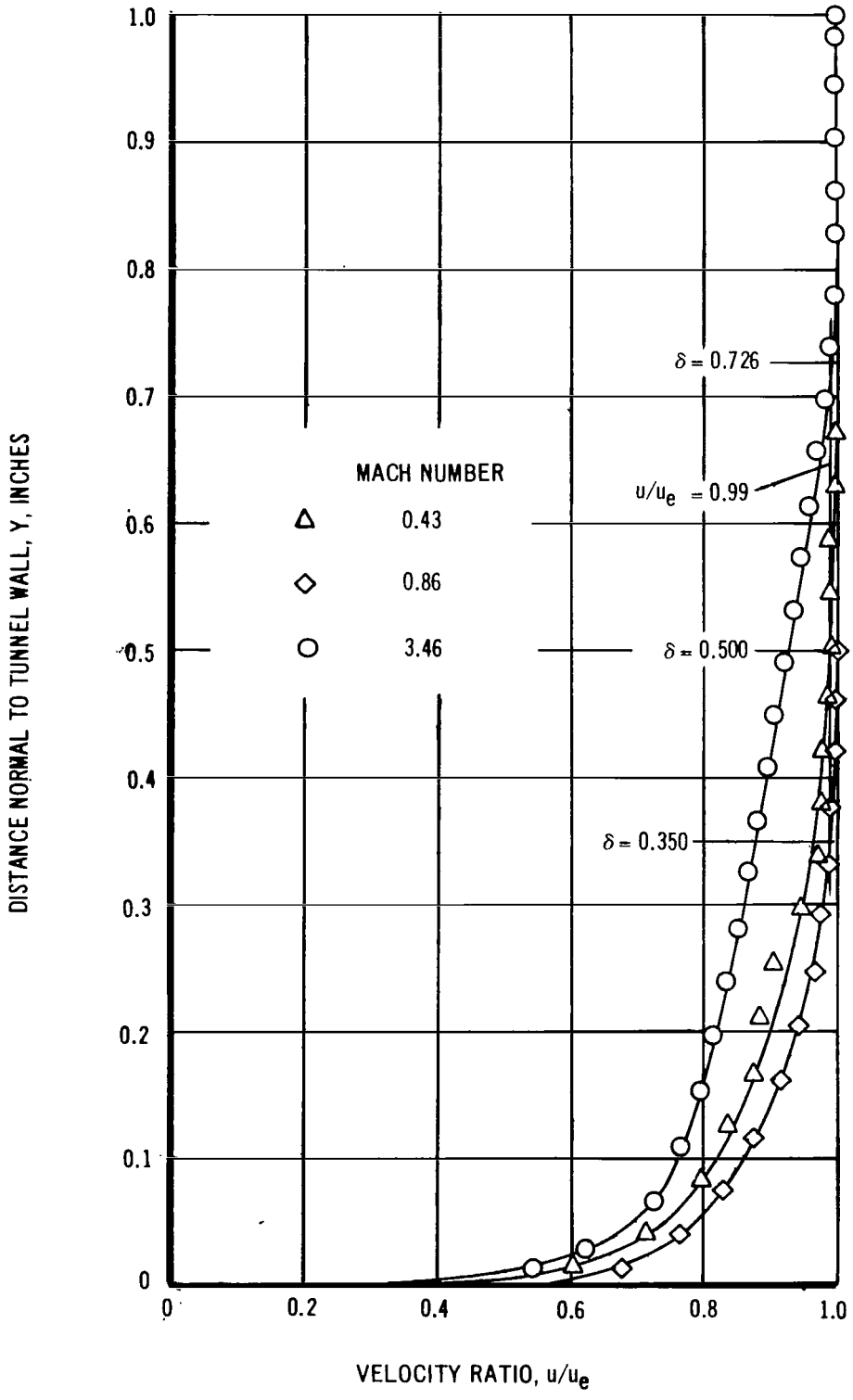

FIGURE 6 – TYPICAL BOUNDARY LAYER VELOCITY PROFILES

NOISE PLATE SHOWING POSSIBLE LOCATIONS OF MICROPHONES AND ACCELEROMETER

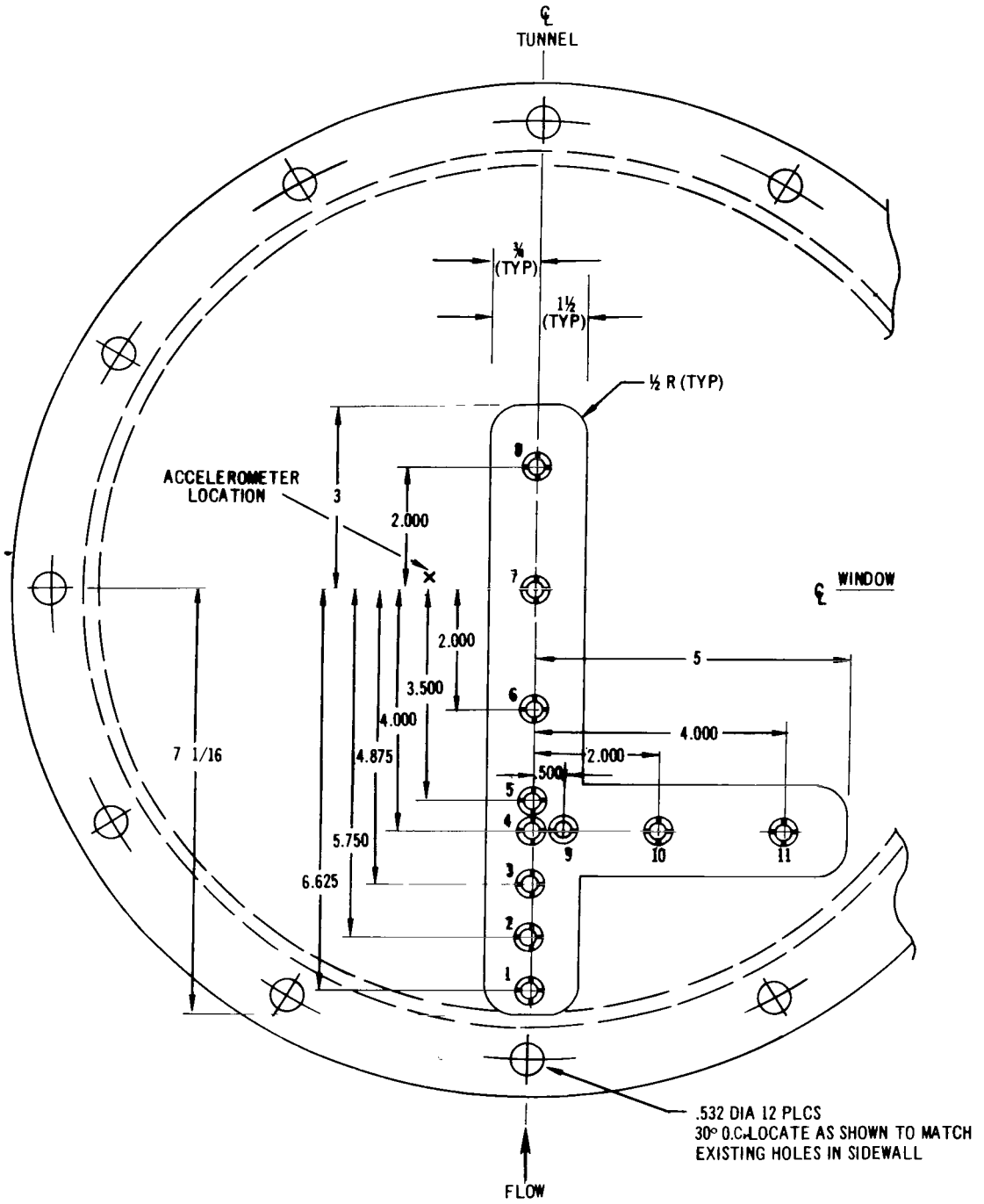

FIGURE 7

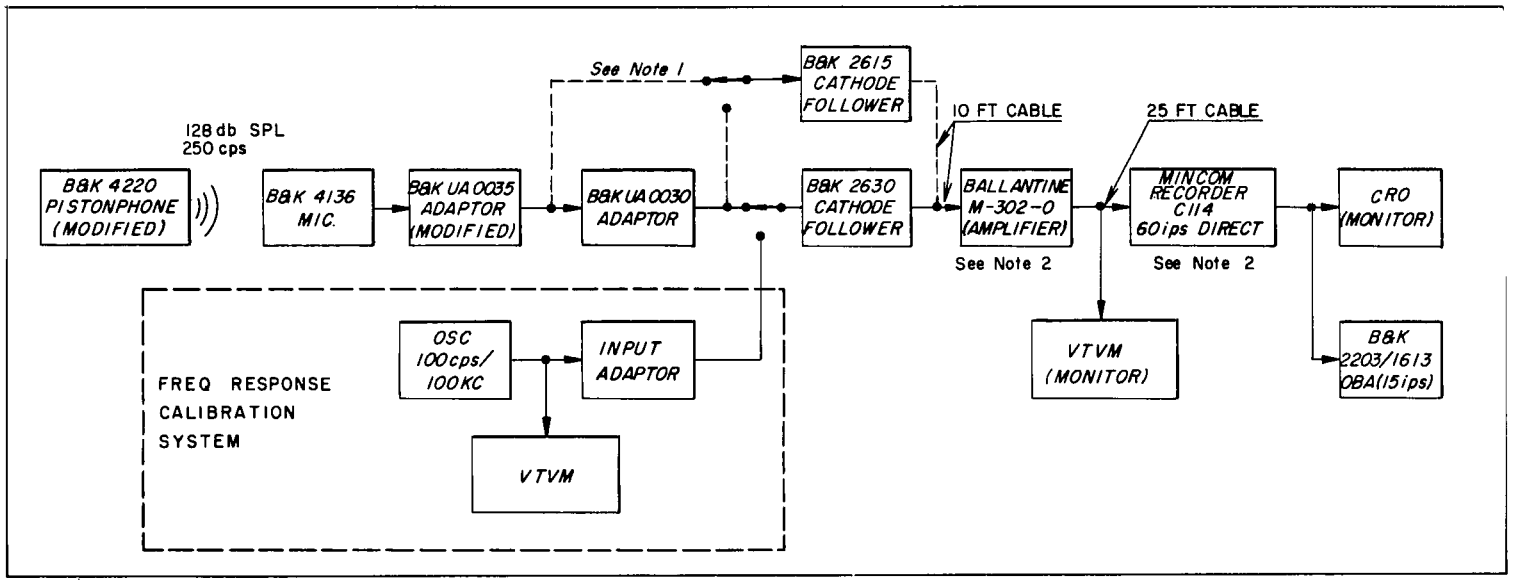

NOTE 1: B + K UA0030 MICROPHONE ADAPTER AND B + K 2630 (BATTERY OPERATED) CATHODE FOLLOWER USED FOR TWO CHANNELS. B + K 2615 ½" CATHODE FOLLOWER AND 2801 POWER SUPPLY USED FOR THREE CHANNELS.

NOTE 2: MARCH '63 TESTS USED SYSTEM SHOWN. NOVEMBER '62 TESTS USED PRECISION INSTRUMENT PI207 WBFM TAPE RECORDER AND NO PREAMPLIFIERS. JANUARY '63 TESTS USED PRECISION INSTRUMENT PS207 WBFM TAPE RECORDER AND COLUMBIA PREAMPLIFIER 6006.

FIGURE 8 — ACOUSTIC DATA ACQUISITION SYSTEM

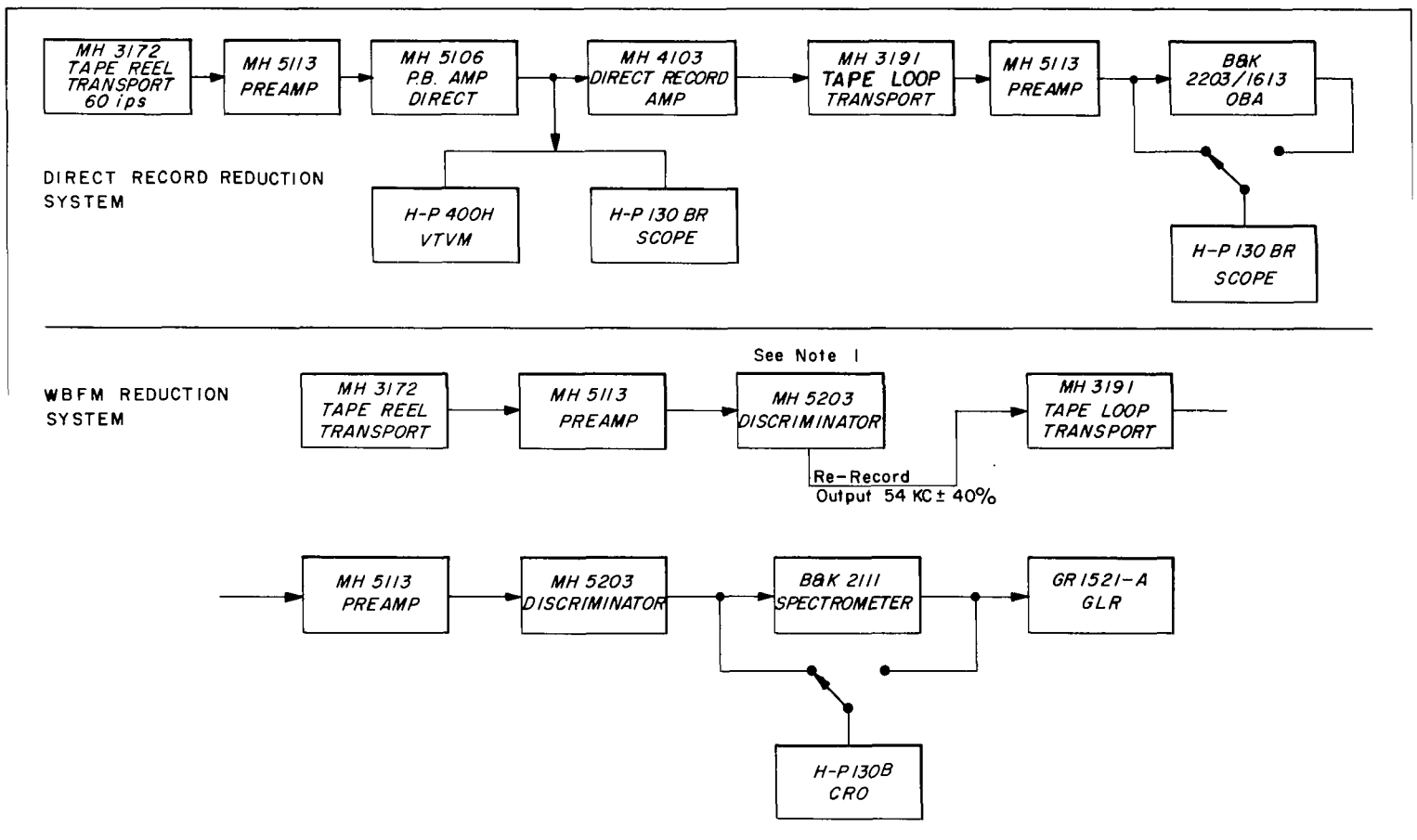

NOTE 1: RE-RECORD OUTPUT IS NOT DISCRIMINATED BUT IS MERELY AMPLIFIED

FIGURE 9 — ACOUSTIC DATA REDUCTION SYSTEMS

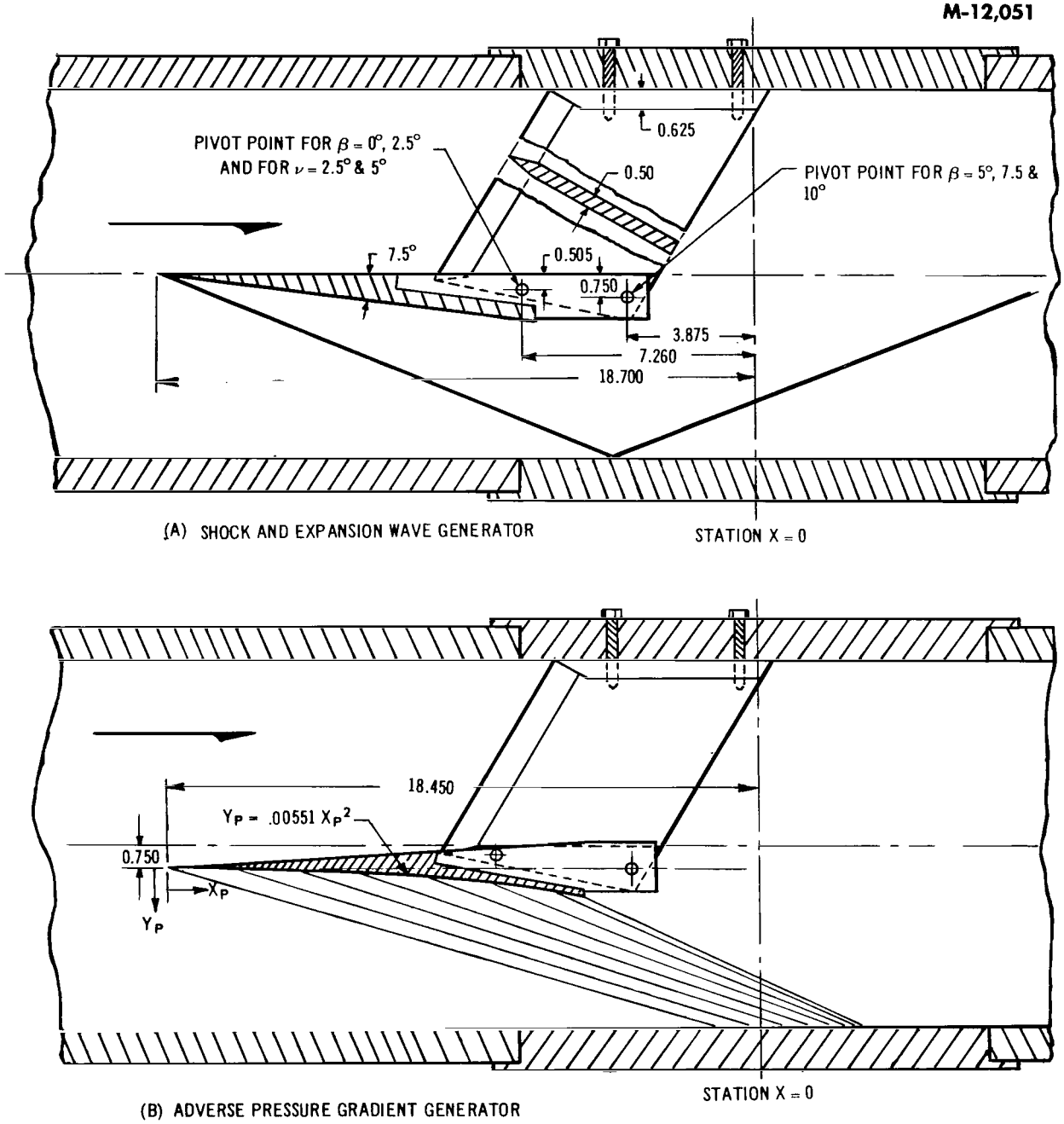

(A) SHOCK AND EXPANSION WAVE GENERATOR

(B) ADVERSE PRESSURE GRADIENT GENERATOR

FIGURE 10 INSTALLATION DETAILS OF SHOCK WAVE AND PRESSURE GRADIENT GENERATORS AT M = 3.46

ROUGHNESS	t
1	0.012
2	0.025
3	0.050
4	0.125

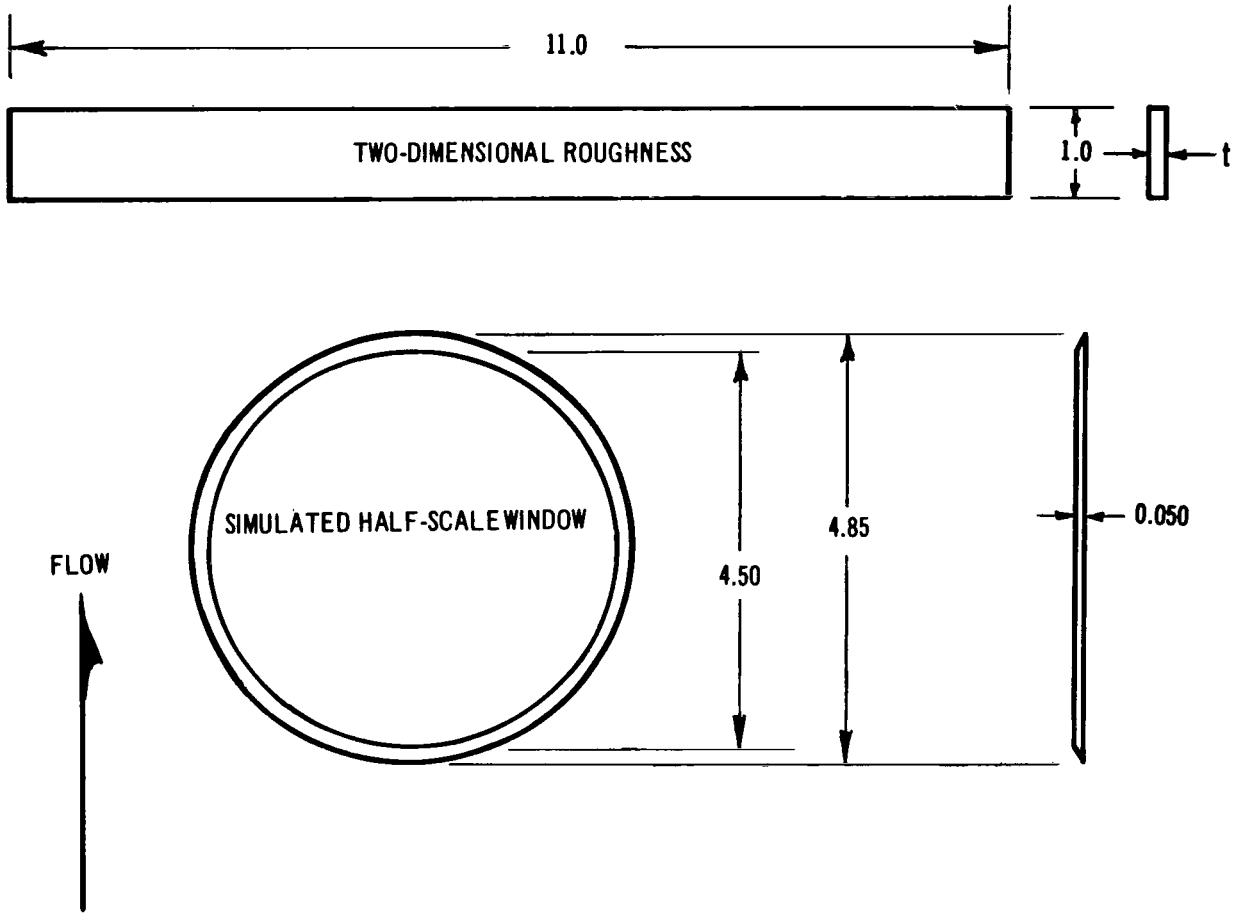

FIGURE 11 — SKETCH OF LOCAL ROUGHNESS ELEMENTS

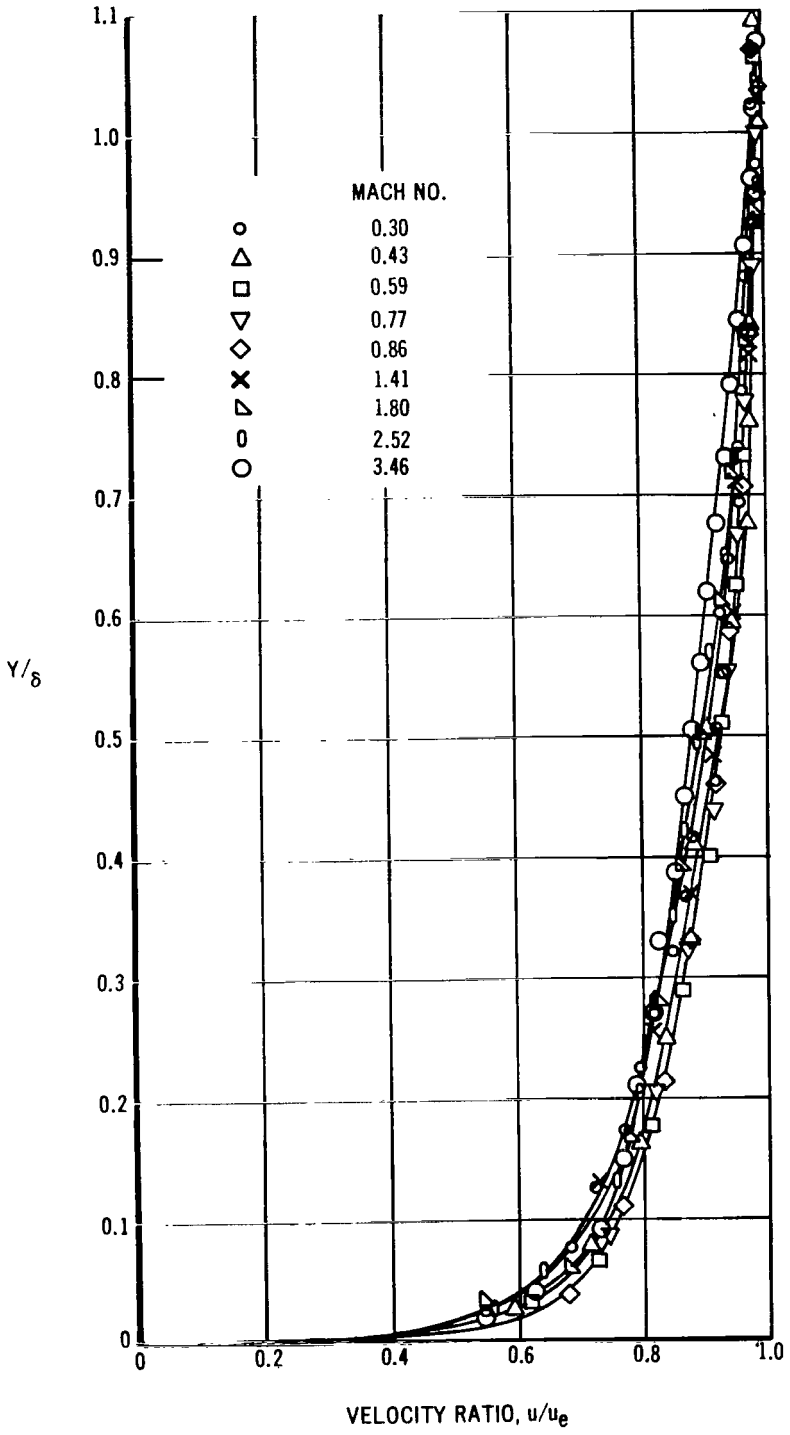

FIGURE 12 — NON-DIMENSIONALIZED BOUNDARY LAYER VELOCITY PROFILES

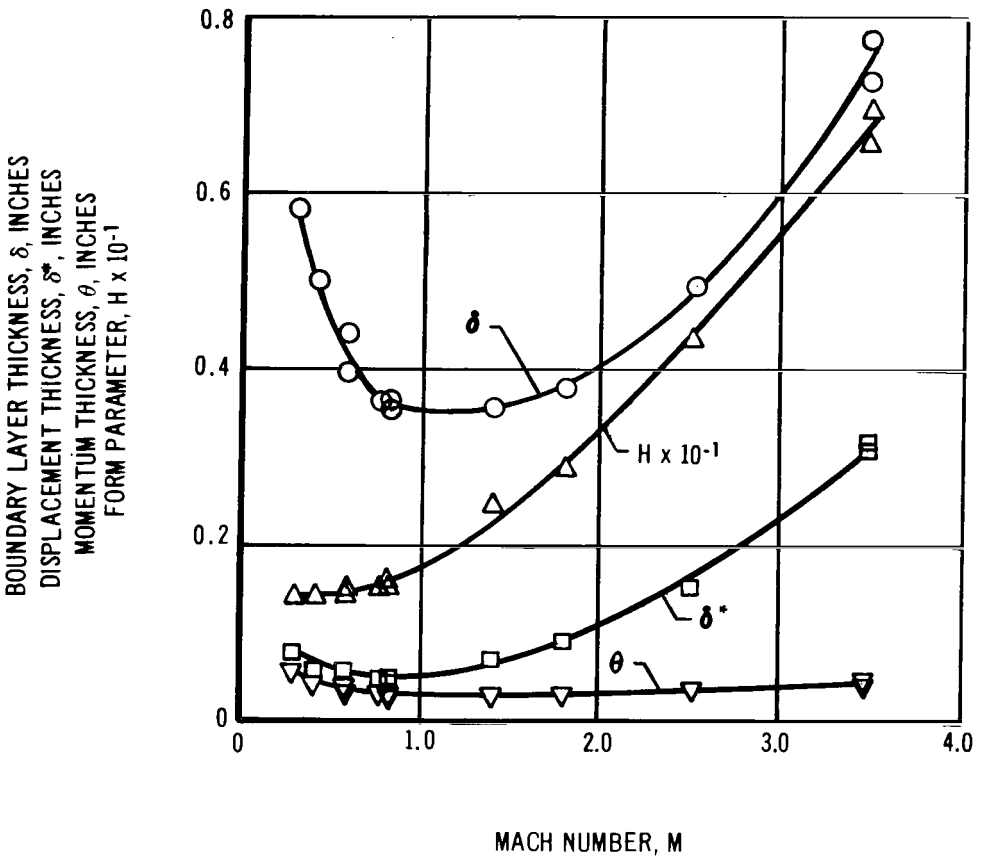

FIGURE 13 – BOUNDARY LAYER PARAMETERS AS FUNCTIONS OF MACH NUMBER

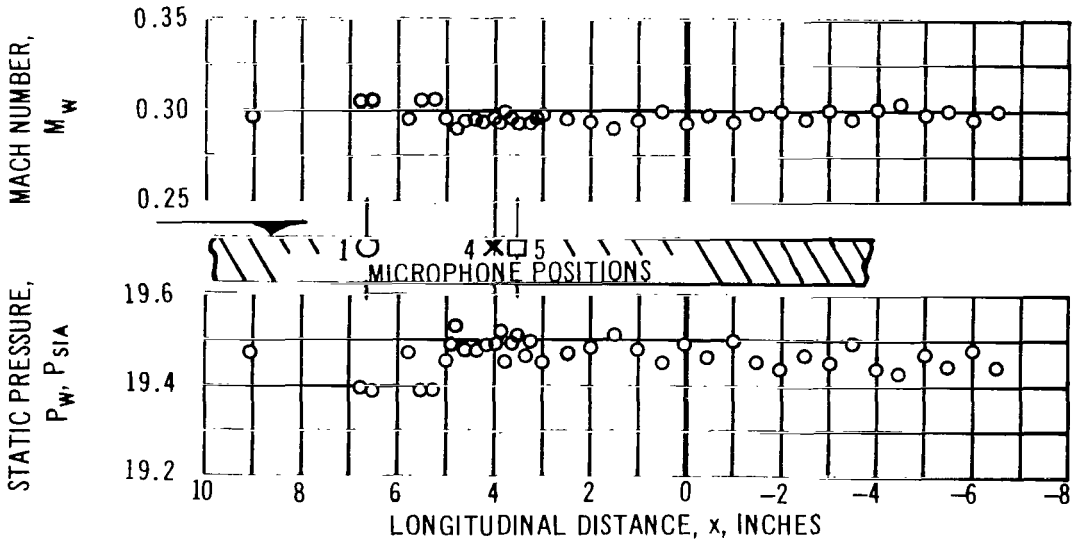

(A) $M_4 = 0.30$

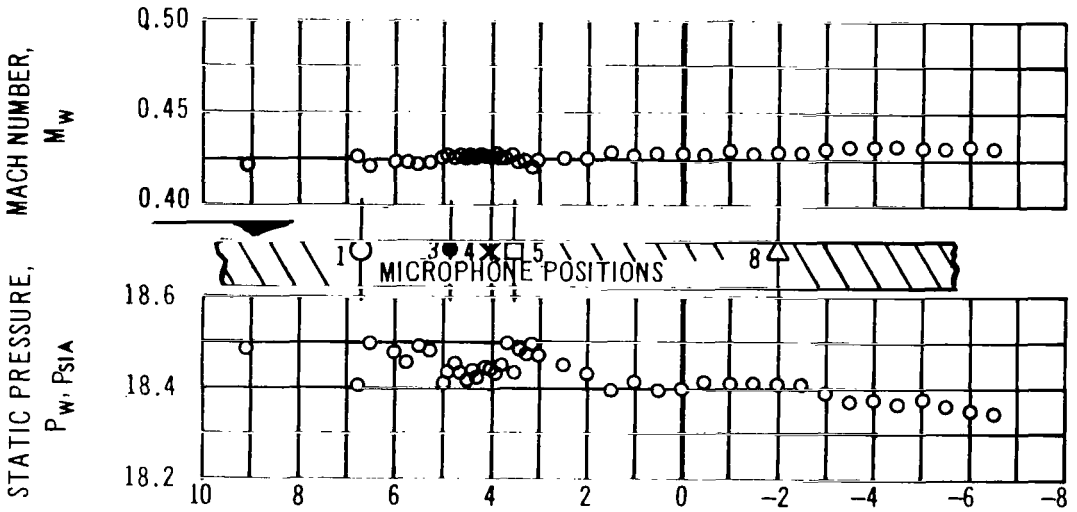

(B) $M_4 = 0.43$

FIGURE 14a – VARIATION OF STATIC PRESSURE AND MACH NUMBER WITH DISTANCE ALONG THE SIDEWALL CENTERLINE

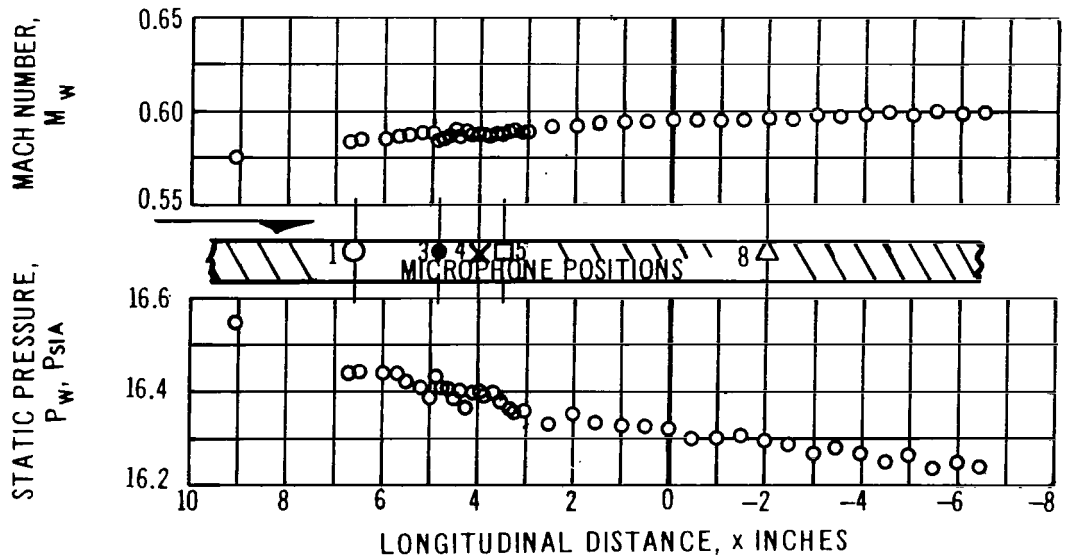

(C) $M_4 = 0.59$

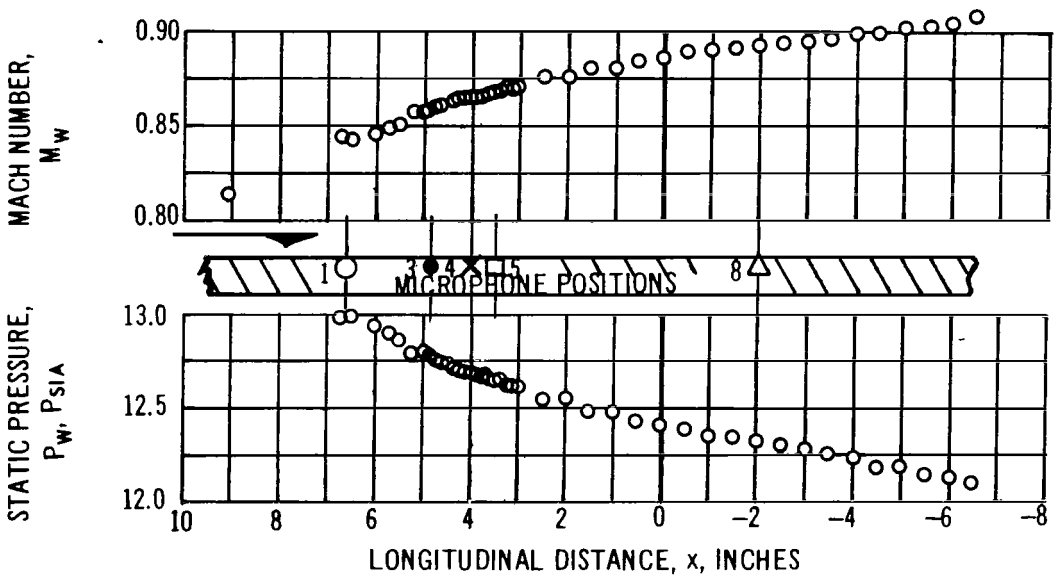

(D) $M_4 = 0.86$

FIGURE 14b —VARIATION OF STATIC PRESSURE AND MACH NUMBER WITH DISTANCE ALONG THE SIDEWALL CENTERLINE

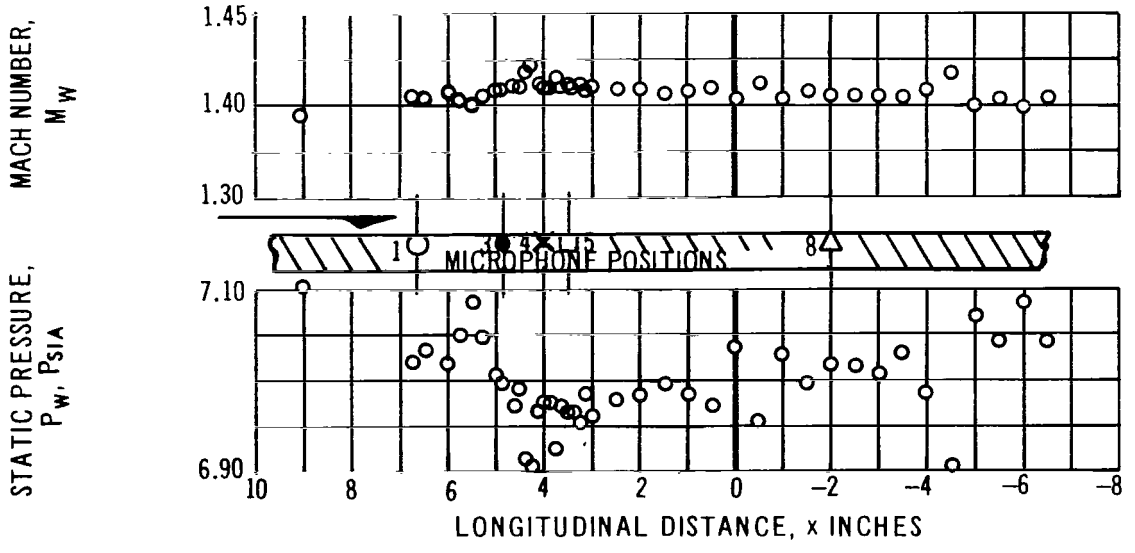

(E) $M_4 = 1.41$

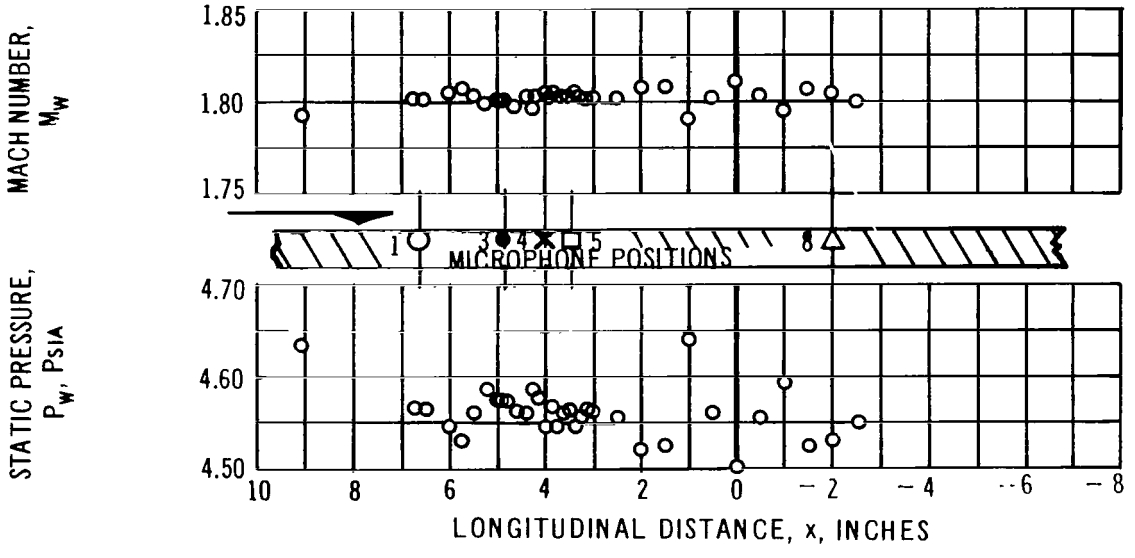

(F) $M_4 = 1.80$

FIGURE 14c — VARIATION OF STATIC PRESSURE AND MACH NUMBER WITH DISTANCE ALONG THE SIDEWALL CENTERLINE

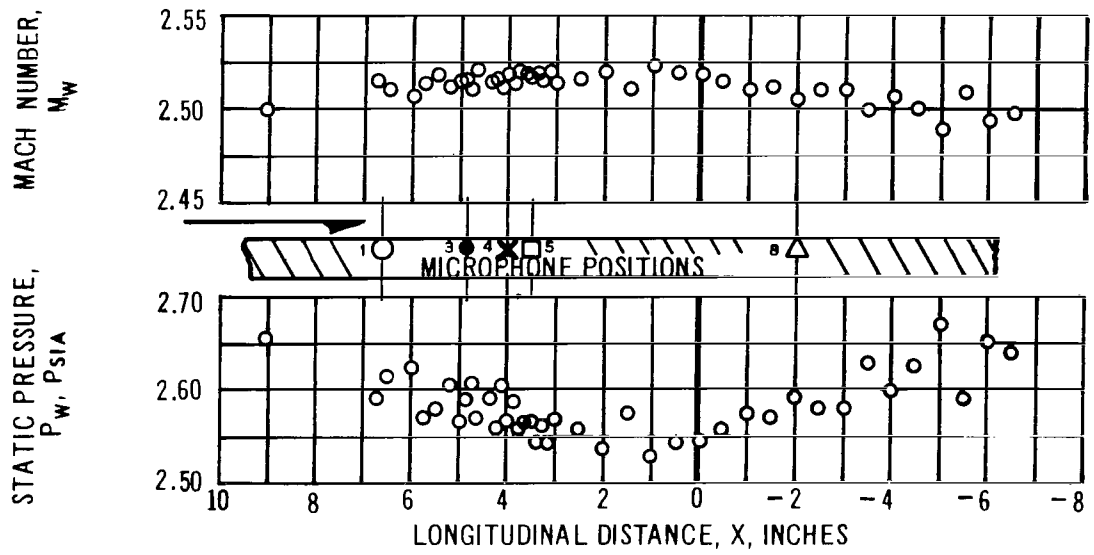

(G) $M_4 = 2.52$

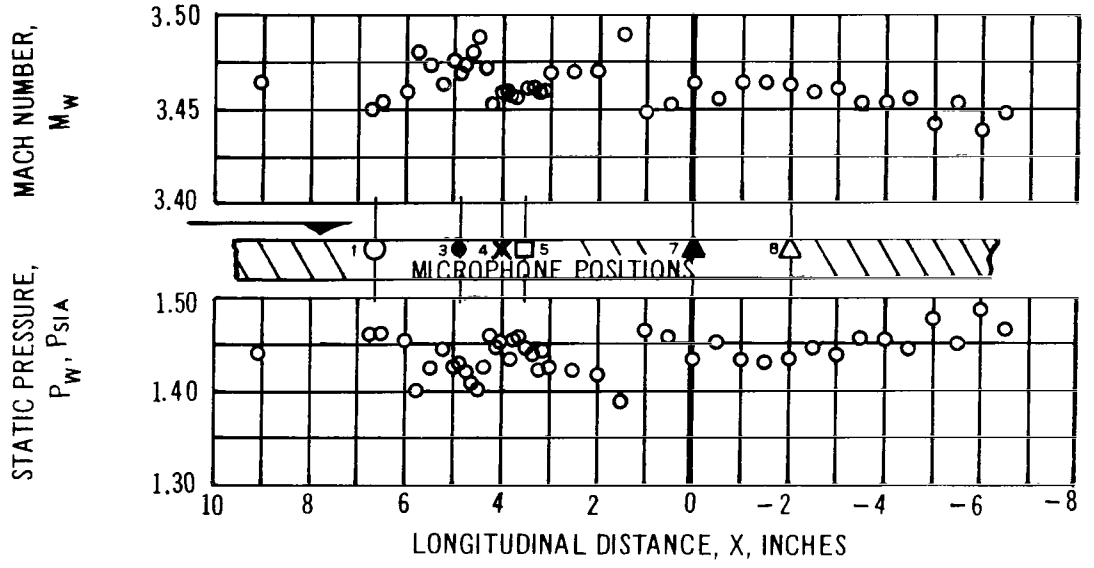

(H) $M_4 = 3,46$

FIGURE 14 d – VARIATION OF STATIC PRESSURE AND MACH NUMBER WITH DISTANCE ALONG THE SIDEWALL CENTERLINE

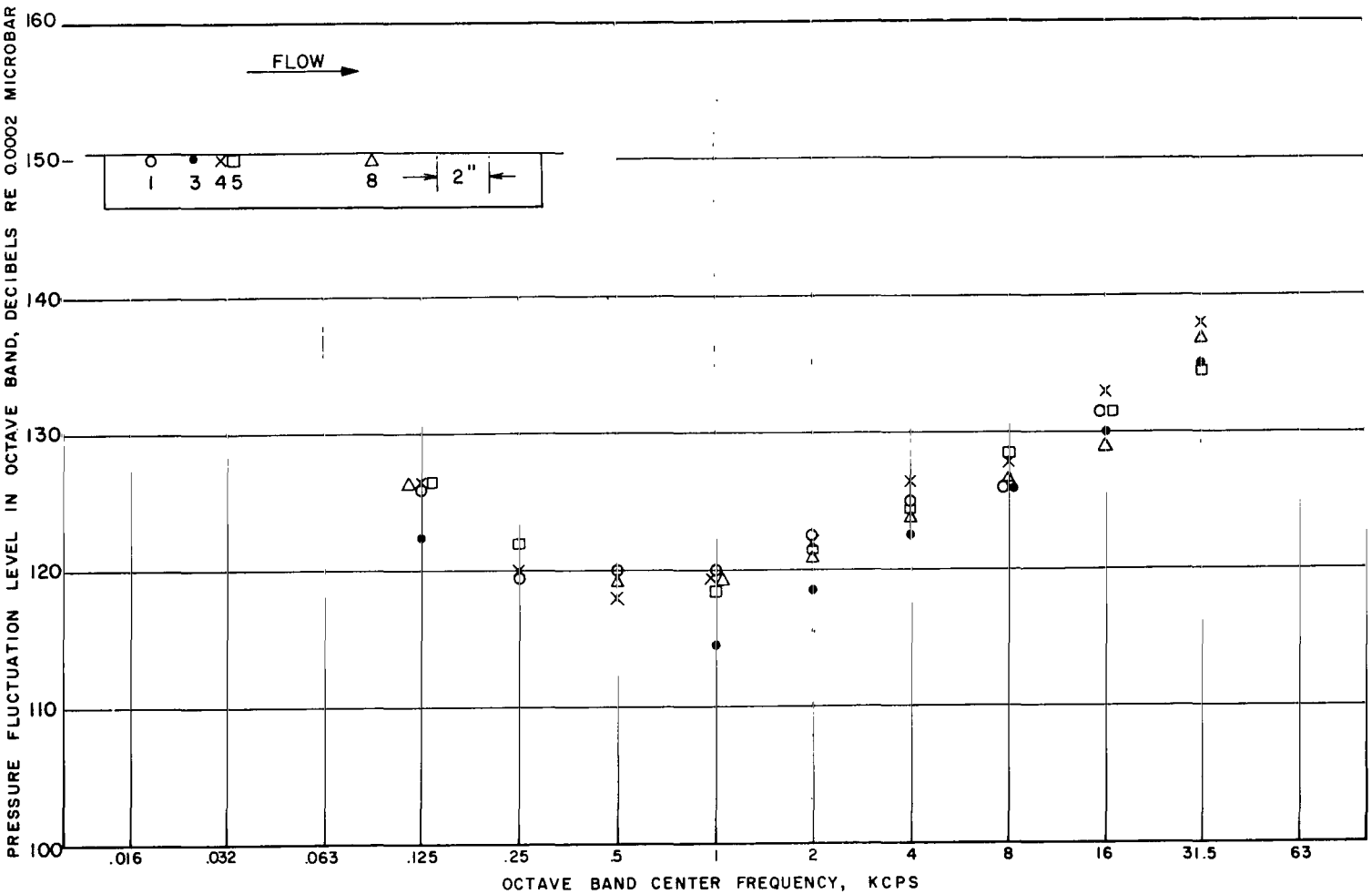

FIGURE 15 BOUNDARY LAYER PRESSURE FLUCTUATION LEVELS AT STATIONS ALONG THE TUNNEL SIDEWALL, $M_4 = 0.43$

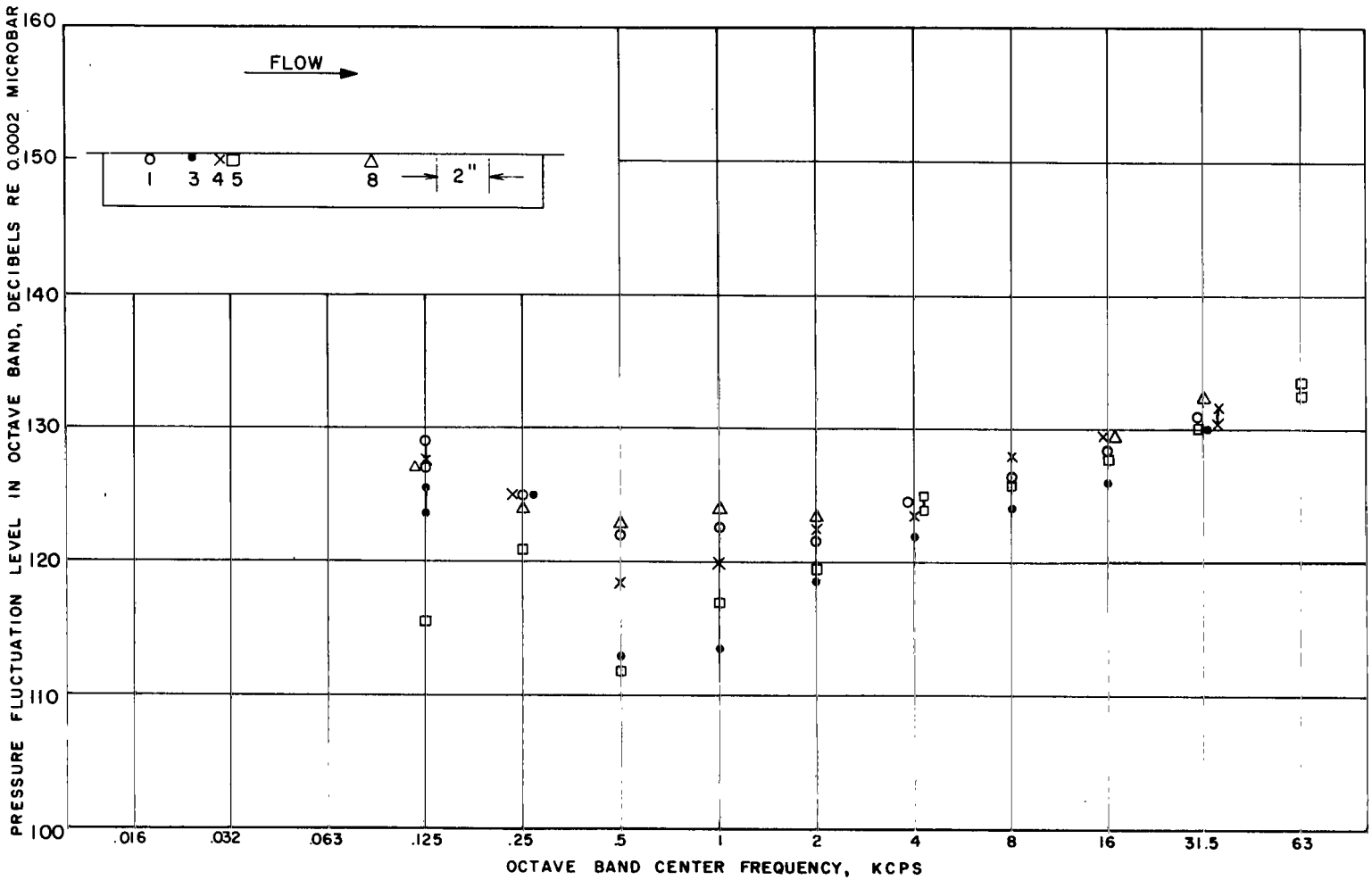

FIGURE 16 BOUNDARY LAYER PRESSURE FLUCTUATION LEVELS AT STATIONS ALONG THE TUNNEL SIDEWALL, $M_4 = 0.59$

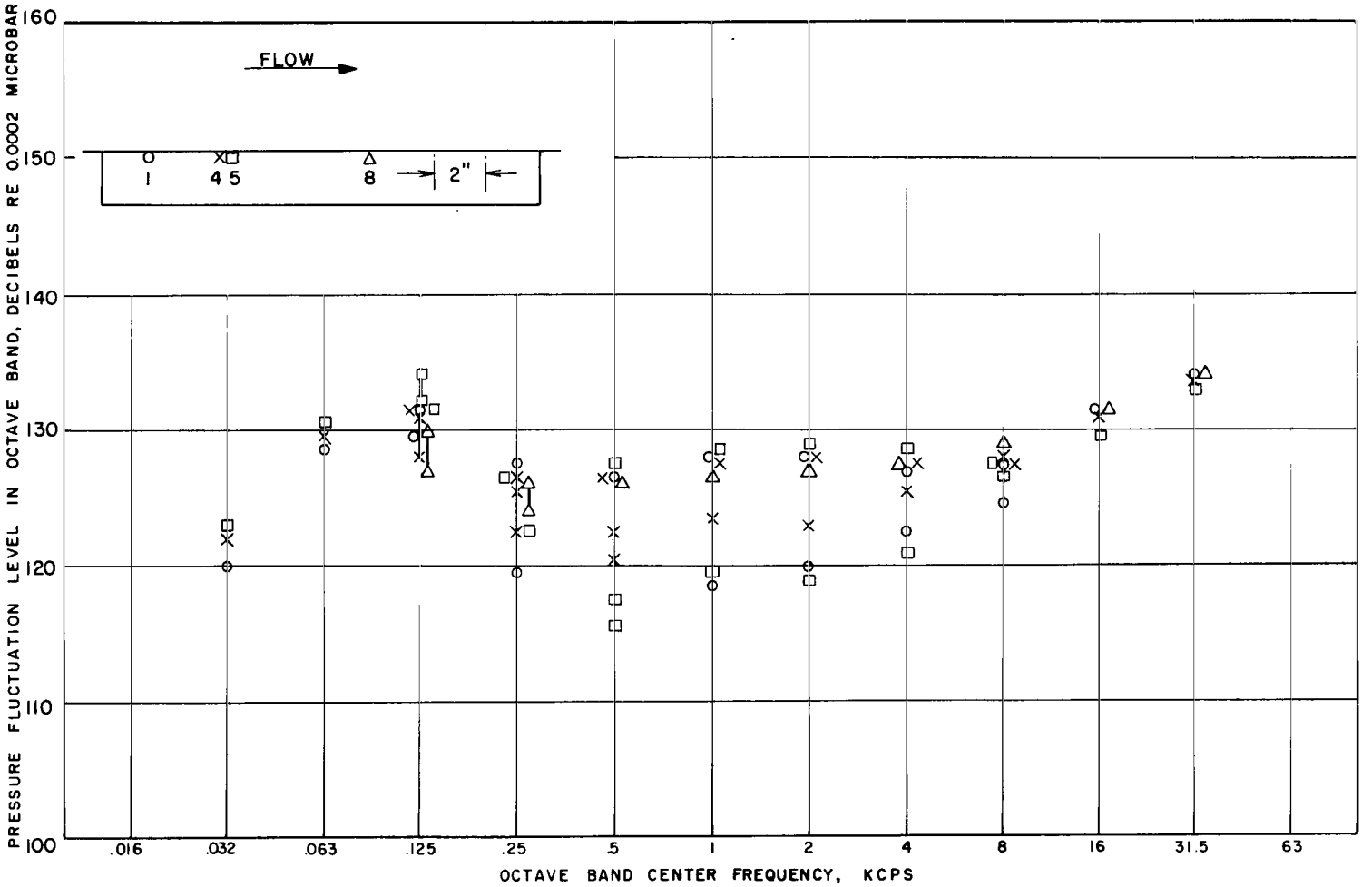

FIGURE 17 BOUNDARY LAYER PRESSURE FLUCTUATION LEVELS AT STATIONS ALONG THE TUNNEL SIDEWALL, $M_4 = 0.86$

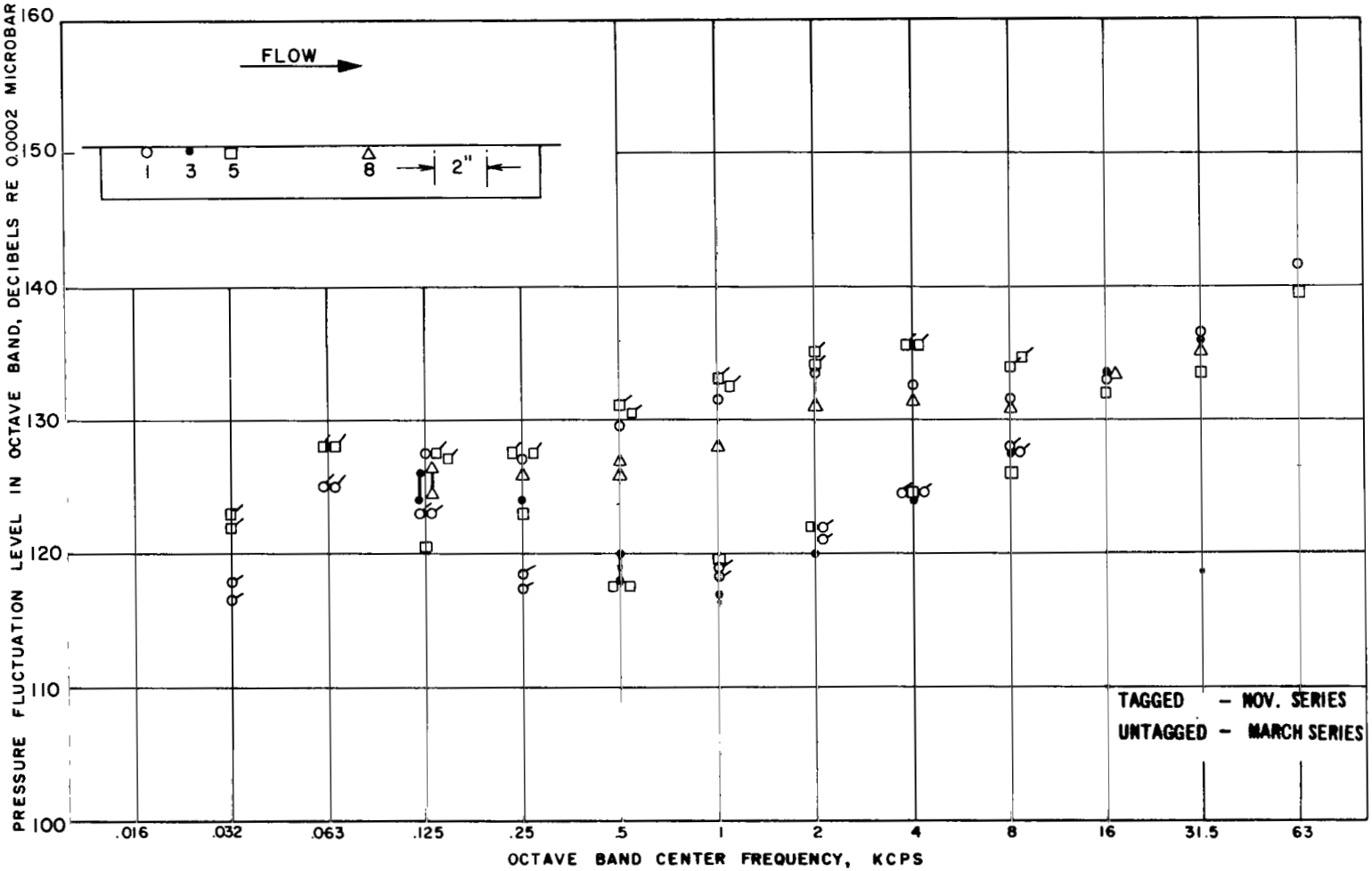

FIGURE 18 BOUNDARY LAYER PRESSURE FLUCTUATION LEVELS AT STATIONS ALONG THE TUNNEL SIDEWALL, $M_4 = 1.41$

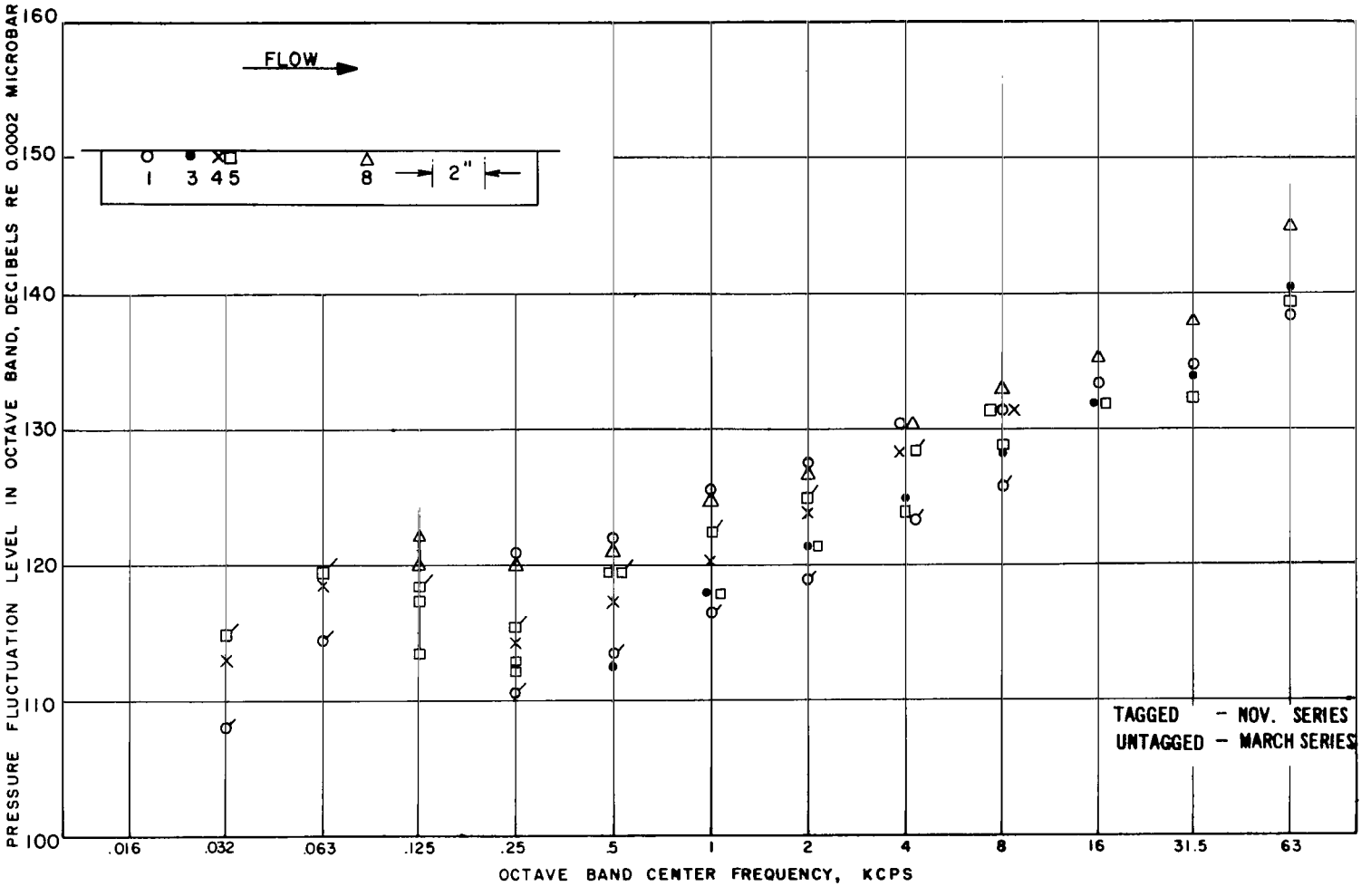

FIGURE 19 BOUNDARY LAYER PRESSURE FLUCTUATION LEVELS AT STATIONS ALONG THE TUNNEL SIDEWALL, $M_4 = 1.80$

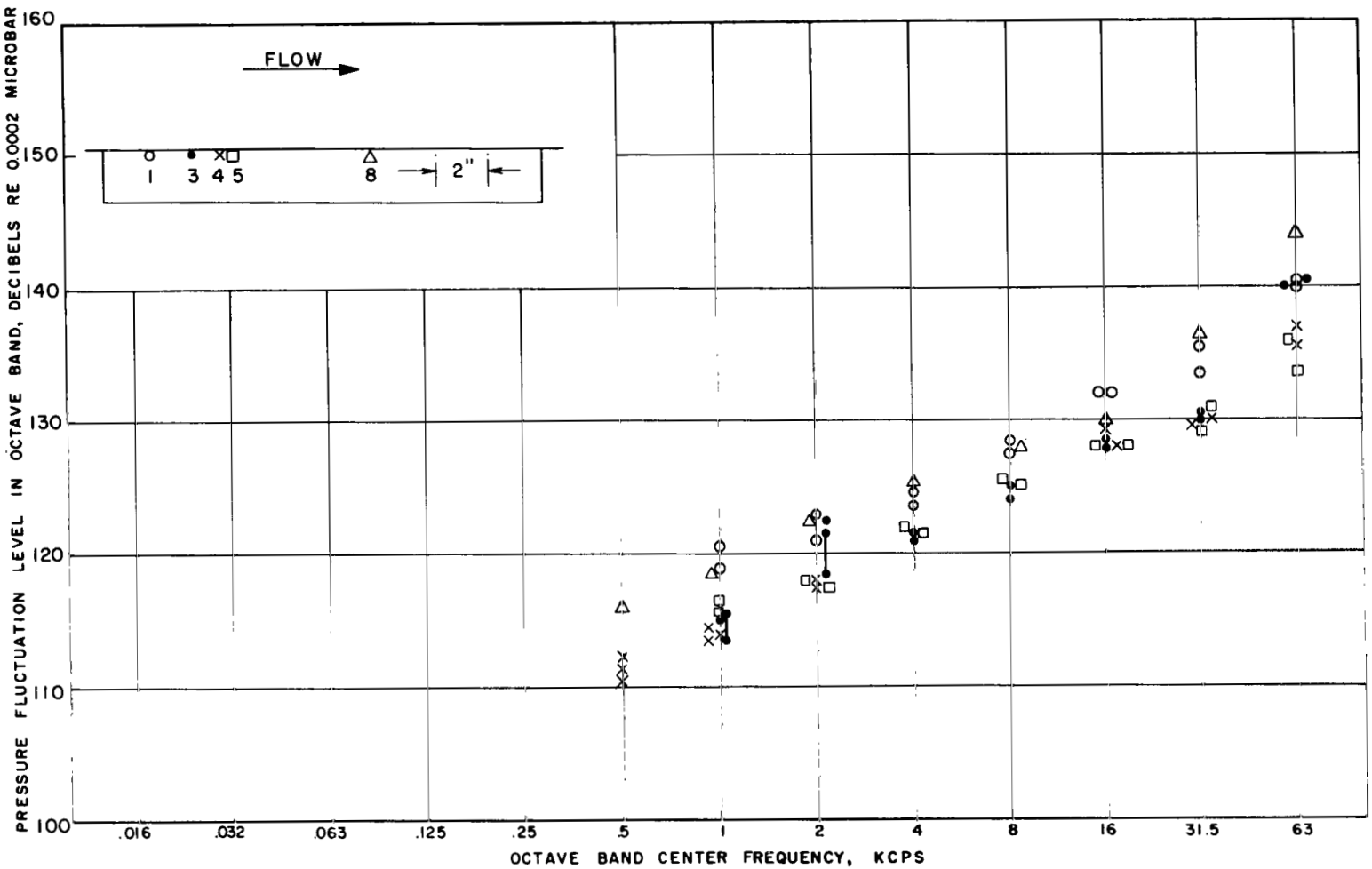

FIGURE 20 BOUNDARY LAYER PRESSURE FLUCTUATION LEVELS AT STATIONS ALONG THE TUNNEL SIDEWALL, $M_4 = 2.52$

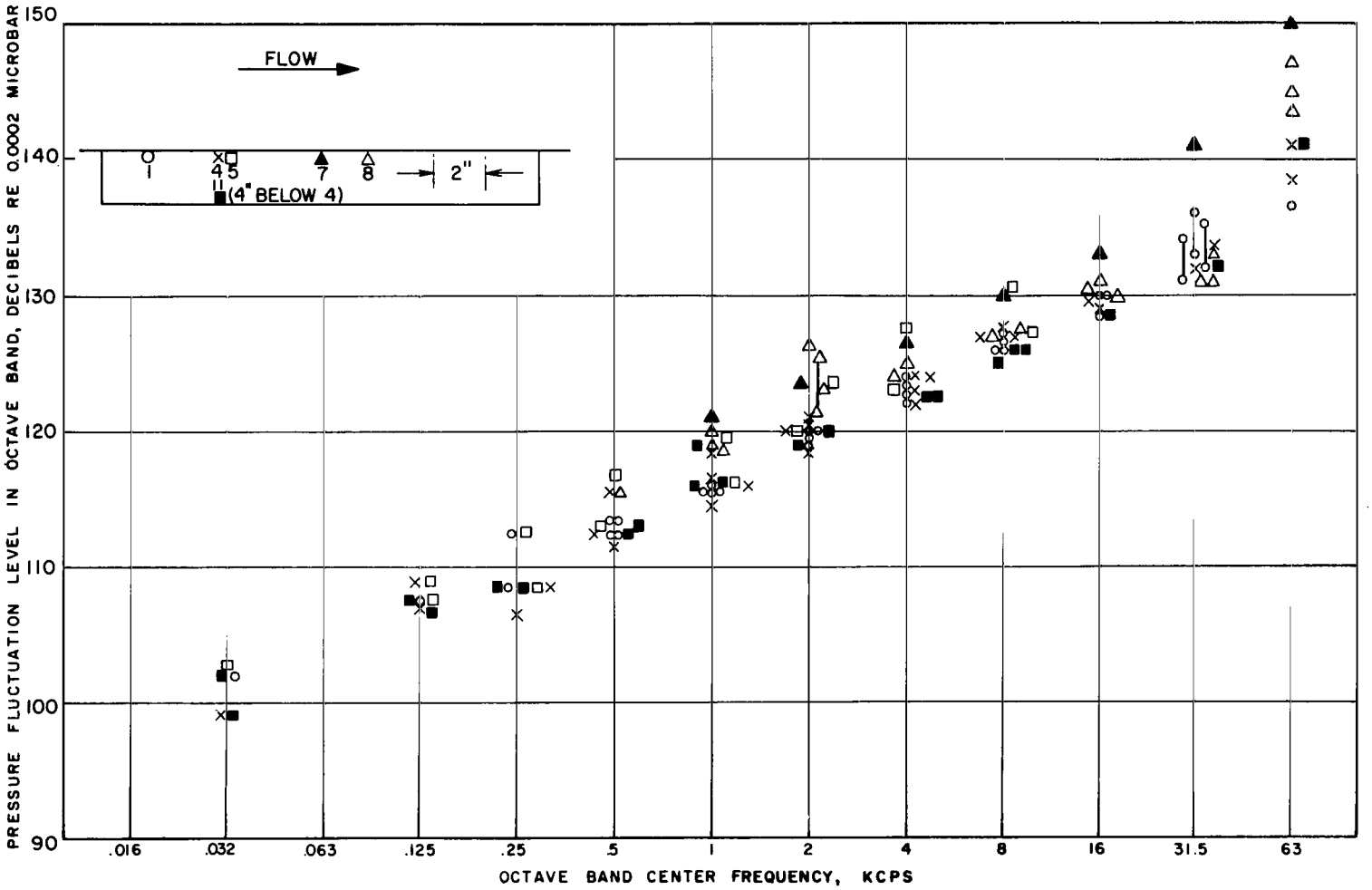

FIGURE 21 BOUNDARY LAYER PRESSURE FLUCTUATION LEVELS AT STATIONS ALONG THE TUNNEL SIDEWALL, $M_4 = 3.46$

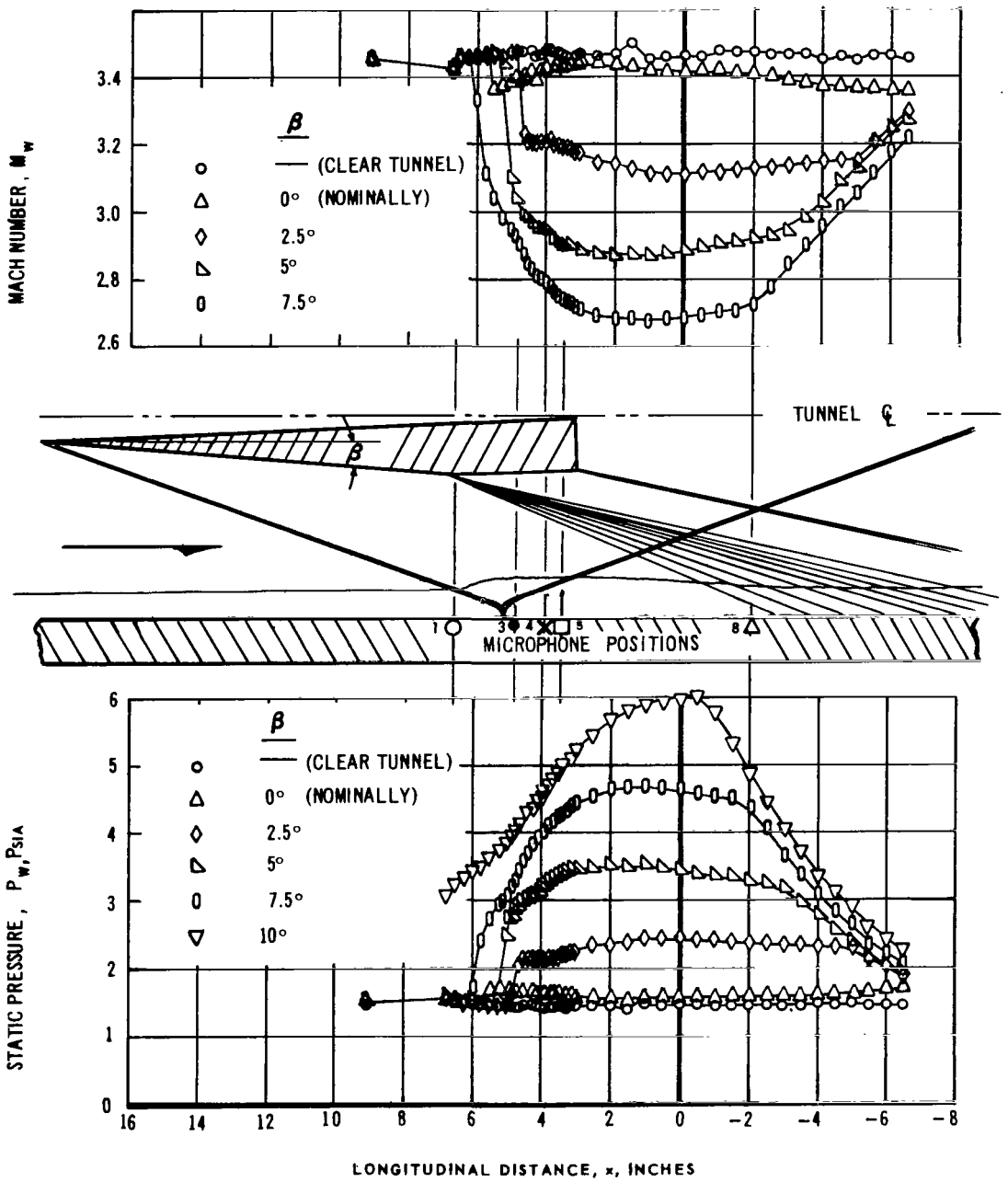

FIGURE 22 – VARIATION OF STATIC PRESSURE AND MACH NUMBER WITH DISTANCE ALONG SIDEWALL CENTERLINE IN THE PRESENCE OF A SHOCK WAVE AT M = 3.46 (ILLUSTRATION INDICATES THE SHOCK POSITION FOR β = 5°)

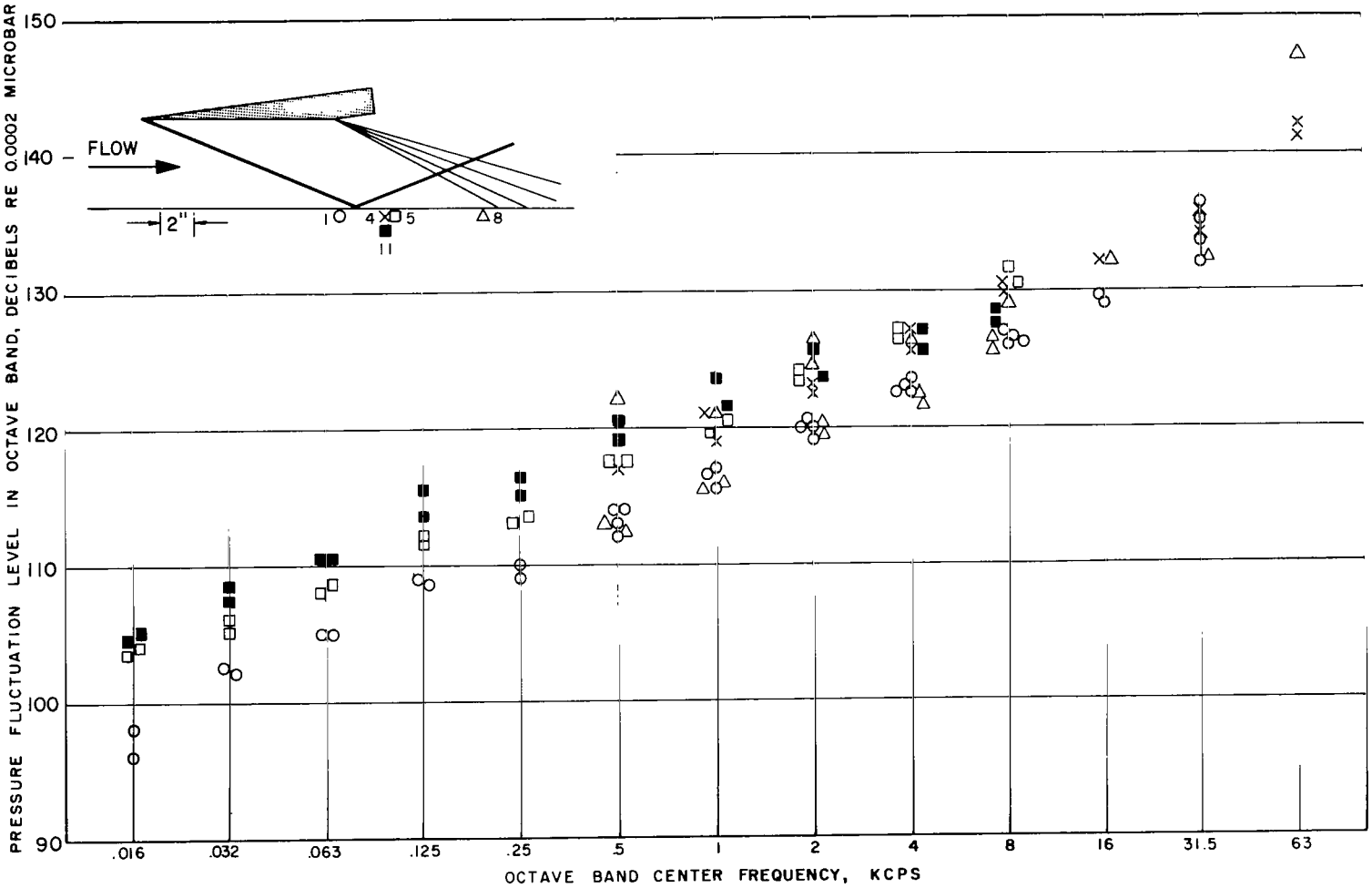

FIGURE 23 BOUNDARY LAYER PRESSURE FLUCTUATION LEVELS AT STATIONS ALONG THE TUNNEL SIDEWALL IN THE PRESENCE OF A SHOCK WAVE, $M_4 = 3.46$ SHOCK GENERATOR ANGLE $\beta = 0°$

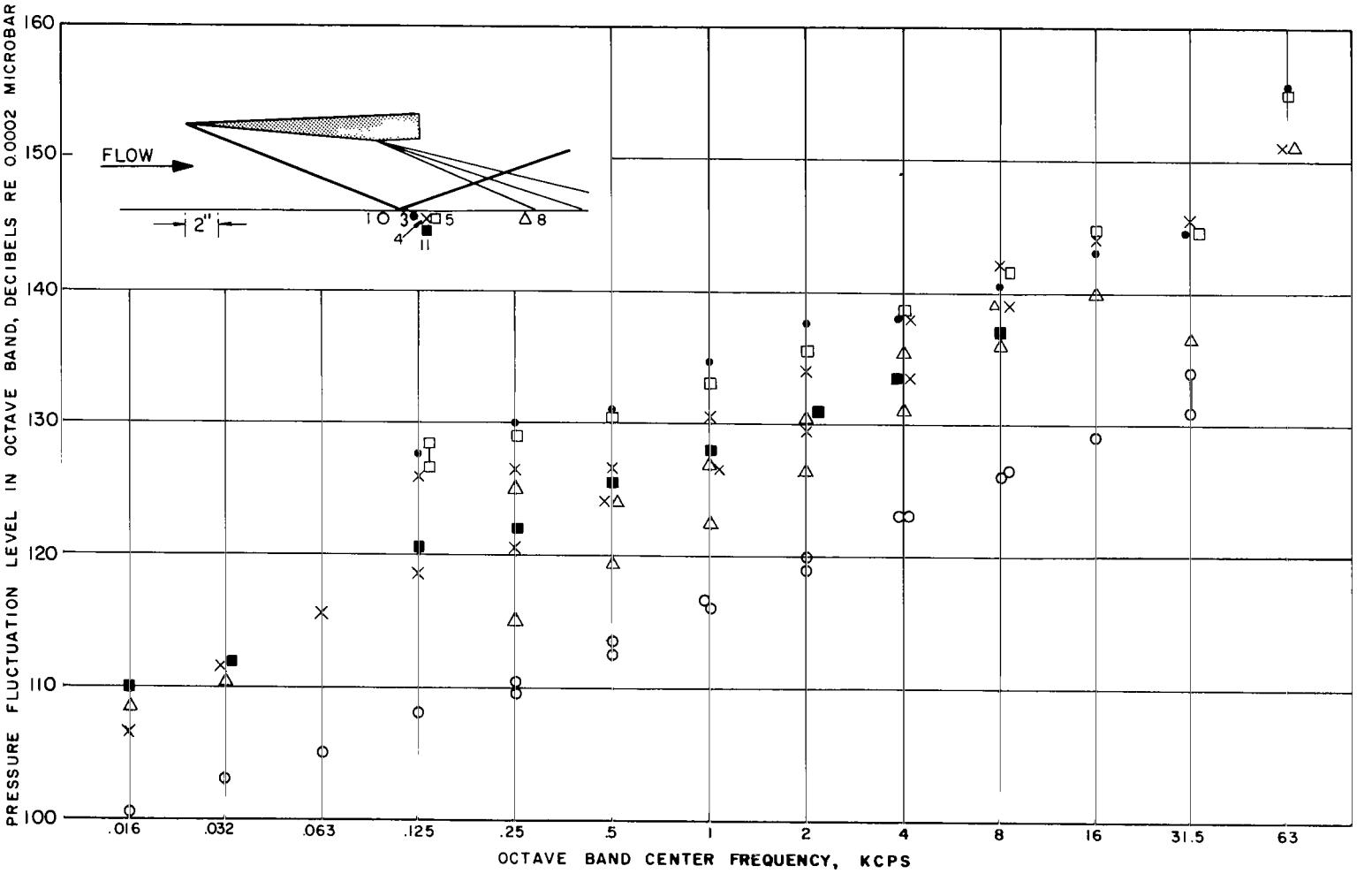

FIGURE 24 BOUNDARY LAYER PRESSURE FLUCTUATION LEVELS AT STATIONS ALONG THE TUNNEL SIDEWALL IN THE PRESENCE OF A SHOCK WAVE $M_4 = 3.46$
SHOCK GENERATOR ANGLE $\beta = 5°$

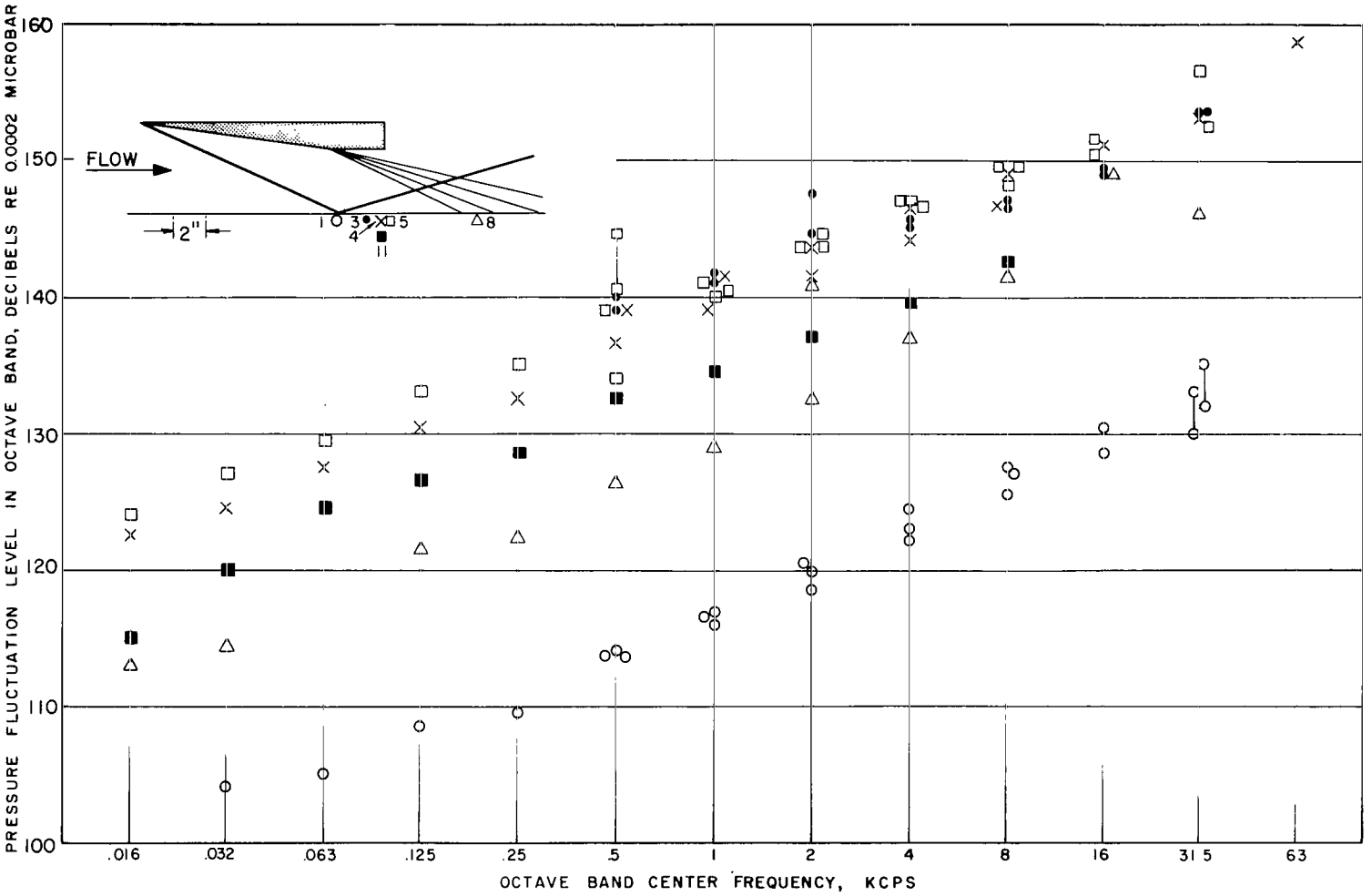

FIGURE 25 BOUNDARY LAYER PRESSURE FLUCTUATION LEVELS AT STATIONS ALONG THE TUNNEL SIDEWALL IN THE PRESENCE OF A SHOCK WAVE AT $M_4 = 3.46$ SHOCK GENERATOR ANGLE $\beta = 7.5°$

M-12,049

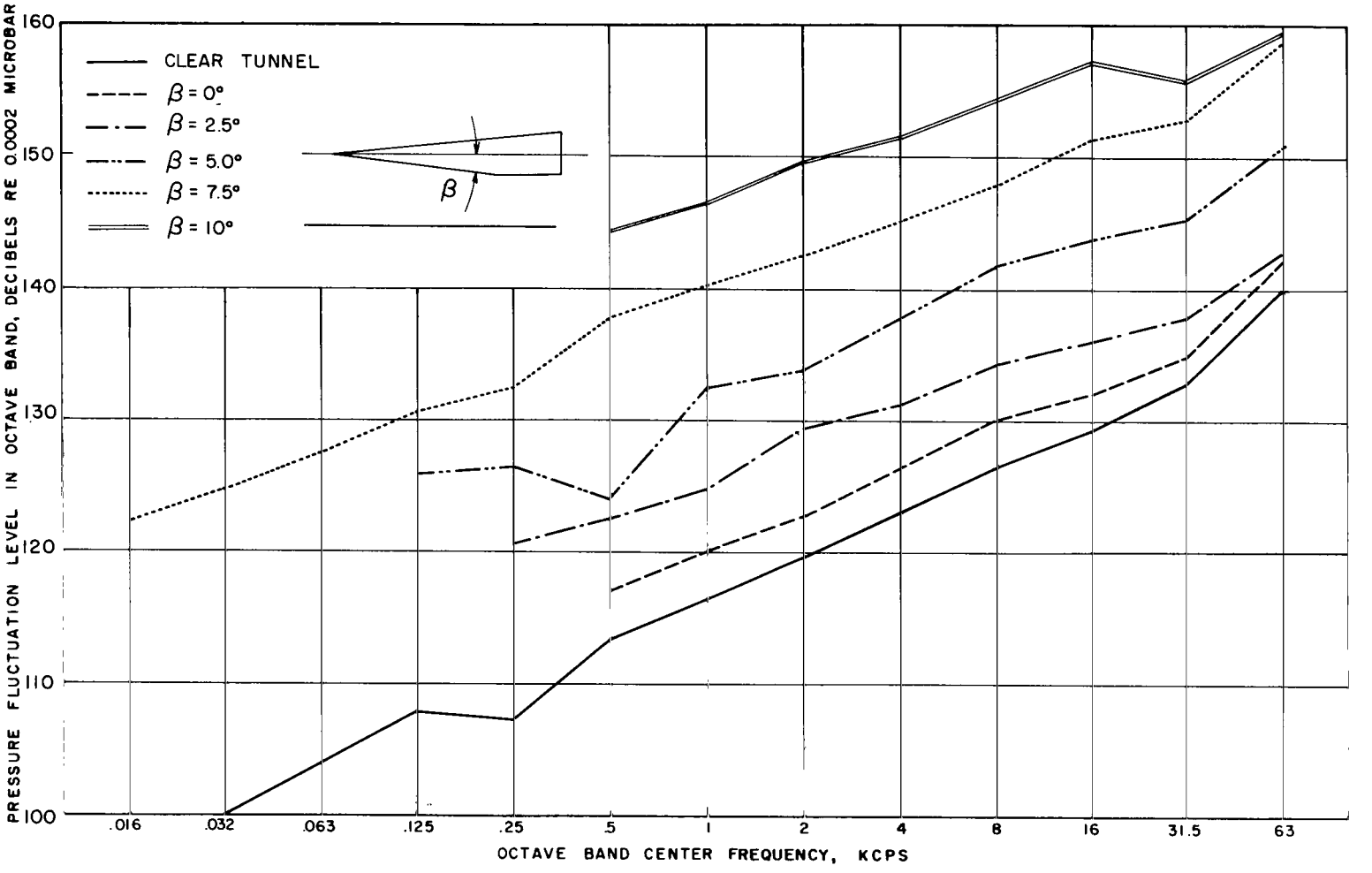

FIGURE 26 BOUNDARY LAYER PRESSURE FLUCTUATION LEVELS AT MICROPHONE LOCATION 4(X = 4") IN THE PRESENCE OF A SHOCK WAVE, $M_4 = 3.46$

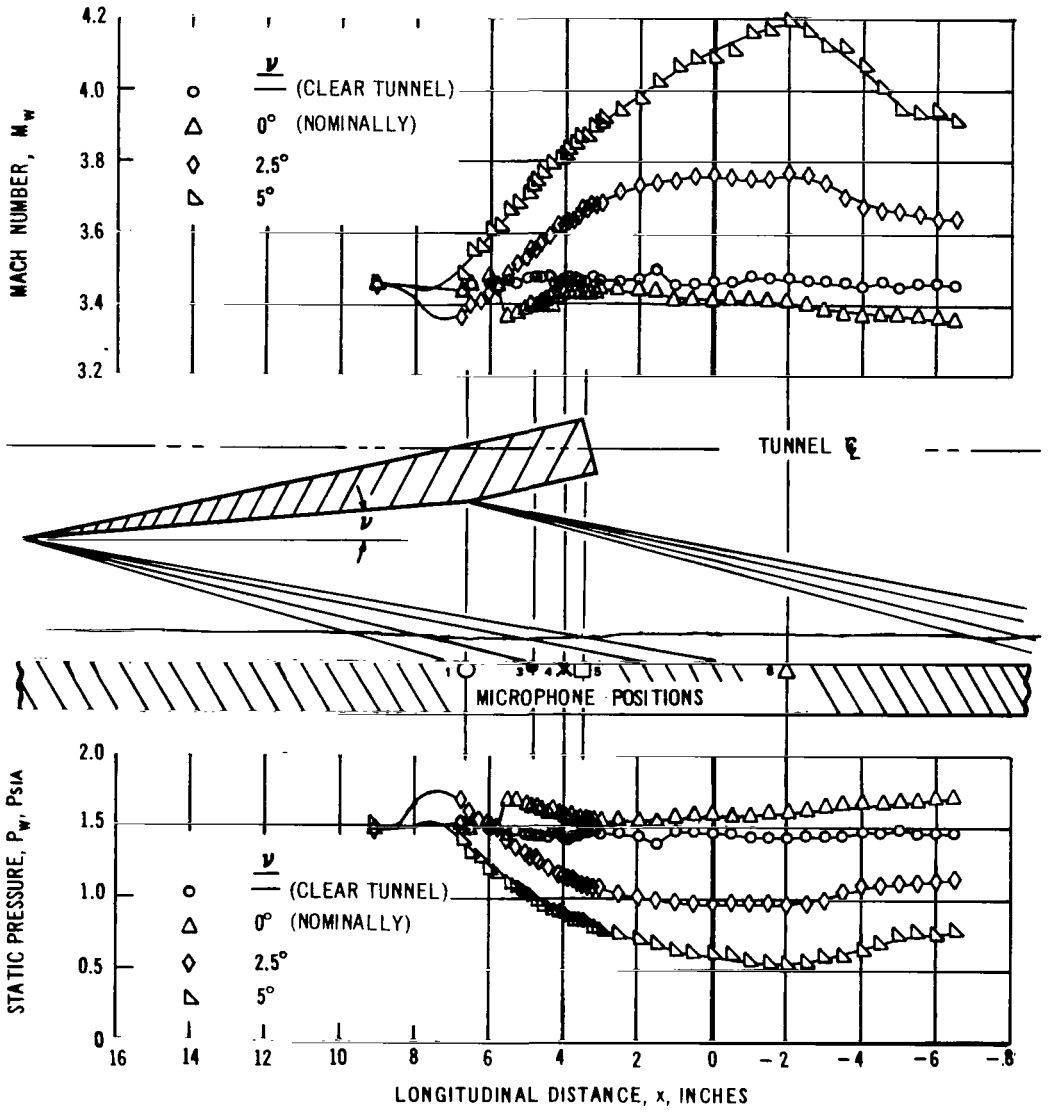

FIGURE 27– VARIATION OF STATIC PRESSURE AND MACH NUMBER WITH DISTANCE ALONG THE SIDEWALL CENTERLINE IN THE PRESENCE OF AN EXPANSION AT $M_1 = 3.46$ (ILLUSTRATION INDICATES THE EXPANSION LOCATION AT $\nu = 5°$.)

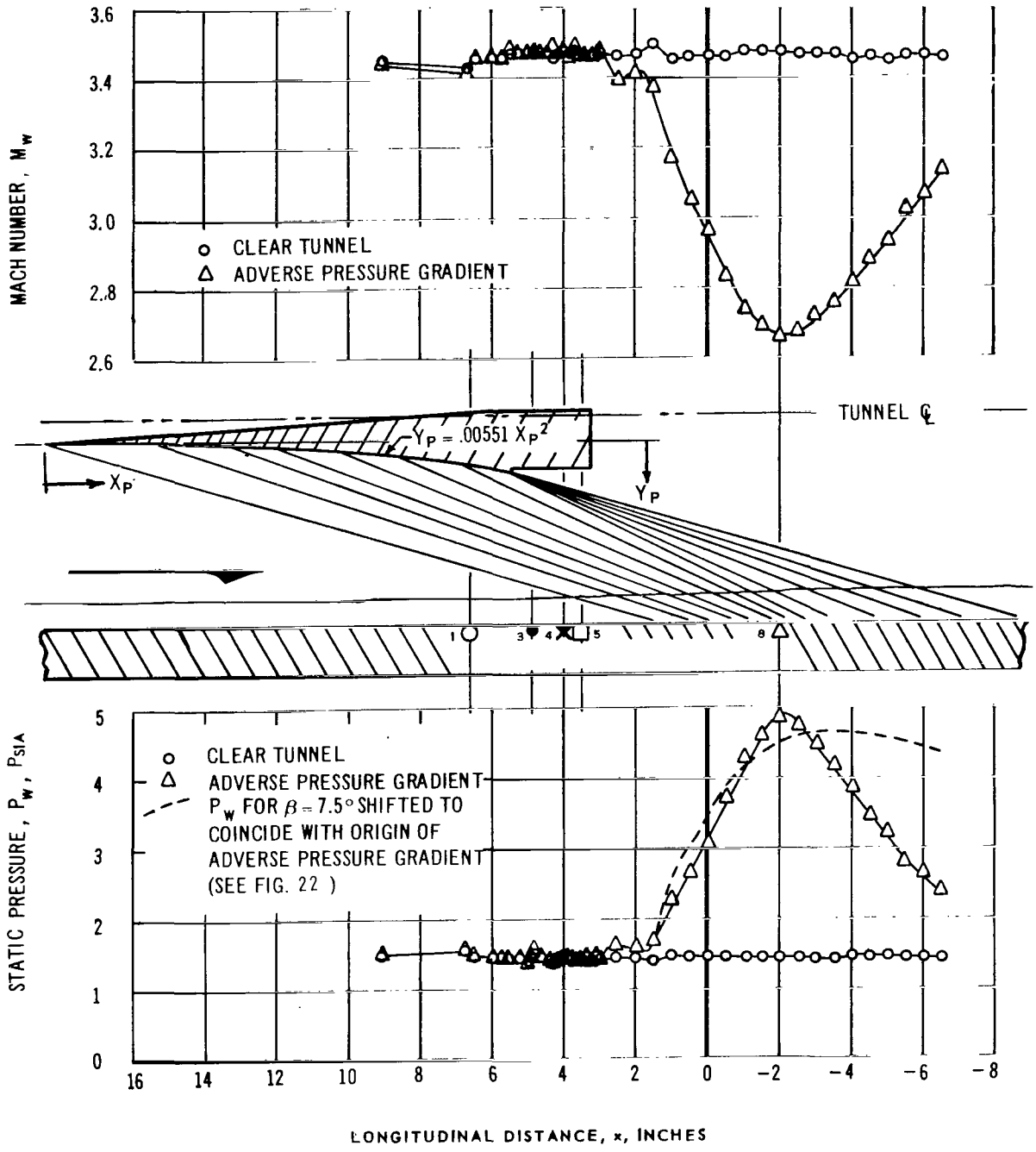

FIGURE 28 – VARIATION OF STATIC PRESSURE AND MACH NUMBER WITH DISTANCE ALONG SIDEWALL CENTERLINE IN THE PRESENCE OF AN ADVERSE PRESSURE GRADIENT $\left(\frac{dP}{dx} = 0.964\ \text{PSI/IN},\ \frac{dM}{dx} = -0.2/\text{IN}\right)$ AT $M_4 = 3.46$

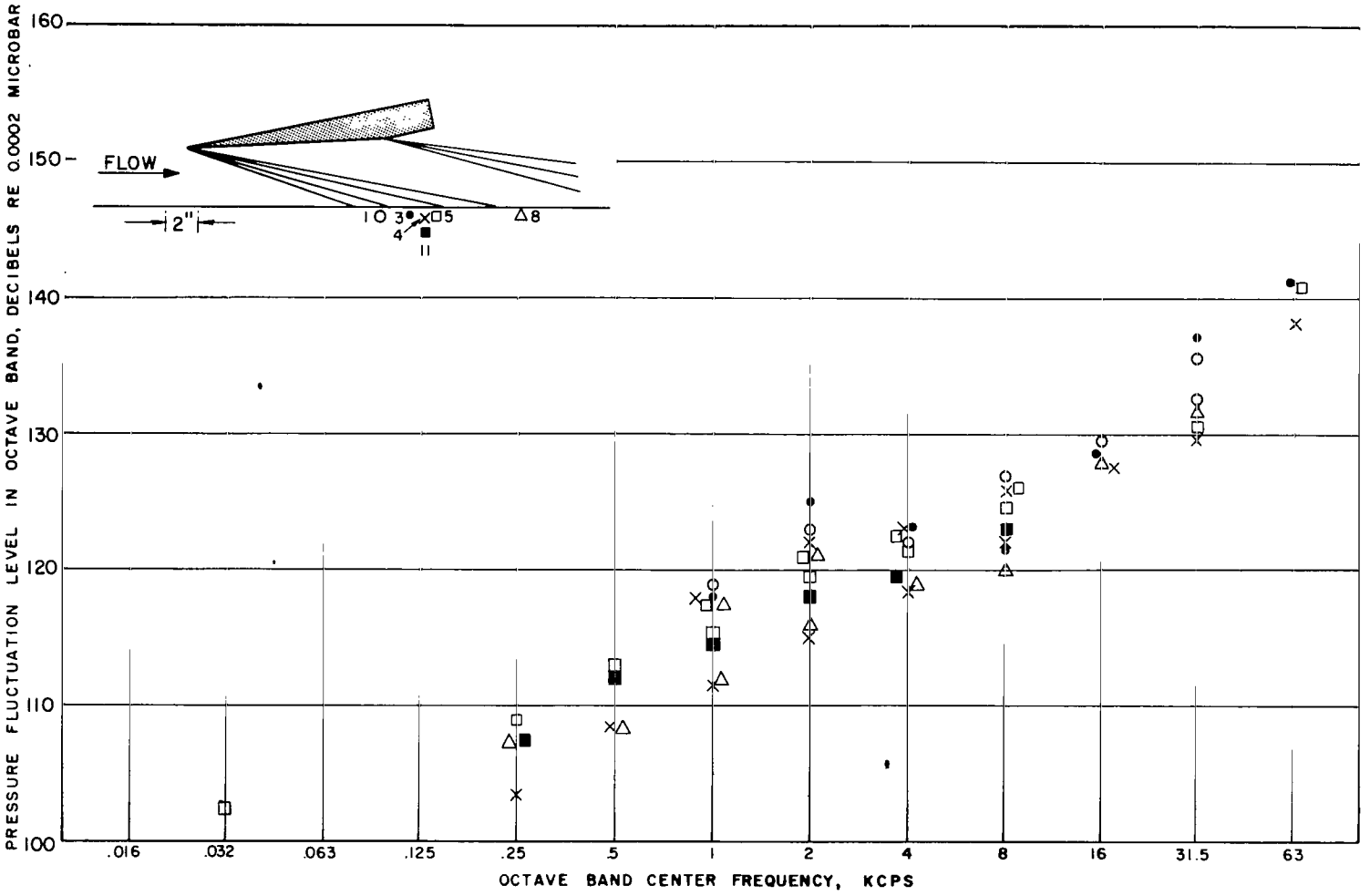

FIGURE 29 BOUNDARY LAYER PRESSURE FLUCTUATION LEVELS AT STATIONS ALONG THE TUNNEL SIDEWALL IN THE PRESENCE OF A FAVORABLE PRESSURE GRADIENT, $M_4 = 3.46$ EXPANSION GENERATOR ANGLE $\nu = 2.5°$

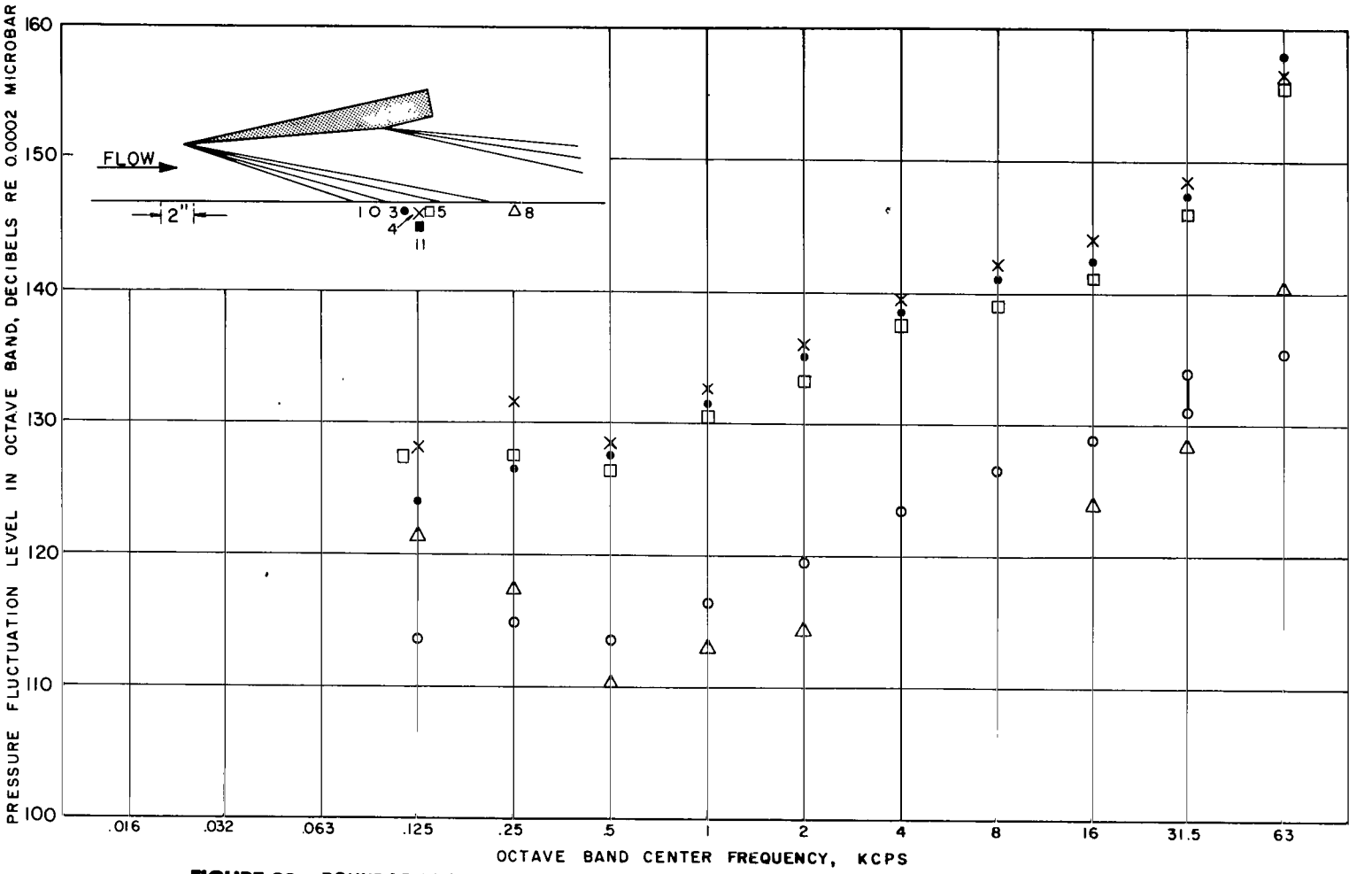

FIGURE 30 BOUNDARY LAYER PRESSURE FLUCTUATION LEVELS AT STATIONS ALONG THE TUNNEL SIDEWALL IN THE PRESENCE OF A FAVORABLE PRESSURE GRADIENT, $M_4 = 3.46$ EXPANSION GENERATOR ANGLE $\nu = 5°$

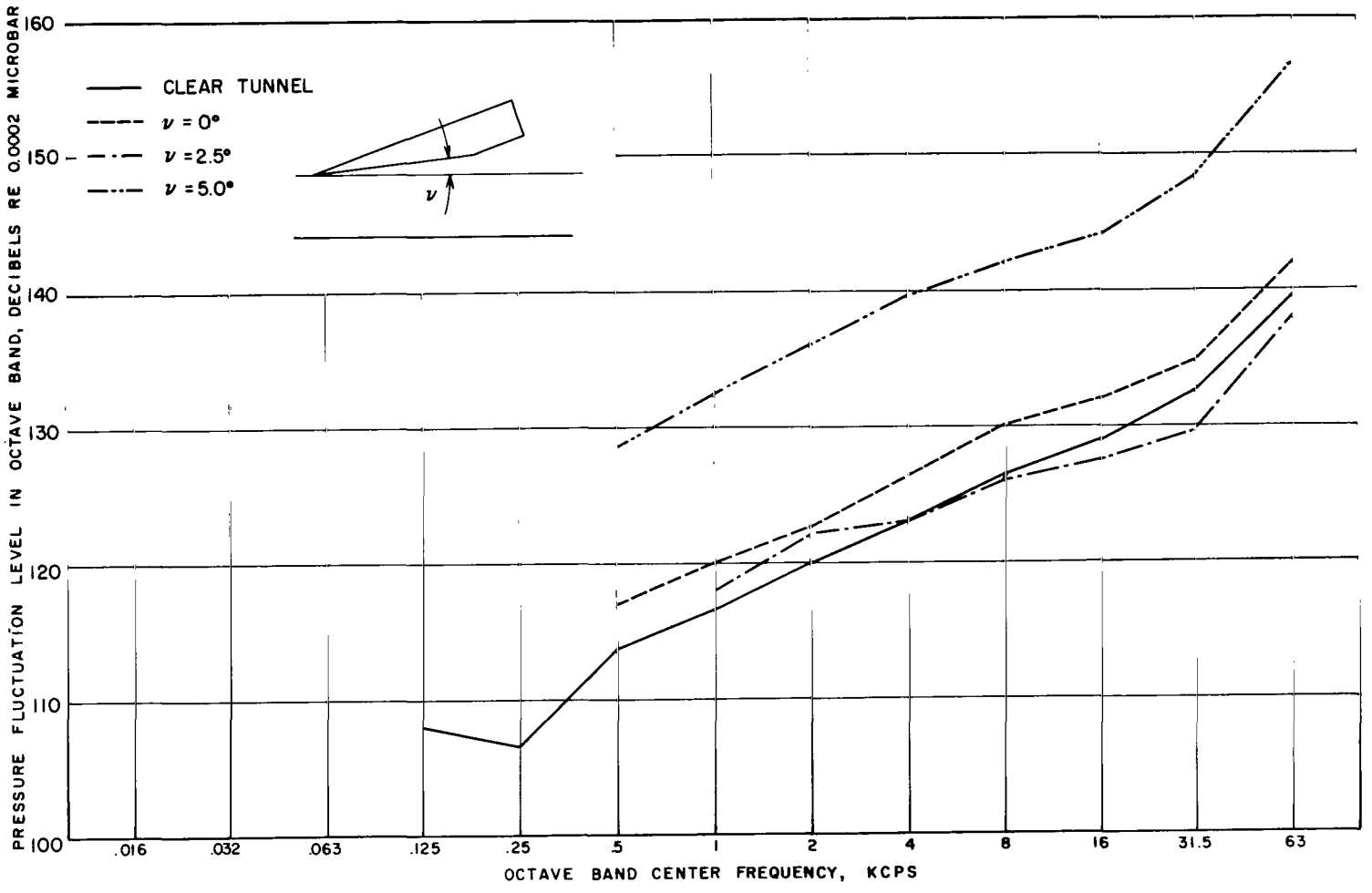

FIGURE 31 BOUNDARY LAYER PRESSURE FLUCTUATION LEVELS AT MICROPHONE LOCATION 4(X = 4'')
IN THE PRESENCE OF A FAVORABLE PRESSURE GRADIENT, $M_4 = 3.46$

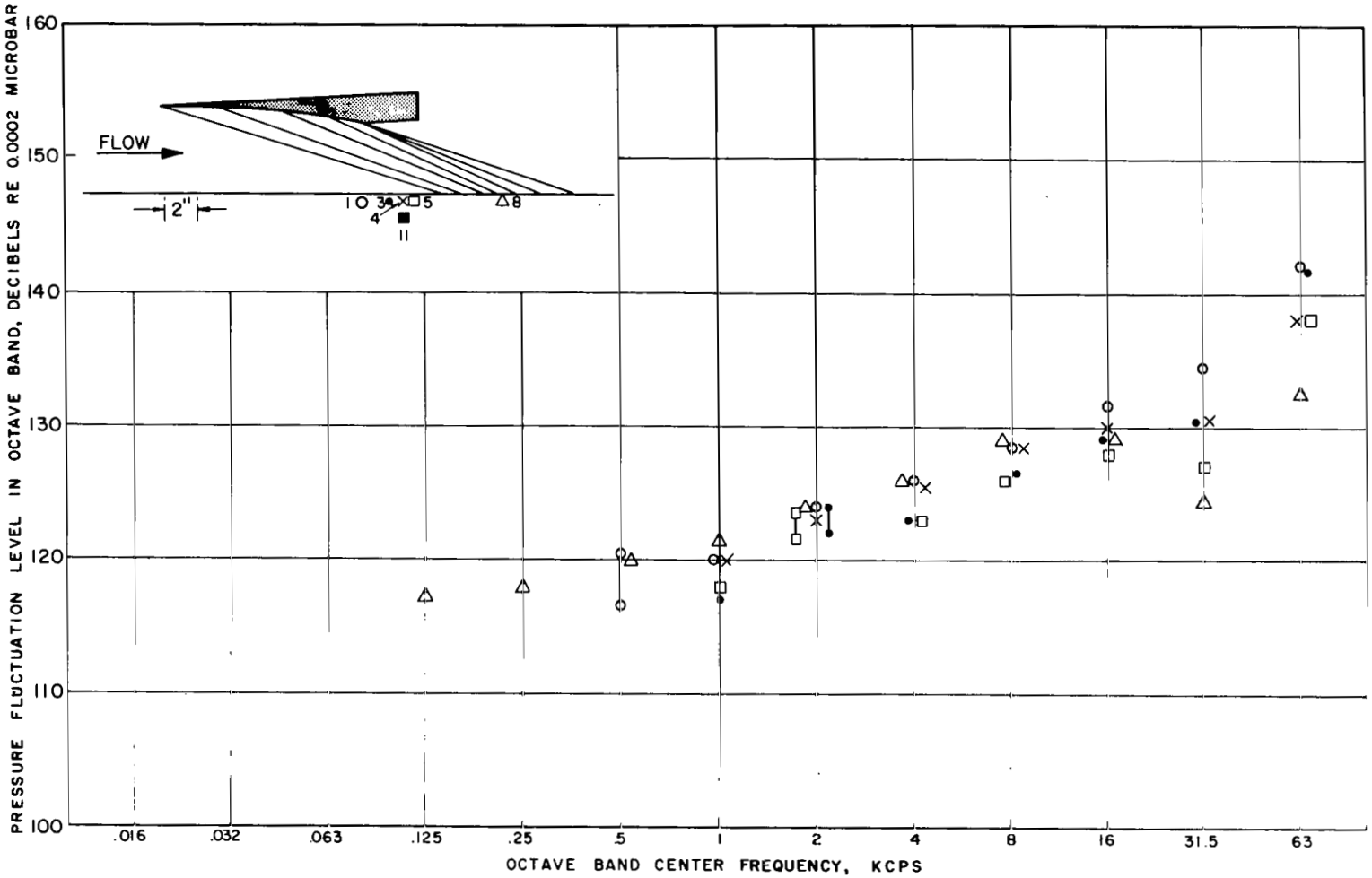

FIGURE 32 BOUNDARY LAYER PRESSURE FLUCTUATION LEVELS AT STATIONS ALONG THE TUNNEL SIDEWALL IN THE PRESENCE OF AN ADVERSE PRESSURE GRADIENT, $M_4 = 3.46$

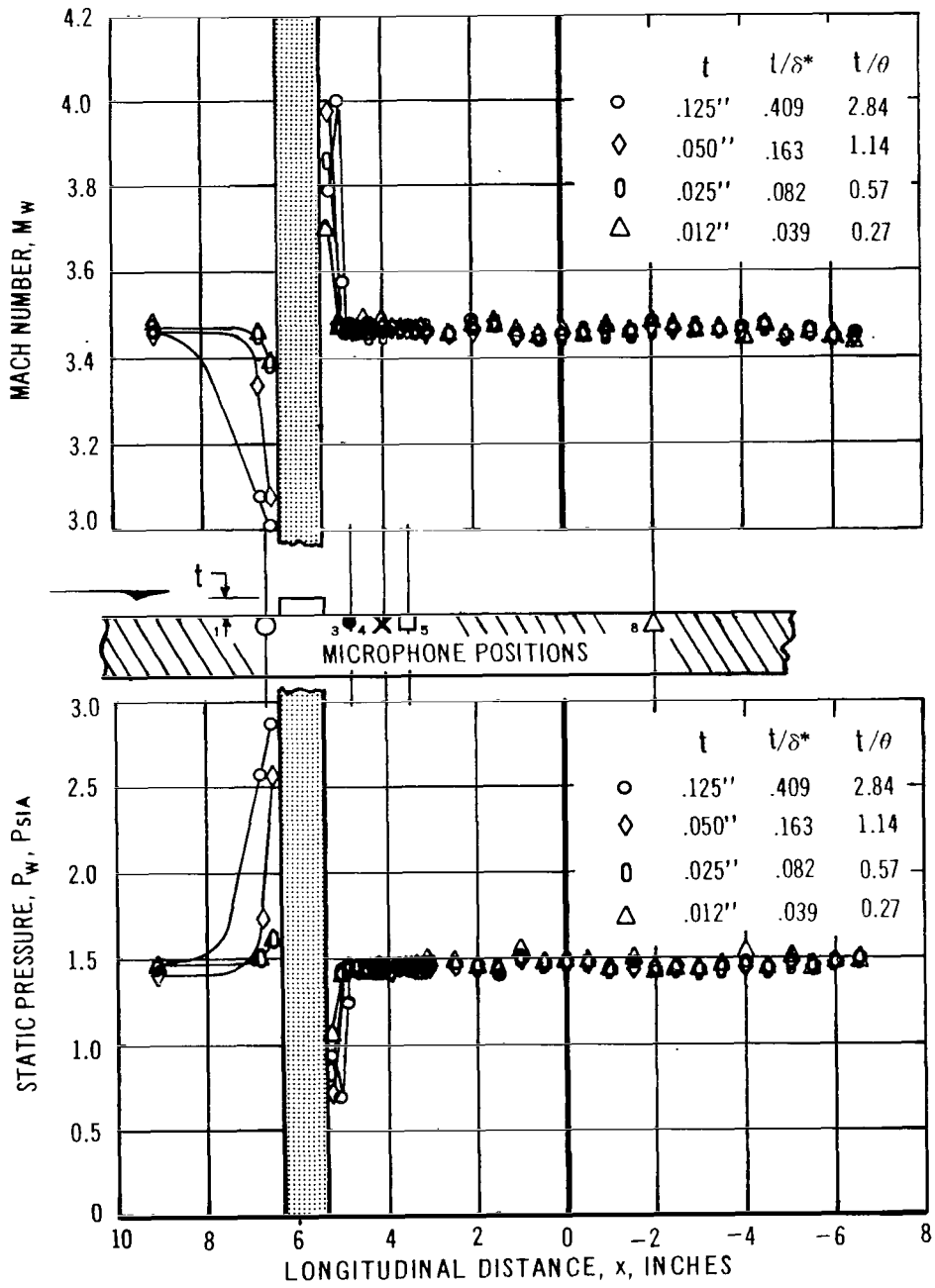

FIGURE 33. VARIATION OF STATIC PRESSURE AND MACH NUMBER WITH DISTANCE ALONG THE SIDEWALL CENTERLINE IN THE PRESENCE OF TWO-DIMENSIONAL SURFACE ROUGHNESS OF VARIOUS THICKNESSES AT $M_4 = 3.46$

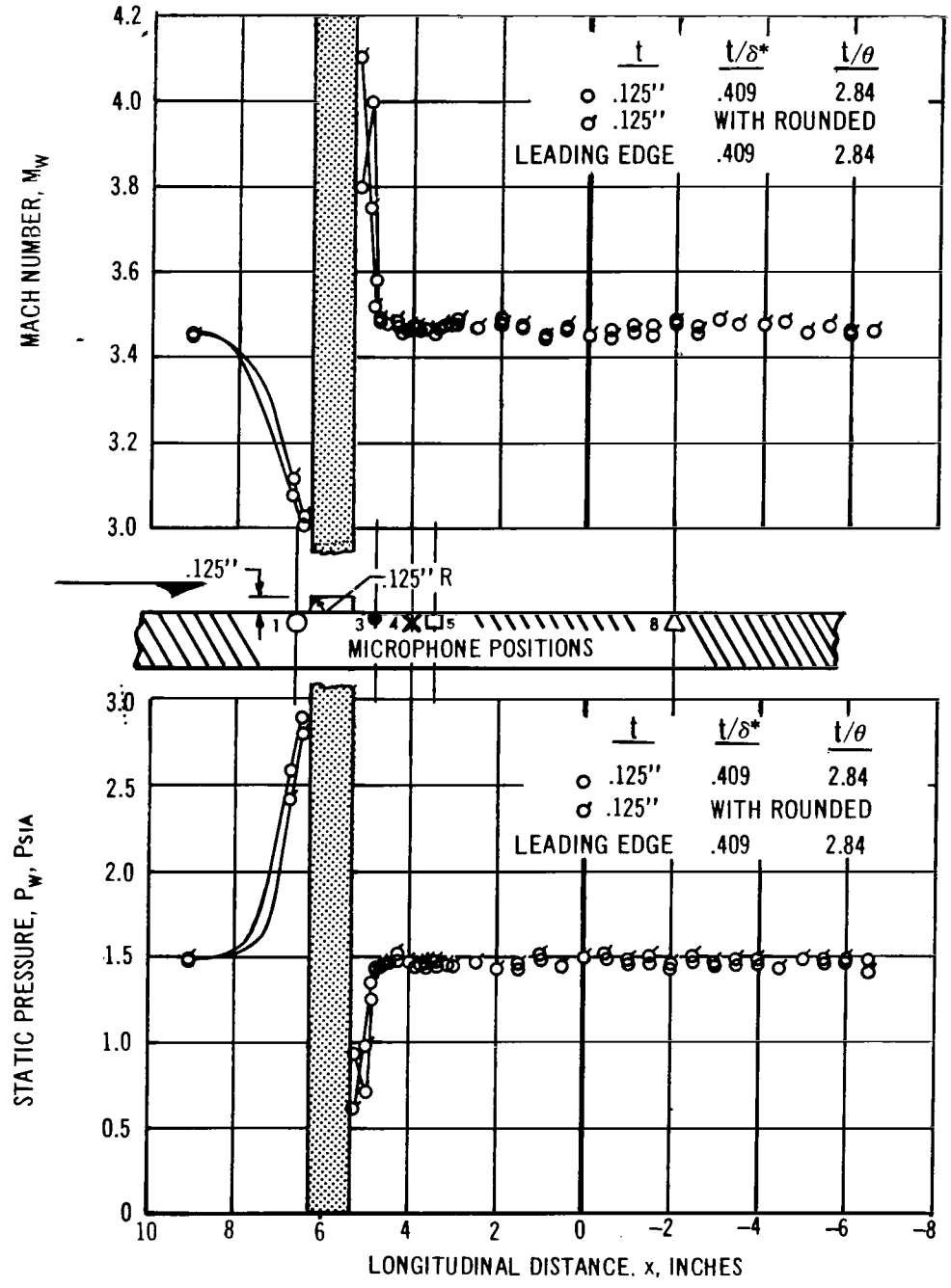

FIGURE 33b – VARIATION OF STATIC PRESSURE AND MACH NUMBER WITH DISTANCE ALONG THE SIDEWALL CENTERLINE IN THE PRESENCE OF A .125" TWO-DIMENSIONAL ROUGHNESS WITH SQUARE OR ROUNDED LEADING EDGE AT $M_4 = 3.46$

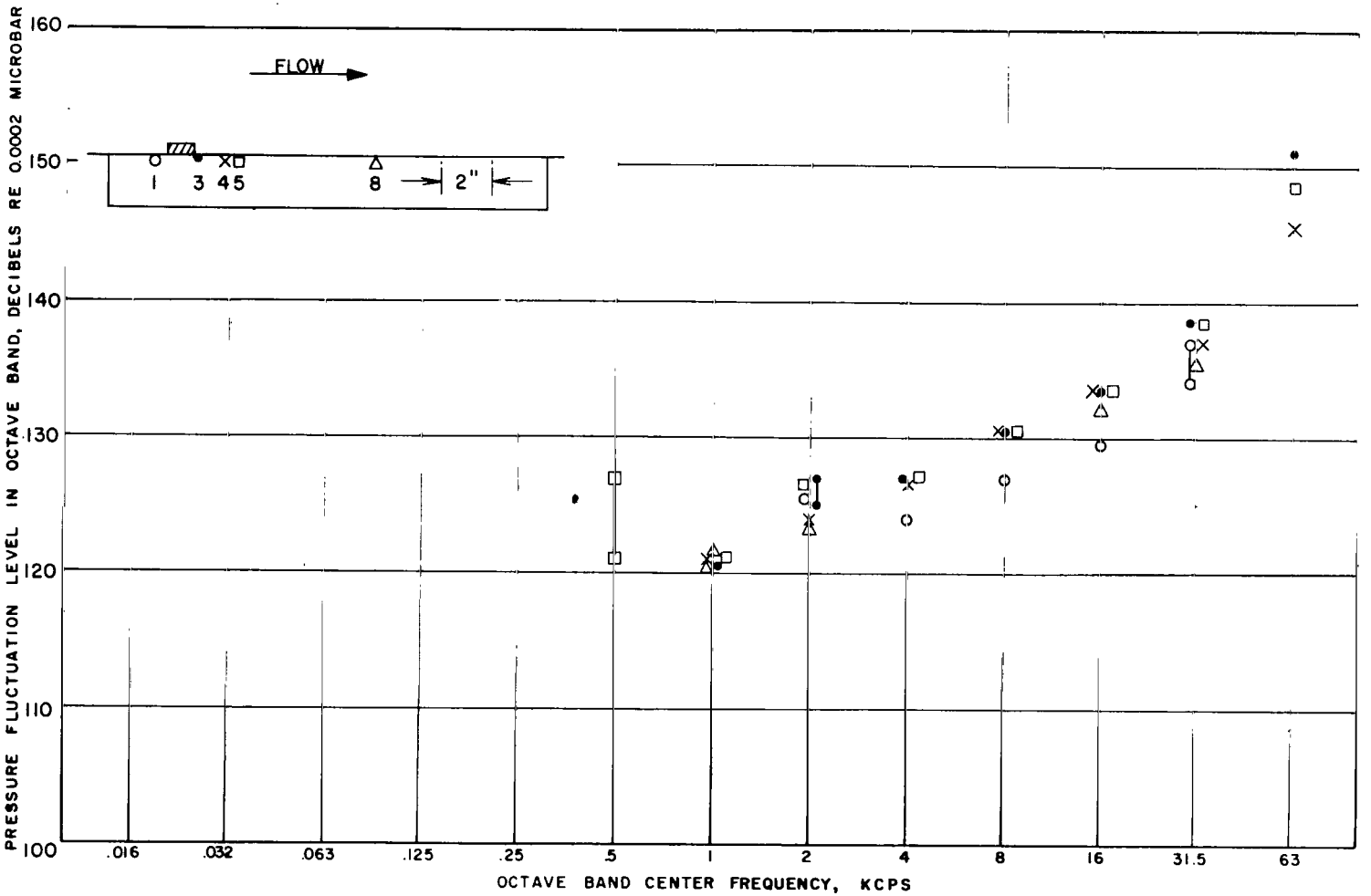

FIGURE 34 BOUNDARY LAYER PRESSURE FLUCTUATION LEVELS AT STATIONS ALONG THE TUNNEL SIDEWALL IN THE PRESENCE OF A ROUGHNESS, $M_4 = 3.46$ ROUGHNESS THICKNESS $t = 0.025'' = 0.08\delta^*$

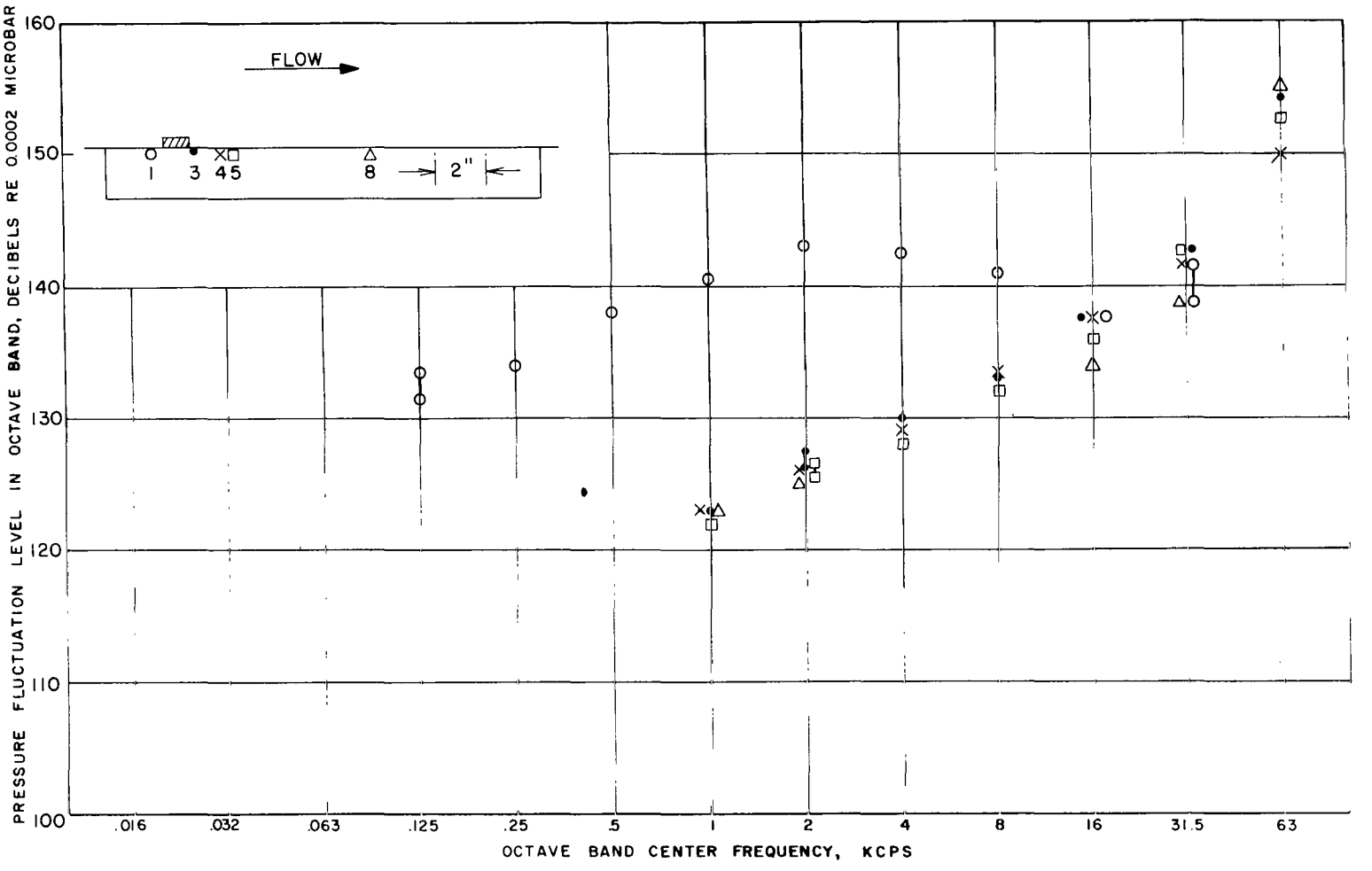

FIGURE 35 BOUNDARY LAYER PRESSURE FLUCTUATION LEVELS AT STATIONS ALONG THE TUNNEL SIDEWALL IN THE PRESENCE OF A ROUGHNESS, $M_4 = 3.46$
ROUGHNESS THICKNESS $t = 0.050'' = 0.16\delta^*$

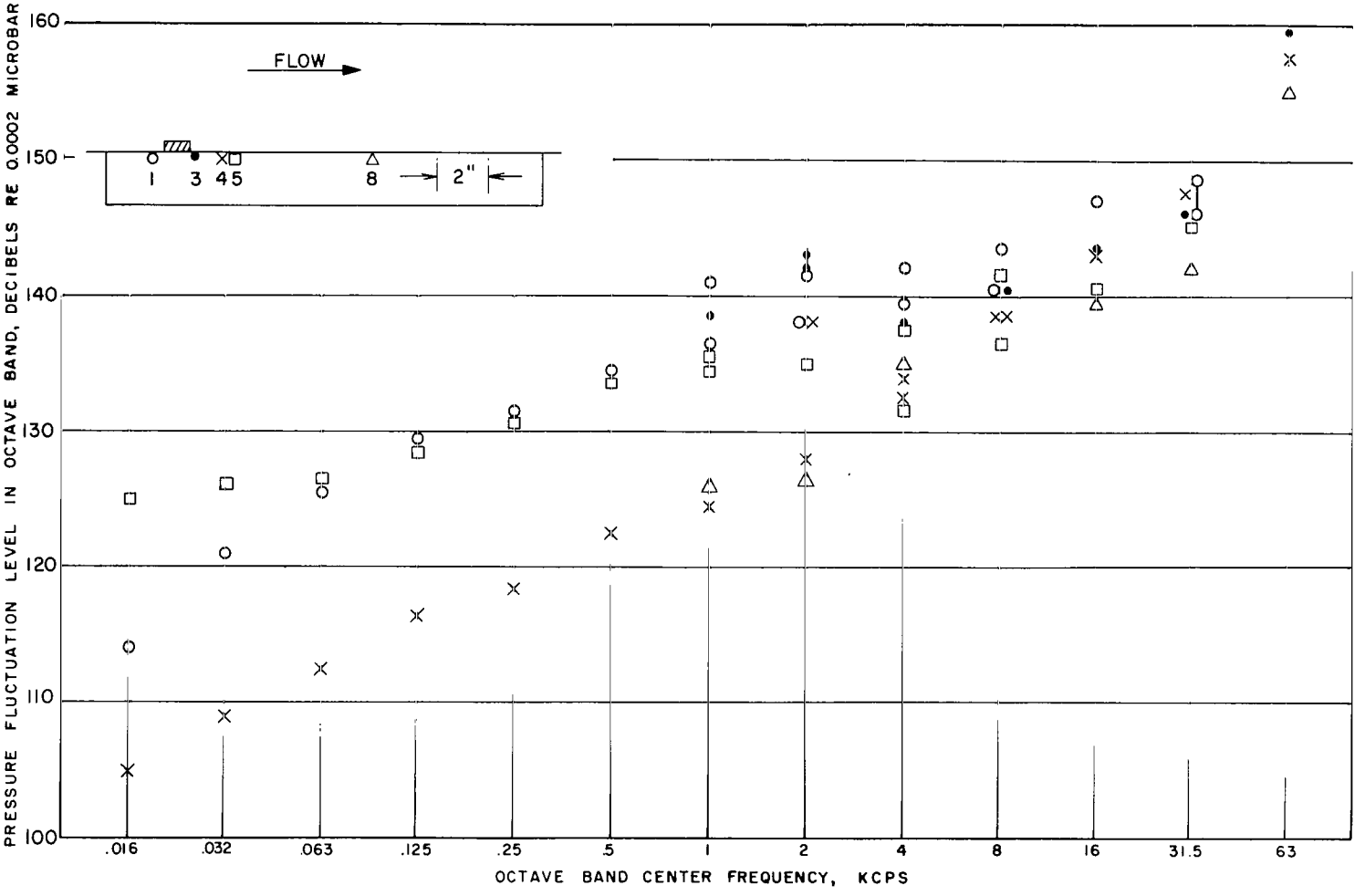

FIGURE 36 BOUNDARY LAYER PRESSURE FLUCTUATION LEVELS AT STATIONS ALONG THE TUNNEL SIDEWALL IN THE PRESENCE OF A ROUGHNESS, $M_4 = 3.46$ ROUGHNESS THICKNESS $t = 0.125'' = 0.408\delta^*$

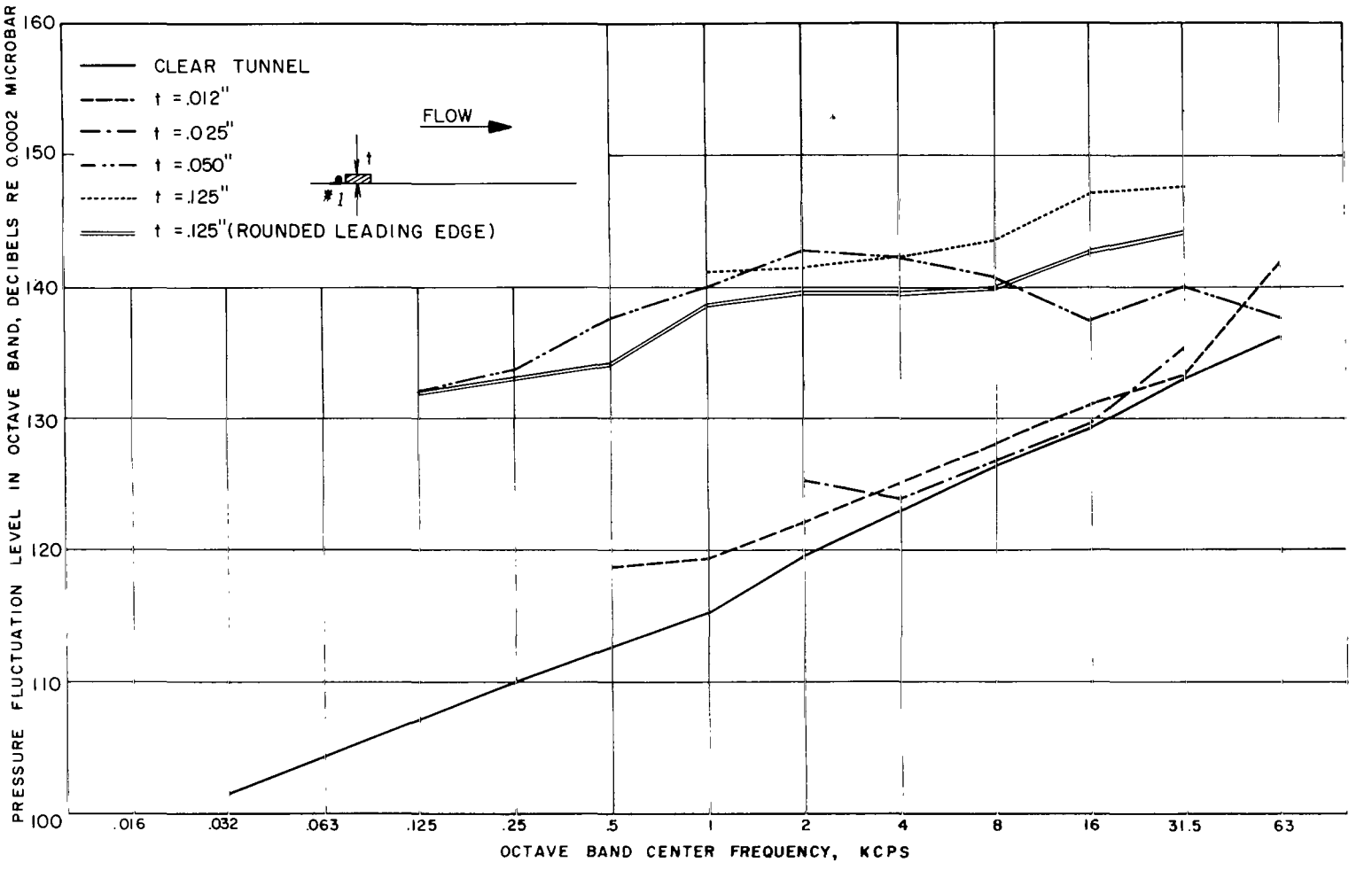

FIGURE 37 BOUNDARY LAYER PRESSURE FLUCTUATION LEVELS AT MICROPHONE LOCATION 1 (X = 6.625") IN THE PRESENCE OF A ROUGHNESS DOWNSTREAM, $M_4 = 3.46$

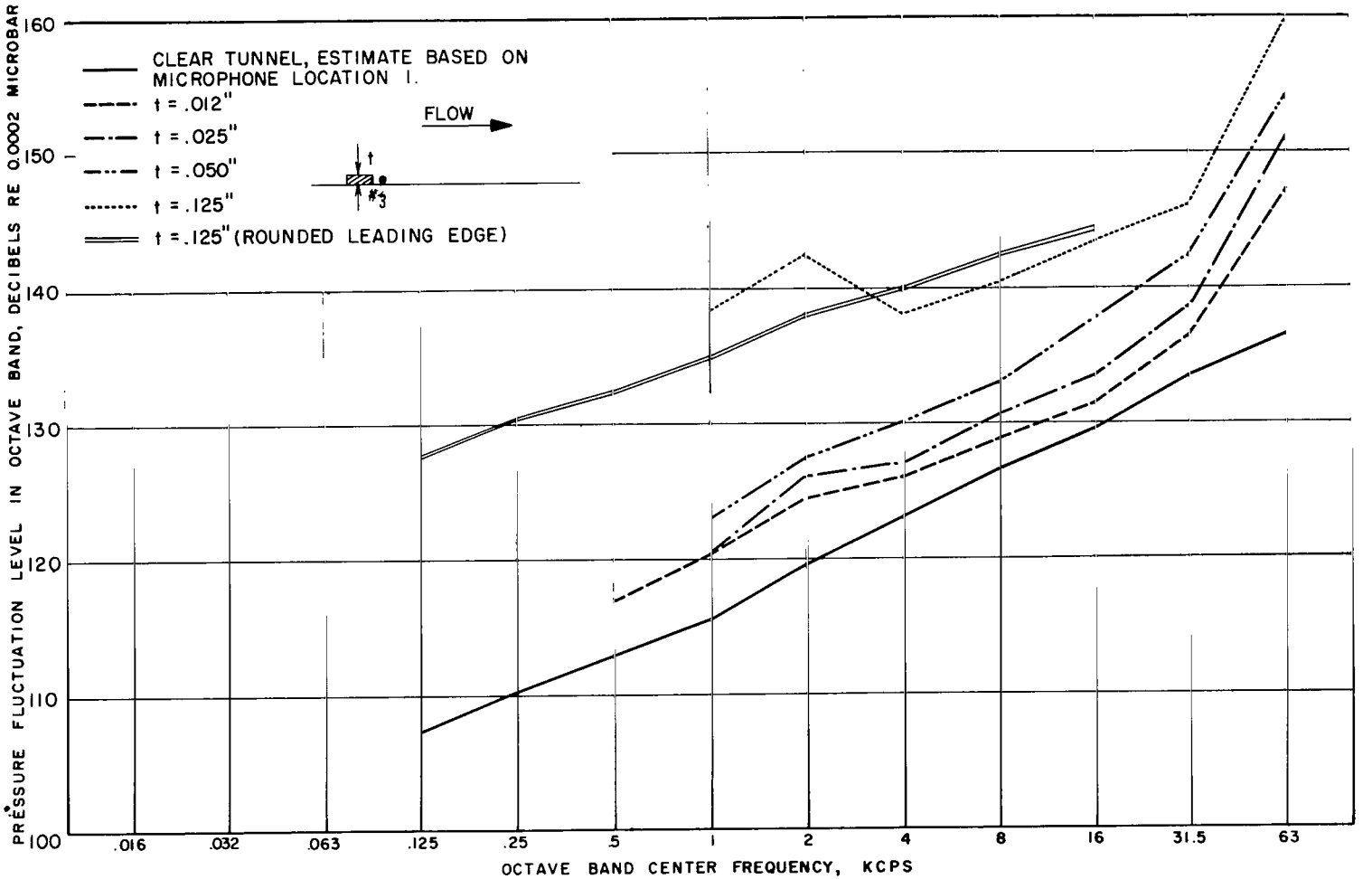

FIGURE 38 BOUNDARY LAYER PRESSURE FLUCTUATION LEVELS AT MICROPHONE LOCATION 3(X = 4.875") IN THE PRESENCE OF A ROUGHNESS DOWNSTREAM, $M_4 = 3.46$

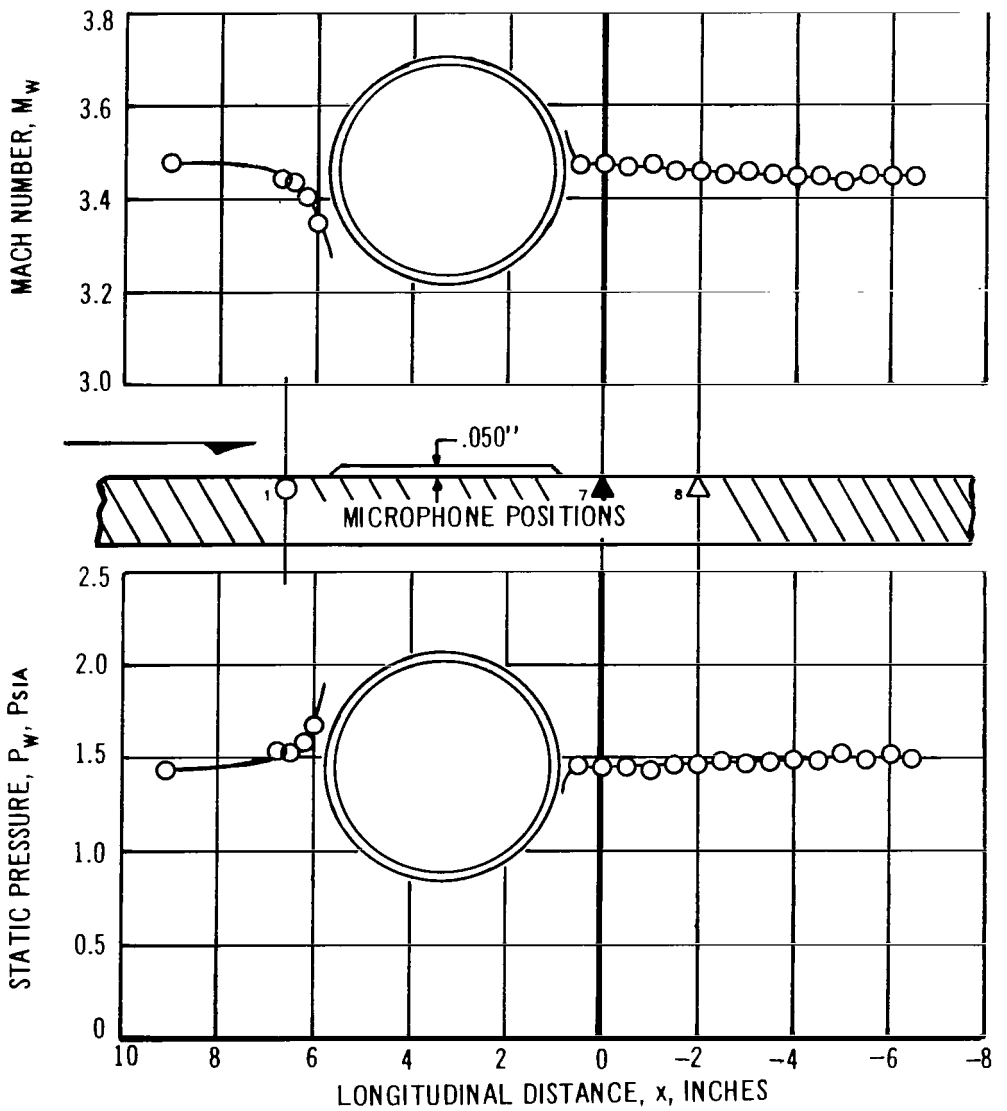

FIGURE 39 VARIATIONS OF STATIC PRESSURE AND MACH NUMBER WITH DISTANCE ALONG THE SIDEWALL CENTERLINE IN THE PRESENCE OF A SIMULATED HALF-SCALE WINDOW AT $M_1 = 3.46$

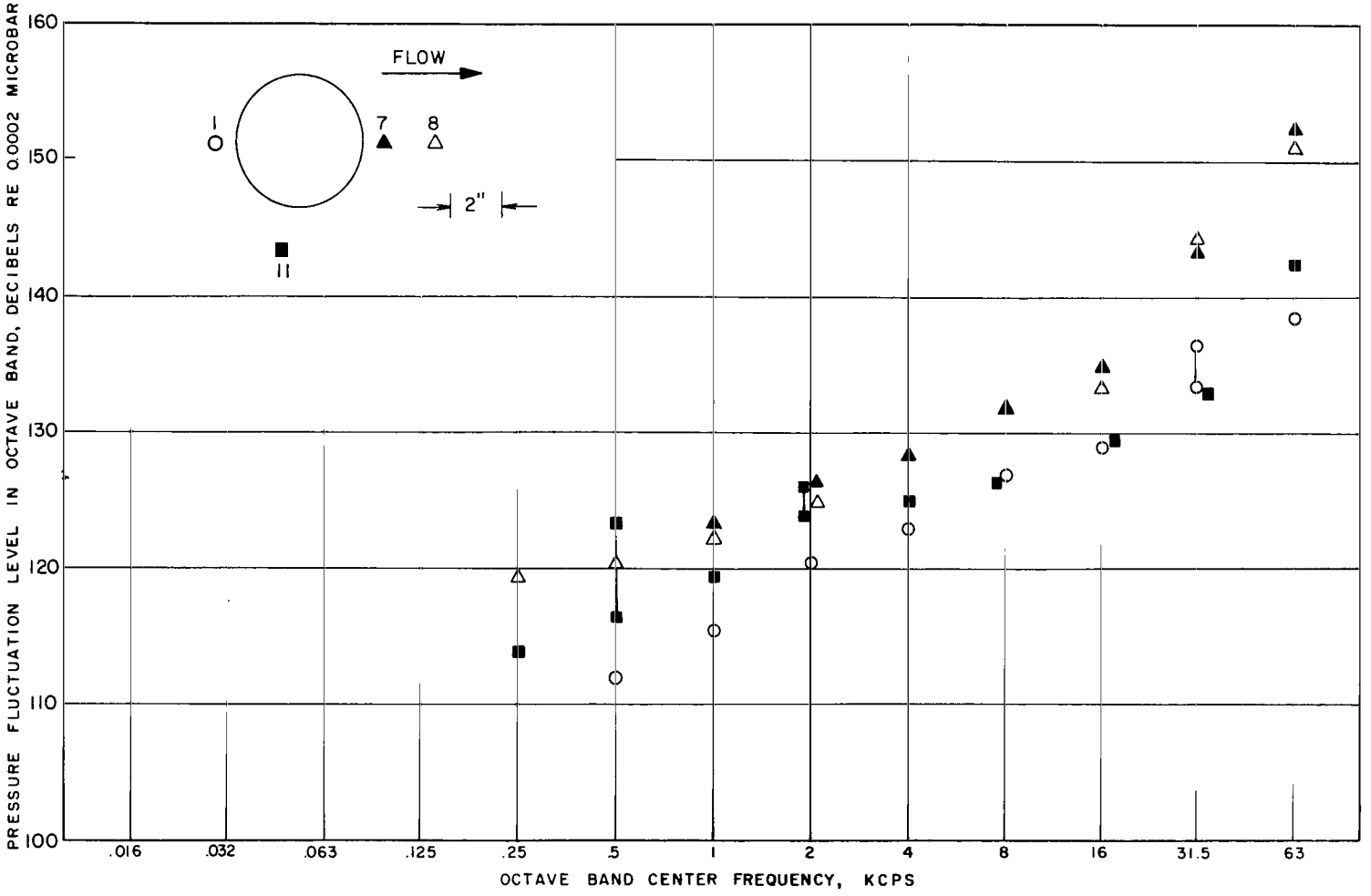

FIGURE 40 BOUNDARY LAYER PRESSURE FLUCTUATION LEVELS ALONG THE TUNNEL SIDEWALL IN THE PRESENCE OF A SIMULATED WINDOW ROUGHNESS, $M_4 = 3.46$ ROUGHNESS THICKNESS 0.050"

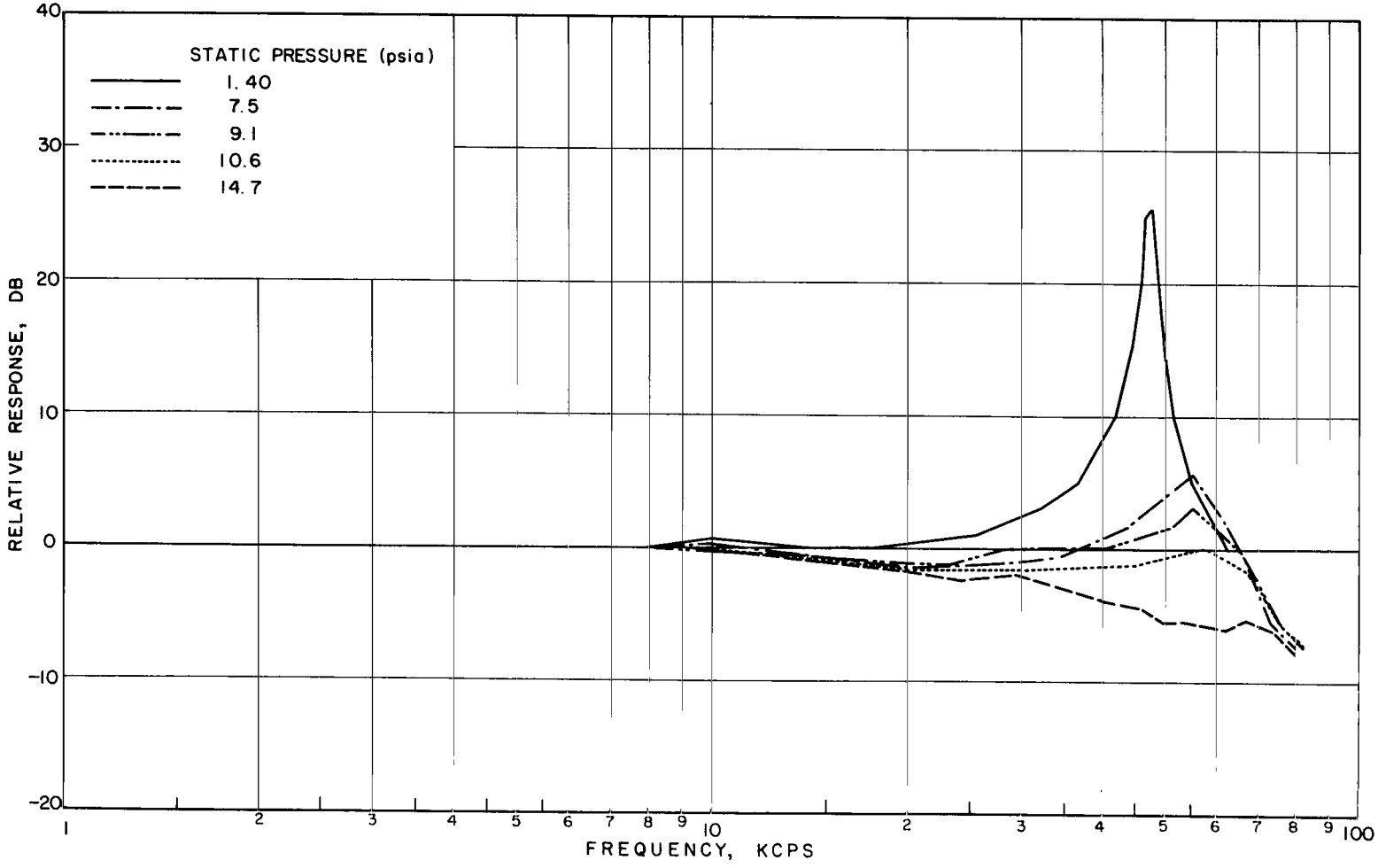

FIGURE 41 PRESSURE RESPONSE CHARACTERISTICS FOR BRUEL AND KJAER QUARTER INCH MICROPHONE TYPE NUMBER 4136, SERIAL NUMBER 77315

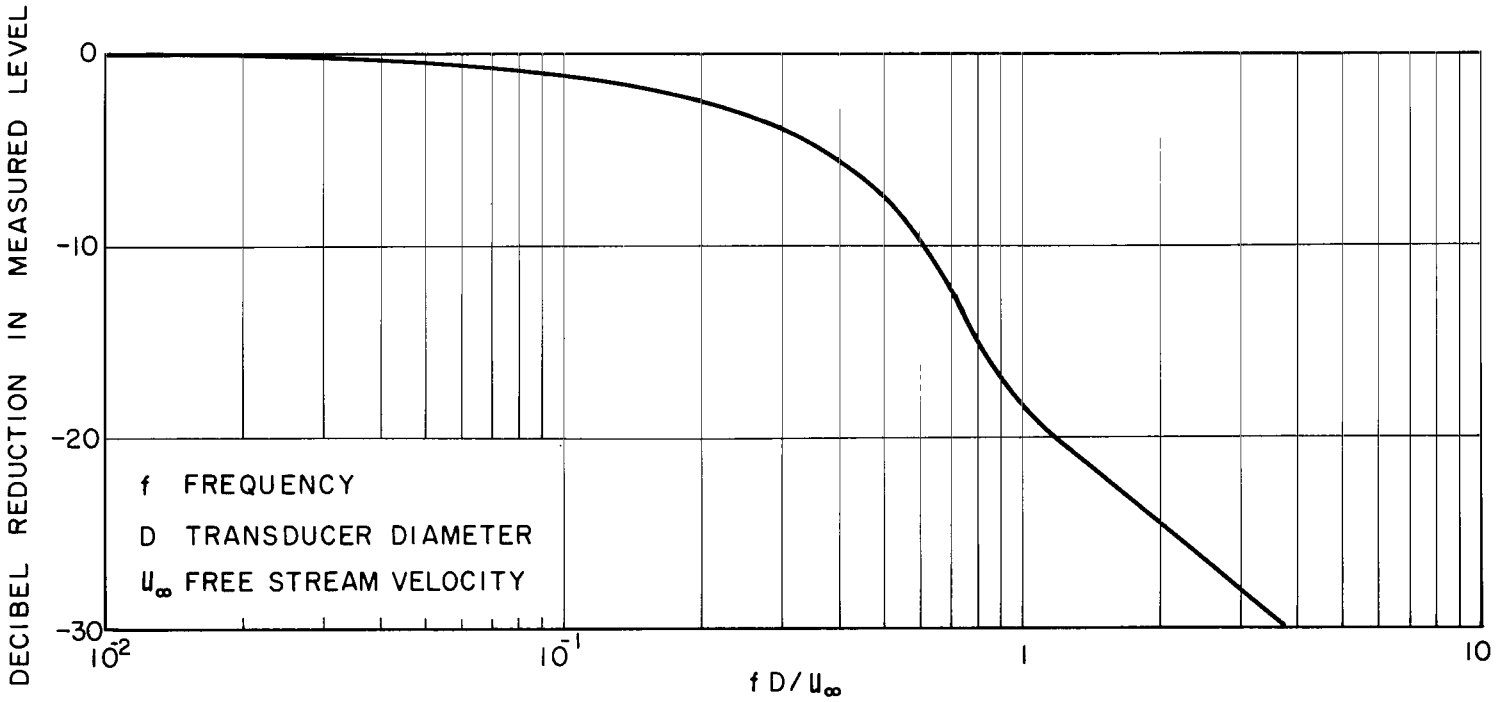

FIGURE 42 TURBULENCE PRESSURE SPECTRUM CORRECTION FOR FINITE SIZE TRANSDUCER BASED ON CORCOS (REF 25)

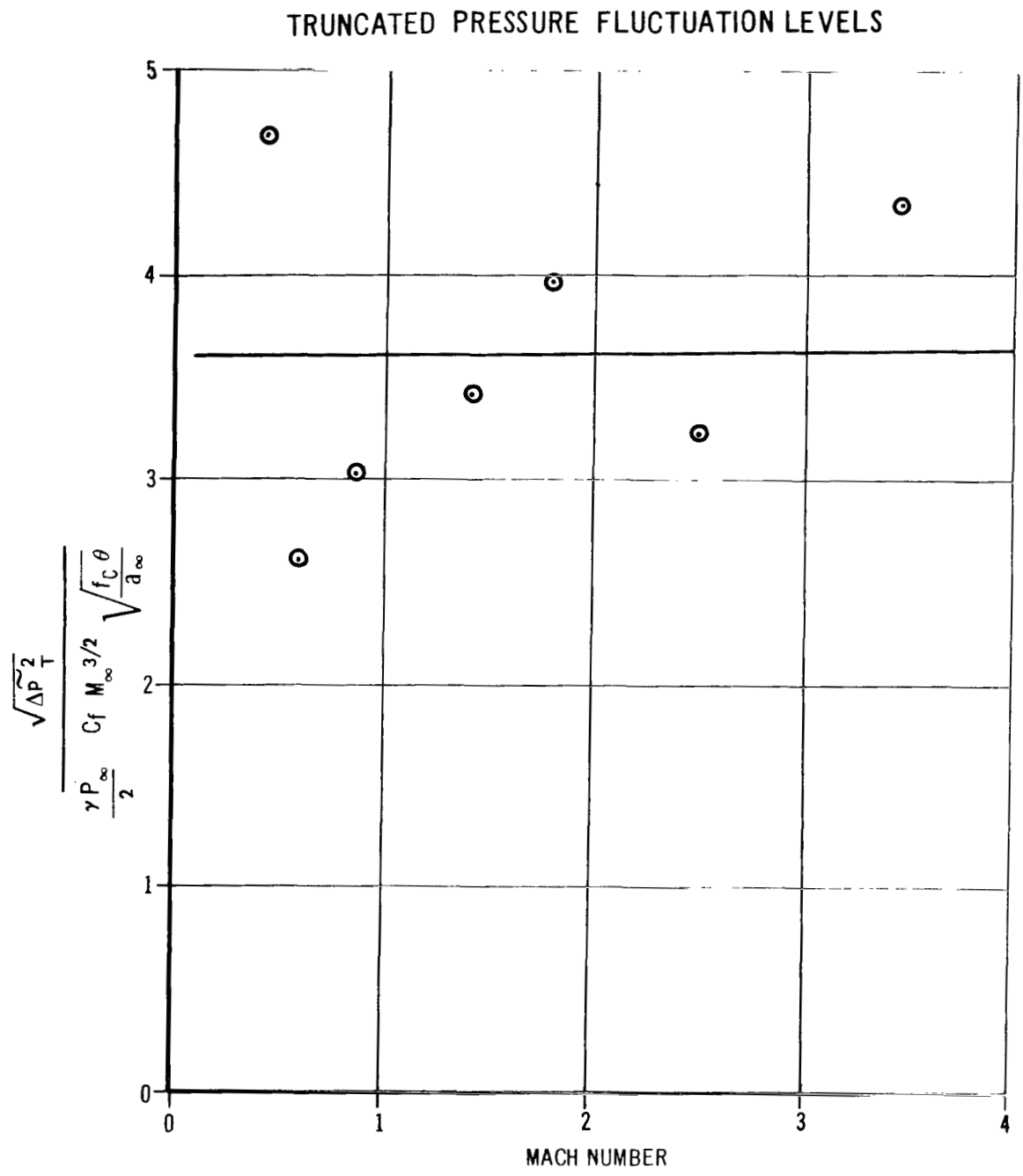
TRUNCATED PRESSURE FLUCTUATION LEVELS
$\frac{\sqrt{\overline{\Delta p_T^2}}}{\frac{\gamma P_\infty}{2} C_f M_\infty^{3/2} \sqrt{\frac{f_c \theta}{a_\infty}}}$
0
1
2
3
4
5
MACH NUMBER

FIGURE 43

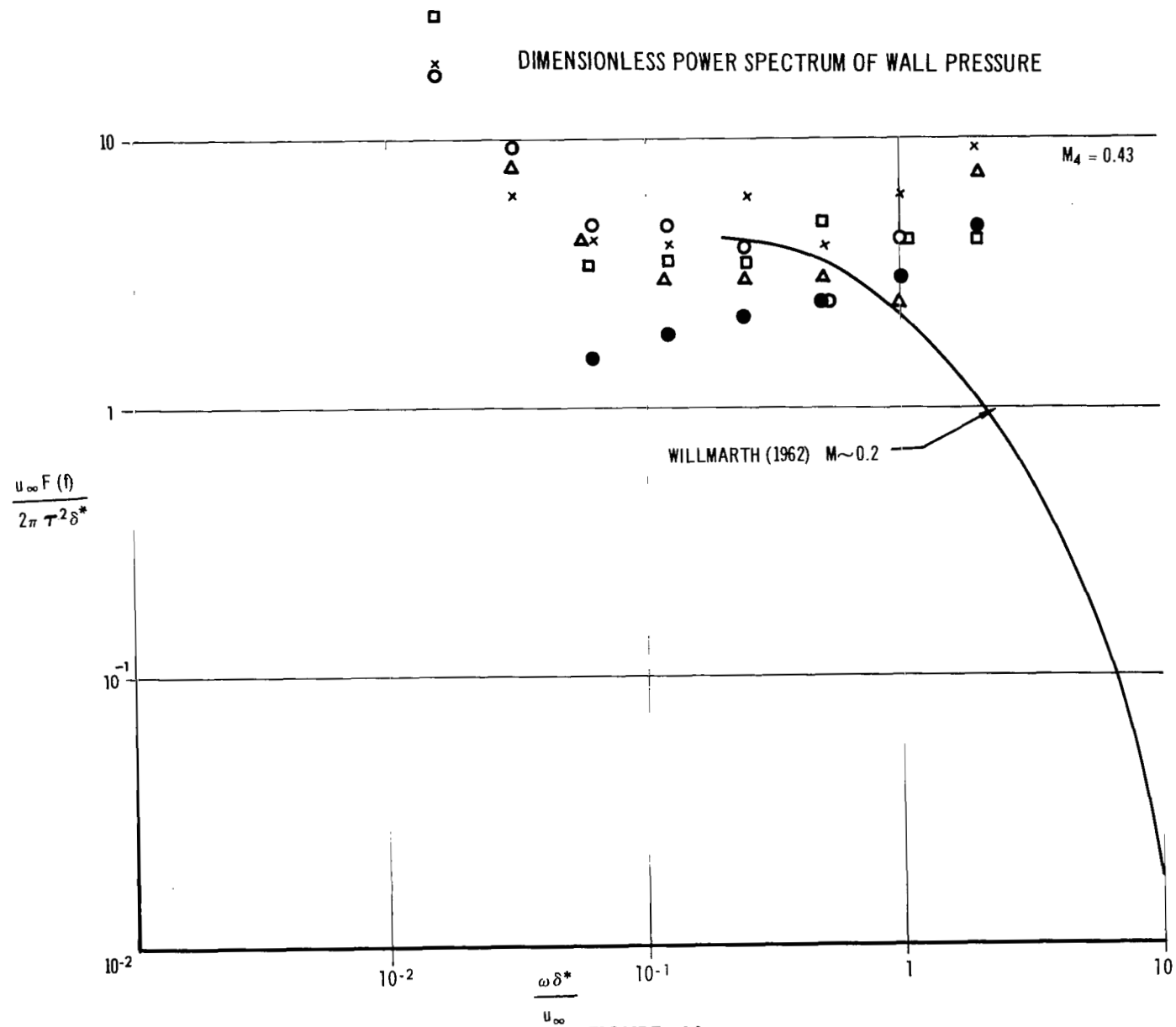
DIMENSIONLESS POWER SPECTRUM OF WALL PRESSURE
$M_4 = 0.43$
WILLMARTH (1962) M~0.2
$\frac{u_\infty F(f)}{2\pi \tau^2 \delta^*}$
$\frac{\omega \delta^*}{u_\infty}$
10
1
10^{-1}
10^{-2}
10^{-2}
10^{-1}
1
10

FIGURE 44 a

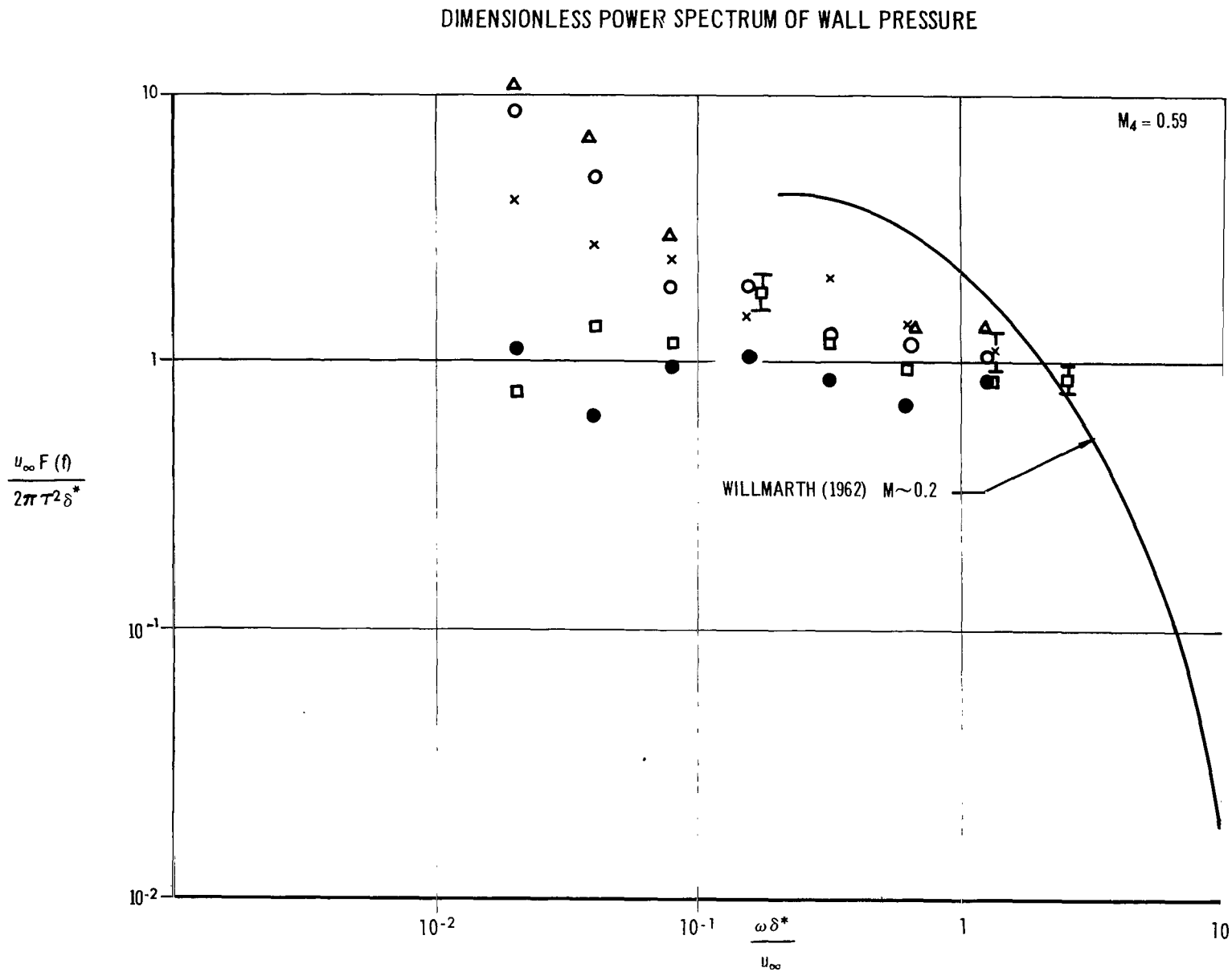
DIMENSIONLESS POWER SPECTRUM OF WALL PRESSURE
$M_4 = 0.59$
WILLMARTH (1962) M~0.2
$\frac{u_\infty F(f)}{2\pi\tau^2\delta^*}$
10
1
10^{-1}
10^{-2}
10^{-2}
10^{-1}
$\frac{\omega\delta^*}{u_\infty}$
1
10

FIGURE 44 b

DIMENSIONLESS POWER SPECTRUM OF WALL PRESSURE

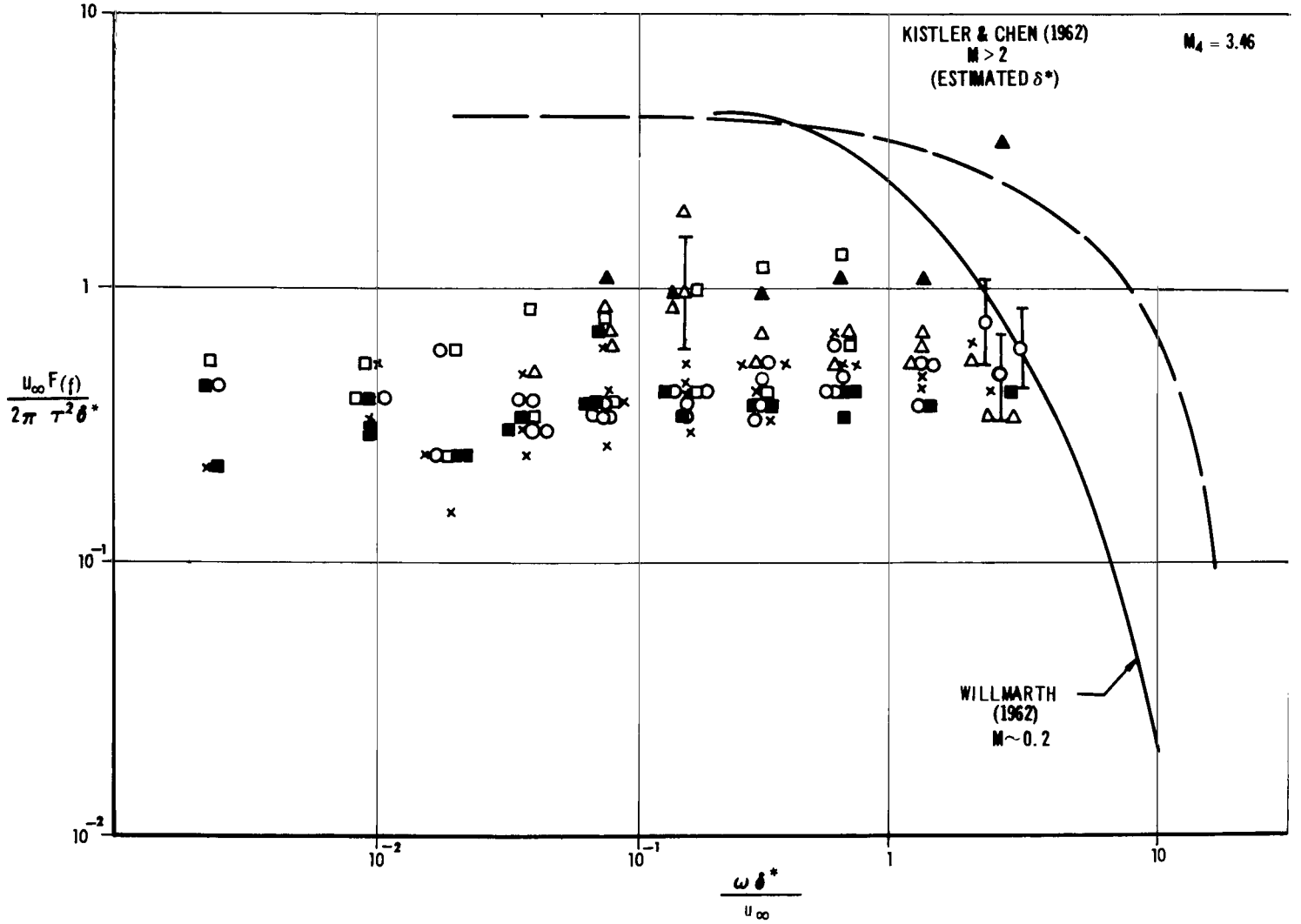

FIGURE 44c